UC Santa Barbara

UC Santa Barbara Electronic Theses and Dissertations

Title

The Effects of Surface Chemistry on Polymer Hydration, Adsorption, and Fouling

Permalink

https://escholarship.org/uc/item/7zs718b9

Author

Barry, Mikayla Elise

Publication Date

2021

Peer reviewed|Thesis/dissertation

eScholarship.org Powered by the California Digital Library
University of California

UNIVERSITY OF CALIFORNIA

Santa Barbara

The Effects of Surface Chemistry on Polymer Hydration, Adsorption, and Fouling

A dissertation submitted in partial satisfaction

of the requirements for the degree

Doctor of Philosophy in Materials

by

Mikayla Elise Barry

Committee in charge:

Professor Rachel A. Segalman, Chair

Professor Craig J. Hawker

Professor Songi Han

Professor Angela A. Pitenis

September 2021

The dissertation of Mikayla Elise Barry is approved.

Professor Craig J. Hawker

Professor Songi Han

Professor Angela A. Pitenis

Professor Rachel A. Segalman, Committee Chair

September 2021

The Effects of Surface Chemistry on Polymer Hydration, Adsorption, and Fouling

Copyright © 2021

by

Mikayla Elise Barry

ACKNOWLEDGEMENTS

As I reflect on my path through graduate school, I'm amazed at the incredible support network I've had. First and foremost, I am indebted to my advisor, Rachel, for her leadership, her scientific insights, and her patience when things go awry. But I most appreciate the way she cares for her students. She balances her students' professional and personal development, and stepped in to help me when I was caught in a pattern of overworking. And her efforts to keep us physically and mentally safe during the COVID-19 pandemic have been nothing short of heroic. I am also especially grateful to her for her commitment to maintaining mentorship during my final year of research spent at Lawrence Berkeley National Laboratory (LBNL).

I am also very grateful to Ethan Crumlin of LBNL, who knowingly took on a student who had never done XPS analysis and welcomed her into his group for over a year. I have benefitted so much from his mentorship: his scientific insight and his passion for learning have helped inspire me to reach farther and discover more as a researcher than I ever thought. He has always made time for me when I've had research or personal challenges, catalyzing my professional and personal growth in the process. I am so thankful for all that he invested in me.

I would also like to express my sincere gratitude for my committee members and their investment in me over these four years. I greatly admire Songi Han and her scientific curiosity; in our meetings together, she has always given exceptional insight and participated extensively in discussions. I am so grateful to Angela for her personal support: during times when I felt weakened by experiments that did not pan out, talking with her

reinvigorated my passion for science and confidence in myself. Lastly, I am very thankful to Craig Hawker, who wielded incredible knowledge yet always made me feel at ease and supported. I appreciate the work that my committee did as a whole, believing in me from my first days through today as I wrap up the end of my graduate work.

I must also express my gratitude for the scholarship and fellowship organizations that made my path possible. I appreciate the confidence placed in me by the National Science Foundation and the Astronaut Scholarship Foundation. I am indebted to the Beckman Foundation for investing in my professional development as a researcher and for pairing me with my amazing undergraduate research advisor, Melissa Grunlan. And I am most grateful for those in the Terry Foundation, who were the first to see potential in me as a high school senior and who have remained involved throughout the years.

I have also been fortunate to have received support from two amazing research groups during my PhD. To the Segalman lab: you all made my time in Santa Barbara so much fun, from weeknight dinners at local restaurants, to the annual "Girls' Night Out," to our summer group retreats. Nicole, I am especially grateful for having had the opportunity to meet you and grow in friendship during my time in Santa Barbara and beyond. I have always enjoyed the time we spent together, from our conversations in between experiments, to cooking dinner together at home, to stargazing in the wilderness. Audra, Keith, Ethan S., and Amanda M.: I could have never asked for better adventure buddies—whether we were hiking in the Santa Barbara backcountry or exploring the Sierra, it was a gift getting to enjoy your company. And to the Crumlin group: I've thoroughly enjoyed the times we've spent together going on hikes, getting pastries and ice cream, and of course engaging in conversations during beamtime. While I will be graduating from the group, I hope to at

least continue joining you for two of those activities. I also must thank Pinar in particular: it was amazing having you as a colleague. Thank you for all your guidance with data collection and analysis, and for the great times and conversations we shared during those long beamtime nights.

I also wish to convey my gratitude to all of my friends here and throughout the country. To Amanda R., Hadass, Sara, Virginia, and the rest of my Materials Department friends, who brightened my days both during classes and outside of work. To my book club friends, whose steady support helped me find joy in things outside of science. To my local Bay Area friends, especially Tony, Julia, Claire, Beth, and Lauren: thank you for welcoming me and for encouraging me to take those much-needed breaks from work. To Amanda L., who went from a collaborator to a close friend over the years. And to all of my friends from high school and my undergraduate studies, for your dedication to maintaining our friendships despite the distance. I look forward to seeing you all again in the future.

And my deepest appreciation goes to my family. For my parents, who nurtured my fascination with science and boundless curiosity from a young age and have loved me through it all. To Matthew, Mariah, and Mitchell, who joined me on adventures ranging from experiments to exploring and are the best siblings I could have ever hoped to have. I am also so grateful for my extended family, the Barrys, Musantes, and Zaryskes, who have always supported me in my endeavors and welcomed me with joy for every visit home. And lastly, I must thank those who may not be family by blood but who have been there for me through it all, from my first days of elementary school through my PhD.

VITA OF MIKAYLA ELISE BARRY

September 2021

EDUCATION

Doctor of Philosophy in Materials *September 2021*
University of California, Santa Barbara

Bachelor of Science in Biomedical Engineering *May 2017*
Texas A&M University

HONORS AND AWARDS

Advanced Light Source Doctoral Fellowship in Residence *2019 – 2020*

National Science Foundation Graduate Research Fellowship *2017 – 2019*

Tau Beta Pi Edward H. Williams Jr. Graduate Fellowship *2017 – 2018*

Astronaut Scholarship *2016 – 2017*

Beckman Scholar *2014 – 2015*

Terry Foundation Scholar *2013 – 2017*

PUBLICATIONS

11. Jiao, S.; DeStefano, A.; Monroe, J. I.; **Barry, M.**; Sherck, N.; Casey, T.; Segalman, R. A.; Han, S.; Shell, M. S. Quantifying Polypeptoid Conformational Landscapes through Integrated Experiment and Simulation. *Macromolecules* **2021**, 54 (11), 5011-5021.

10. Sherck, N.; Webber, T.; Brown, D. R.; Keller, T.; **Barry, M.**; DeStefano, A.; Jiao, S.; Segalman, R. A.; Fredrickson, G. H.; Shell, M. S.; Han, S. End-to-End Distance Probability Distributions of Dilute Poly (ethylene oxide) in Aqueous Solution. *Journal of the American Chemical Society* **2020**, 142 (46), 19631-19641.

9. Aydogan Gokturk, P.; **Barry, M.**; Segalman, R.; Crumlin, E. Directly probing polymer thin film chemistry and counterions influence on water sorption. *ACS Applied Polymer Materials* **2020**, 2 (11), 4752-4761.

8. **Barry, M. E.**; Landsman, M. R.; Nomaan, S. M.; Aydogan Gokturk, P.; Cooper, C. M.; Kienzle, B. A., McKay, C.; L. E. Katz. Expanding the Use of Synchrotron Techniques for Water Treatment: From Minerals to Membranes. *Synchrotron Radiation News* **2020**, 33 (4), 3-12.

7. Monroe, J.; **Barry, M.**; DeStefano, A.; Gokturk, P. A.; Jiao, S.; Robinson-Brown, D.; Webber, T.; Crumlin, E. J.; Han, S.; Shell, M.S. Water Structure and Properties at Hydrophilic and Hydrophobic Surfaces. *Annual Review of Chemical and Biomolecular Engineering* **2020**, 11, 523-557.

6. Ngo, B. K. D.; **Barry, M. E.**; Lim, K. K.; Johnson, J. C.; Luna, D. J.; Pandian, N. K.; Jain, A.; Grunlan, M. A. Thromboresistance of Silicones Modified with PEO-Silane Amphiphiles. *ACS Biomaterials Science & Engineering* **2020**, 6 (4), 2029-2037.

5. **Barry, M. E.**; Davidson, E. C.; Zhang, C.; Patterson, A. L.; Yu, B.; Leonardi, A. K.; Duzen, N.; Malaviya, K.; Clarke, J. L.; Finlay, J. A.; Clare, A. S.; Chen, Z.; Ober, C. K.; Segalman, R. A. The role of hydrogen bonding in peptoid-based marine antifouling coatings. *Macromolecules* **2019**, 52 (3), 1287-1295.

4. Zouaghi, S.; **Barry, M. E.;** Bellayer, S.; Lyskawa, J.; André, C.; Delaplace, G.; Grunlan, M. A.; Jimenez, M. Antifouling amphiphilic silicone coatings for dairy fouling mitigation on stainless steel. *Biofouling* **2018** 34 (7), 769-783.

3. Rufin, M. A.; Ngo, B.; **Barry, M. E.**; Page, V. M.; Hawkins, M. L.; Stafslien, S. J.; Grunlan, M. A. Antifouling silicones based on surface-modifying additive amphiphiles. *Green Materials* **2017**, 5 (1), 4–13.

2. Rufin, M. A; **Barry, M. E.**; Adair, P. A.; Hawkins, M. L.; Raymond, J. E.; Grunlan, M. A. Protein resistance efficacy of PEO-silane amphiphiles: dependence on PEO-segment length and concentration in silicone. *Acta Biomaterialia* **2016**, 41, 247-252.

1. **Barry, M**.; Pearce, H.; Cross, L.; Tatullo, M.; Gaharwar, A. Advances in nanotechnology for the treatment of osteoporosis. *Current Osteoporosis Reports* **2016**, 14 (3), 87-94.

CONFERENCE PRESENTATIONS

4. **Barry, M. E.;** Aydogan, P.; Segalman, R. A.; Crumlin, E. J. "Investigating Amphiphilic Polymer Surface Chemistry in Conditions from Vacuum to Hydration with Ambient Pressure XPS." Presented at the MRS Virtual Spring 2021 Meeting, April 17-23, 2021. [oral]

3. **Barry, M. E.;** Aydogan, P.; Crumlin, E. J.; Segalman, R. A. "Studying surface hydration of polymers with Ambient Pressure XPS." Presented at the ACS Fall 2019 Meeting, August 25-29, 2019. [oral]
2. **Barry, M. E.**; Davidson, E. C.; Crumlin, E. J.; Segalman, R. A. "(Near-) Ambient Pressure XPS (AP-XPS) for studying surface reconstruction of hydrated polymers." Presented at the American Physical Society March Meeting 2019, Boston, MA, United States, March 4-8, 2019. [oral]
1. **Barry, M. E.**; Davidson, E. C.; Zhang, C.; Patterson, A. L.; et al. "The role of hydrogen bonding in peptoid-based marine antifouling coatings." Presented at the 19th International Congress on Marine Corrosion and Fouling, Melbourne, FL, United States, June 25-29, 2018. [poster; **2nd Place Student Award.**]

ABSTRACT

The Effects of Surface Chemistry on Polymer Hydration, Adsorption, and Fouling

by

Mikayla Elise Barry

Polymers are commonly used in applications requiring long-term exposure to water and aqueous mixtures including as medical implants, marine antifouling coatings, and water purification membranes. In all of these, the chemistry and structure of the polymer surfaces determine the effectiveness of the final material via interactions with water, dispersed solutes, and larger biomolecular structures. In the past, scientific progress has been made primarily through empirical results derived from chemically distinctive coatings and membranes, but design rules are essential for improving the rate of advancement.

This work leverages a two-pronged approach for relating surface chemistry to its effects on interactions at the water–polymer surface. Design of surfaces containing sequence-defined, peptidomimetic "peptoid" side chains provides fine control over both chemistry and the relative spacing between functional groups, while self-assembled monolayers (SAMs) allow for investigation of model surfaces consisting of a single functional group with negligible surface roughness. This work also includes the development of ambient pressure X-ray photoelectron spectroscopy (APXPS) for studying the chemistry and surface interactions in hydrated polymer surfaces. First, the presence or lack of hydrogen bonding in marine antifouling coatings is found to alter both the polymer's interactions with water and with soft algal foulers. Afterwards, the capability of

side chains to present at the surface and modify polymer hydrophilicity is investigated using APXPS. Finally, the effects of functional group chemistry on the adsorption of small organic molecules are explored in APXPS experiments on model SAM surfaces. The findings of this work indicate that polymer surface chemistry can be modulated by minor changes in composition, and that these changes can have large effects on surface interactions with water, organic molecules, and organisms.

TABLE OF CONTENTS

Chapter 1
Introduction

Polymers are commonly used in applications that entail long-term exposure to water and aqueous mixtures. Two of these applications are of particular interest for the energy and environmental sectors and share many of the same design challenges. The first, marine antifouling coatings, prevents the adhesion of marine organisms and biomolecules on the surfaces of ships and other marine structures that would otherwise severely increase fuel consumption[1] and provide a platform for the spread of invasive species. The second, water purification membranes, requires polymers that allow for selective transport of water or certain solutes through the membrane. Here fouling is a similarly strong concern, as the total flux through the polymer membrane decreases dramatically when the surface is blocked by layers of salt or organic molecules.

In both of these applications, the polymer surface is exposed to a complex aqueous mixture containing both ionic and organic solutes. Our fundamental understanding of the ways that polymer surfaces interact with water and with solutes is limited, however, leaving researchers to leverage a largely empirical approach that depends upon comparisons of chemically distinct coating or membrane materials. The outcomes of these comparisons inform, sometimes unpredictably, the design and development of novel materials.

Systematic research would be dramatically improved by understanding the relationship between surface chemistry and the resulting interactions that determine membrane success and failure. The present work introduces a two-pronged approach to this challenge (1) by the use of sequence-defined materials for marine antifouling applications and (2) by developing ambient pressure X-ray photoelectron spectroscopy (APXPS) as a tool for characterizing polymer surfaces.

1.1 Polymers in underwater applications

1.1.1 Marine antifouling coatings

Marine fouling, or the undesirable deposition of marine organisms, is a problem that affects all ocean-going vessels and begins nearly immediately upon immersion. Over four thousand different species are known to colonize and foul manmade oceanic structures that range from the microscopic (e.g., bacteria and diatoms) to macroscopic (e.g. mussels, algae).[2,3] These organisms, when attached, roughen the hulls of ships, reducing hydrodynamic efficiency and dramatically increasing the cost of transport: effective antifouling coatings would be predicted to save $150 billion USD worldwide every year.[1,4] Furthermore, fouled ships contribute to the expansion of non-native species, as has been observed with the marine mussel *Mytella strigata* in southeast Asia.[5,6] While biocidal coatings containing tributyltin and cuprous oxide have historically been used to prevent adhesion, their accumulation in the ocean poses a risk to other marine life. Increasingly strict regulations (use of tributyltin has already been banned worldwide) and environmental impacts make the search for alternative coating technologies increasingly urgent.[7]

Non-toxic marine antifouling coatings represent an environmentally benign solution to adhesion by reducing attachment with no harmful effects on the organisms. These coatings typically follow two distinctive pathways to prevent permanent adhesion. Antifouling coatings completely prevent the settlement and growth of marine organisms by preferentially interacting with water at the surface. The majority of these coatings are made from various hydrophilic polymers including poly(ethylene oxide) (PEO), zwitterionic polymers, polyvinyl alcohol, polysaccharides, and hydrogels.[3,8] Conversely, fouling release coatings permit adhesion to the surface, but have a low surface energy that minimizes attachment strength and allows movement through water to shear off adhered organisms. Most fouling release coatings are made from polydimethylsiloxane (PDMS) or fluoropolymers.[8–10]

Because marine species have independently evolved unique mechanisms to attach to surfaces, development of a universally antifouling coating has been remarkably difficult. Amphiphilic materials that incorporate both hydrophilic and hydrophobic chemistries are currently heavily studied in the hopes of designing coatings with both antifouling and fouling release capabilities. These coatings form heterogeneous surfaces with domains on the micro- or nano-scale that prevent organisms from finding a suitable, sufficiently large surface for attachment.[9,11] To date, fluorinated, PDMS, and PEG-based chemistries are among the most prevalent in amphiphilic coatings.[12–14] For instance, fluorinated side chain chemistries incorporated into PEO-based block copolymers reduced settlement and enhanced release of *Ulva* algae, which are known to adhere well to hydrophilic polymers.[15] PDMS copolymers containing PEGylated-fluoroalkyl modified polystyrene or acrylate blocks demonstrated improved algal fouling release of *Ulva*,[16] as well as reduced barnacle

settlement (*Balanus amphitrite*) and fouling upon immersion.[17] Incorporation of PEO-siloxane amphiphiles into crosslinked siloxane coatings has been shown to improve coating performance against bacteria and diatoms, as well as reduce microfouling on samples submersed in the Atlantic Ocean for up to twenty weeks.[18] Crosslinked siloxane-polyurethanes with PEG co-macromers similarly resist diatom, algae, and barnacle adhesion.[19]

1.1.2 Water purification membranes

Maintaining and expanding worldwide access to clean water has become recognized as one of the most significant challenges in the upcoming years, made difficult by the limited amount of relatively clean water sources.[20–22] Water purification membranes consist of a thin, often polymeric, interphase separating adjacent aqueous phases. These display selective permeability between the aqueous phases by either size-exclusion, electrostatic, or solute–membrane interactions and therefore serve as energy-efficient candidates (versus thermally based mechanisms) for water treatment.[23,24] Today, various polymer membranes are used for water purification and energy applications including reverse osmosis, microfiltration and ultrafiltration, electrodialysis, photoelectrochemical cells and fuel cells, but are inadequate for purification of highly impaired water that contains large amounts of organic or saline contaminants.[25,26] Current membranes have low selectivity for many neutral contaminants, such as boron,[27] are poor at discriminating among ions of the same valence,[27] are limited by fouling,[28–30] and must also balance the permeability–selectivity trade-off.[22,31] As water supplies expand to highly complex, non-traditional water sources, significant technological advances are needed in order for

membranes to sufficiently improve fresh water production, resource recovery, and energy generation.[22,27,32]

Improvement of purification membranes is hindered by the glaring gaps in current understanding of the processes that govern passage of water and solutes through membranes at the molecular level.[22] As noted before, a major challenge limiting further adoption of membranes for water purification is the tradeoff between permeability (i.e., how fast molecules pass through a membrane) and selectivity (i.e., the extent to which desirable solutes are separated from the rest).[27,33] In addition, fouling of membrane surfaces and the interior of membrane pores by solutes reduces water flux, decreases permeate water quality, and increases energy consumption.[22,34] Both of these challenges are inherently affected by the surface chemistry of the membrane–water interface. A fundamental understanding of the surface interactions with solutes and water in such materials, especially the influence of polymer chemistry on these interactions, is crucial for developing next-generation membranes with improved properties.

Surface modification of polymer membranes has been crucial for preventing fouling on membranes during operation, as hydrophobic materials that are useful for maintaining membrane structural integrity in hydrated conditions tend to experience severe fouling.[22,32] Surface modifying macromolecules have thus been heavily studied for improving flux during operation and are already developed by commercial sources.[32,35,36] Copolymerization with PEO end blocks or side chains, for instance, has been shown to improve fouling resistance and flux for polysulfone membranes (PSf),[37] poly(ether sulfone) (PES),[38] and polymethacrylate/poly(vinylidene fluoride) blends[39] and during operation. Similarly, modification of poly(vinylidene fluoride) membranes with poly(methacrylic

acid) and poly(oxyethylene methacrylate) side chains was found to reduce protein adhesion.[40] In addition to incorporation of hydrophilic polymers, low surface energy fluorinated chemistries have been investigated. Incorporation of fluorinated macromolecules into PES membranes suggested improved fouling resistance by their ability to maintain higher flux in oil/water emulsions.[41] Other approaches include coupling small molecules such as zwitterions[42] sulfonation to hydrophobic polymers,[43,44] interfacial or layer-by-layer polymerization of polyamide monomers on the membrane surface,[45,46] plasma treatment,[47–49] and modification with polydopamine.[50–52]

1.2 Controlled chemistries for improving materials design

In both marine antifouling and water purification, polymer surfaces have been explored extensively to mitigate fouling, and do so by directing interactions with water, dispersed solutes, and larger biomolecular structures. The chemistry of polymer surfaces is understood to directly affect overall hydrophilicity but modelling further predicts that the nanoscale spacing of these moieties modulates hydration water dynamics and water mobility.[53] Polymers containing sequence-defined side chains can provide fine control over both chemistry and the relative spacing between functional groups, and are therefore excellent model systems for understanding the interactions at polymer–aqueous interfaces (**Figure 1-1**).

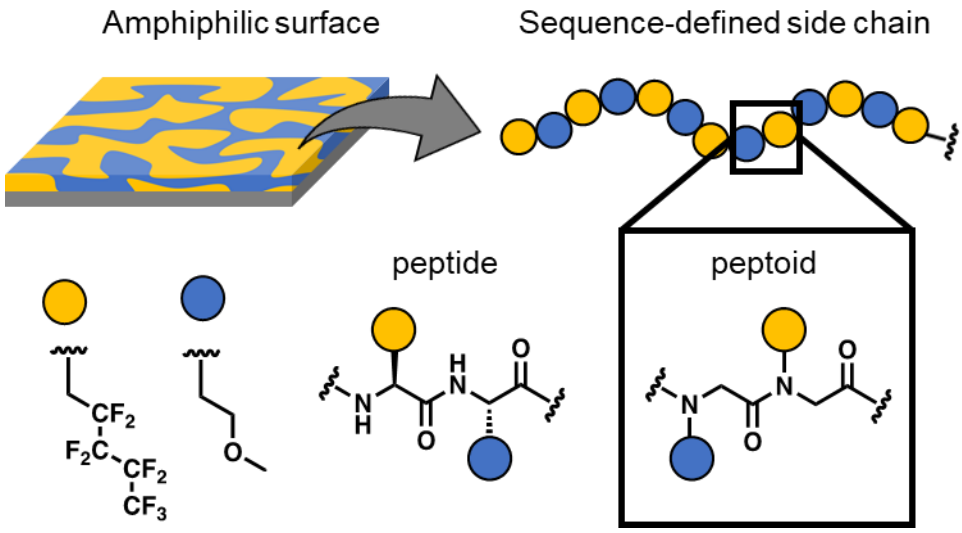

Figure 1-1. Amphiphilic surfaces can be created by incorporating sequence-defined chemistries such as peptides or biomimetic peptoids as side chains.

One method for providing molecular-scale patterning in a polymer is via incorporation of sequence-defined peptidomimetic *N*-substituted glycine oligomers, or peptoids. Peptoids enable control of monomer type in defined sequences along the chain through an iterative synthesis of sub-monomer units.[54,55] Because the formation of the amide group in each peptoid monomer is divided into two reactions, virtually any primary amine can be incorporated into the chain, with a higher yield per reaction that allows for increased (gram-scale) batch size and polymeric chain lengths compared to peptide synthesis. Furthermore, *N*-substitution in peptoids results in a tertiary amide that inherently lacks hydrogen bond donors, enabling finer control over the functionalities present in the final material. Consequently, peptoids are suitable materials for understanding the role of surface chemistry and distribution in applications such as marine antifouling and water purification.

While peptoids provide excellent scale for controlling monomer chemistry and order on a polymer surface, control over spatial distribution of functional groups is still limited and the presented surface is chemically complex. For fundamental inquiries requiring simple surfaces, self-assembled monolayers (SAMs) are advantageous. These densely packed monomolecular layers are formed by the adsorption and spontaneous assembly of organic molecules, and which enable study of singular functional group chemistries on a flat, homogeneous surface.[56,57] These molecules contain a head group that presents at the outer surface, a (typically alkyl) backbone of oligomer size, and a reactive linker that binds to a metal substrate. Several distinctive classes of SAM molecular chemistries have been formed. The most prevalent consist of thiols linked to gold or other oxide-free metals, or silanes bound to hydroxylated surfaces such as silica. Phosphonates, fatty acids, peptides, peptoids, and many others have also been used to form self-assembled monolayer chemistries.[58]

Surfaces formed with peptoids or SAMs are particularly useful for relating chemistry to interfacial interactions, which determine the ultimate success or failure of marine antifouling coatings and membranes. Intermolecular forces that govern macromolecule interaction, including London dispersion forces,[59] dipole-dipole interactions, and hydrogen bonding, heavily shape adsorption of both solutes and marine fouling organisms. Dispersion forces resulting from temporary dipole fluctuations can occur between all molecules, but are low in magnitude.[59] Similar interactions can occur between molecules that have permanent dipoles, where the atoms in the molecule differ locally in electron density due to the non-uniform sharing of electrons dependent on each atom’s electronegativity. Atoms in these molecules have permanent partial charges can

interact with oppositely charged atoms in other molecules or with atoms having temporary dipoles. These interactions are stronger than London dispersion forces, but require polar bonds that distribute electrons between the atoms unequally.

However, hydrogen bonding likely has the greatest impact on marine fouling organisms due to the role played by proteins in the adhesion process. Though the magnitude of this interaction is only on the order of a tenth of that of a covalent bond, hydrogen bonds are recognized to have great impacts on cohesive properties of materials, causing deviations in melting temperature, density, and even enabling the secondary structure used by biological systems.[60] Hydrogen bonding very strongly affects adhesive strength in biologically-sourced materials. Amide groups, as found in proteins, contain both a hydrogen bond donor (in the nitrogen-linked hydrogen) and hydrogen bond acceptor (in the carbonyl oxygen). The oxygen in ether and ester groups can act as hydrogen bond acceptors, but cannot engage in hydrogen bonding without a donor. Marine fouling organisms are known to depend on proteins with large numbers of hydrogen bond donors, particularly polyphenols, in adhesive plaques.[61] Polymers containing these and other hydrogen-bonding groups have already been designed for adhesive and self-healing applications,[62,63] but ongoing research is still investigating appropriate materials to prevent attachment of these chemistries for marine antifouling and membrane applications.

1.3 Surface characterization of membranes and underwater coatings

Investigation of interfacial intermolecular interactions, such as those between water molecules and a surface, requires the use of *in situ* characterization methods. Because

polymer surfaces are capable of restructuring between dry and aqueous conditions, *in situ* methods are also necessary for evaluating the surface chemistry in conditions similar to membrane or marine antifouling coating operation. Contact angle goniometry has traditionally been used to characterize the hydrophilicity and restructuring of polymer surfaces in response to water conditions, but is limited to qualifying surface energy. Spectroscopic and microscopic characterization of surfaces *in situ* and *in operando* has advanced significantly in the last few decades,[64] and greatly improved our ability to probe polymer surfaces under aqueous conditions.

Modern microscopy methods have become especially useful for characterizing water–surface interactions and topography, with sub-molecular spatial resolution.[65] Underwater atomic force microscopy (AFM) is commonly used to investigate the topography of hydrated polymer materials,[66] as well as the effects of secondary conditions such as temperature[67] and pH[68] on the surface. Interactions between the surface and an AFM cantilever tip, such a bubble probe, allow for quantification of hydrophobic interactions[69,70] and hydrogen bonding[71] in aqueous media. Scanning tunneling microscopy (STM) has also been used to understand aggregation of nucleic acid polymers underwater.[72,73] Both STM and AFM enable observation of one- and two-dimensional water hydrogen bonding structures on simple surfaces,[74–76] hinting at further potential for characterization of water–polymer interfaces.

Vibrational spectroscopy has also become an essential tool for understanding chemistry-specific interactions underwater. This group of techniques measures the vibrational energy of chemical bonds, where both the position and relative intensity of spectral features provide insight on chemistry and interactions. While Raman, infrared (IR),

attenuated total reflection (ATR) IR, and THz absorption have been useful for characterizing water at interfaces,[65] sum-frequency generation (SFG) spectroscopy is particularly advantageous for characterizing the surface's chemistry and its interactions with water and solutes. In contrast to IR and Raman that inherently derive signal from bulk as well as interfacial species, SFG vibrational spectroscopy probes molecular vibrations that take place exclusively at the interface (**Figure 1-2**). Specifically, resonant IR light excites particular vibrational modes that are then further interact with non-resonant visible light pulse in an anti-Stokes scattering process. Light is then released with a frequency equivalent to the sum of the visible and IR pulses and with a phase dependent on molecule orientation (and therefore sensitive to the surface over disorganized bulk).

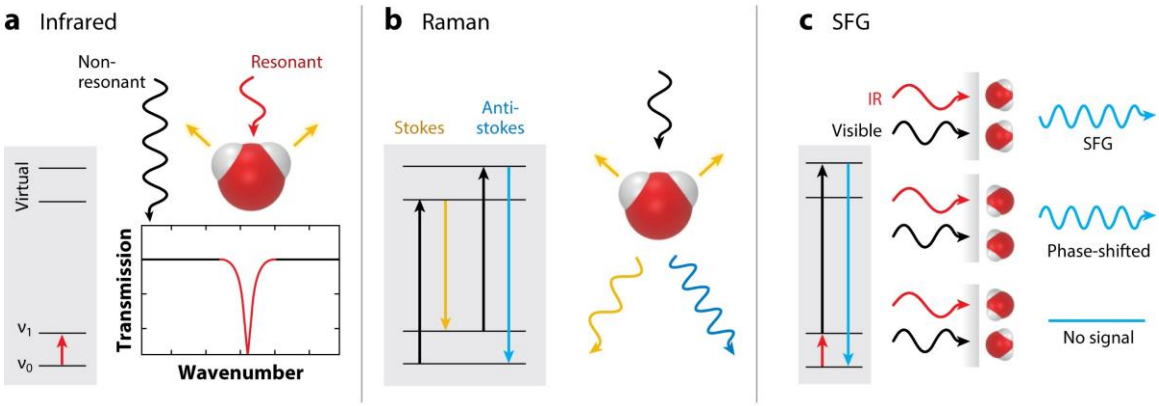

Figure 1-2. Sum-frequency generation (SFG) spectra result from the combination of infrared (IR) and Raman processes. Briefly, (a) IR operates by absorption of radiation corresponding to bond vibrational energies, whereas (b) Raman spectra result from inelastic scattering (41). Together, IR and Raman yield a summed frequency wave with a phase dependent on the exact orientations of interfacial water (c). Disordered water at the surface does not induce signal owing to destructive interference. (Adapted from Ref. 64 with permission from Annual Reviews Chemical and Biomolecular Engineering.)

Like IR, SFG vibrational spectroscopy distinguishes bond vibrational energies of surface species. It is also capable of detecting interfacial water alignment and orientation, as well as the degree of hydrogen bonding, via the position and intensity of the OH

stretch.[77,78] Because SFG vibrational spectroscopy is compatible with measurements ranging from ambient air to aqueous solutions, it has been used for identifying restructuring in a wide array of polymers.[78] Understandably, polymer restructuring was found to vary among different surfaces, ranging from no response to changes in side chain orientation to large scale backbone restructuring. The polymer surface is complementarily capable of affecting surface water orientation as seen in SFG and Raman spectroscopy: water molecules are known to orient differently around hydrophobic surfaces versus hydrophilic ones,[79] while polyampholytes with balanced ratios of positively and negatively charged monomers showed minimized disruption of bulk water orientations.[80–82] This was seen to correlate with reduced fouling by proteins and cells, suggesting biocompatibility and fouling resistance are heavily influenced by perturbations of water structure.[80]

These techniques, while all useful, would benefit from pairing with a quantitative characterization of polymer surface chemistry. However, traditional electron-detecting spectroscopies such as X-ray photoelectron spectroscopy (XPS), Auger electron spectroscopy (AES), and near edge X-ray absorption fine structure (NEXAFS) require the use of high vacuum environments.[83] As demonstrated by SFG, investigation of polymer surface chemistry for hydrated conditions must be done *in situ*. Ambient pressure XPS allows for characterization of surfaces in hydrated conditions, making it particularly appealing as a complementary technique for understanding the surface chemistry and the way it changes underwater as well as quantifying affinity for water in terms of sorption.

1.4 Ambient Pressure XPS for characterizing surface chemistry *in situ*

1.4.1 Fundamentals of ambient pressure X-ray photoelectron spectroscopy

XPS is a standard surface-sensitive chemical analysis technique primarily employed to identify quantitative atomic surface concentration of solid materials. In this technique, X-rays are used to excite and eject electrons in nonbinding core levels of an atom in a process known as the photoelectric effect.[84] By detecting the kinetic energy of these ejected photoelectrons (using a hemispherical analyzer), the binding energy can be found according to energy conservation. Specifically, the electron binding energy (E_b) is equivalent to the difference between the total photon energy ($h\nu$) and the measured kinetic energy (E_k) with the work function of the particular electron analyzer (ϕ).[85]

$$E_b = h\nu - E_k - \phi \qquad \text{(Eqn 1.1)}$$

The binding energy of an electron is mostly affected by the quantum state of the atomic orbital from which it comes (e.g., 1s, 2s, etc.) but is also affected by minute changes in chemical environment imposed by interatomic bonding. These shifts allow XPS to elucidate a more detailed description of surface presentation beyond simple atomic composition, making it especially useful.

Because photoelectrons are detected in XPS, their probability of reaching the detector after emission simultaneously provides XPS with its surface sensitivity and necessitates measurement under vacuum conditions. While X-rays penetrate far further into the sample (typically 0.1-10 μm depending on photon energy),[86] the attenuation of photoelectrons in a solid material limits electron escape out from the surface. This phenomenon is often referenced in terms of the inelastic mean free path (IMFP), which

describes the average distance that electrons travel before losing energy from interactions with matter. The IMFP of photoelectrons through solid material is on the order of nanometers, largely determined by the chemistry of the material with some further dependence on the electron's kinetic energy. Bulk photoelectrons thus provide a negligible portion of XPS signal, and most detected electrons come from the top few nanometers of the surface.[84] However, the presence of a gas or vapor atmosphere would still rapidly attenuate signal; water vapor at only 1 Torr limits photoelectrons (E_k = 100 eV) to an IMFP of ~1 mm.[87,88] Consequently, XPS systems are traditionally run at ultrahigh vacuum (UHV; $<10^{-7}$ Torr).[83]

However, great demand for measurements under *in situ* or *operando* conditions prompted the development of ambient pressure X-ray photoelectron spectroscopy (APXPS).[64,89] This technique allows for *in situ* surface chemistry measurements with vapor or gas phase present, and addresses two fundamental challenges. APXPS systems overcome the limited IMFP of photoelectrons by leveraging a differential pumping system between the analysis chamber and analyzer (**Figure 1-3**).[90] Ejected electrons travel ~100 μm through ambient conditions before passing through a conical aperture into a series of chambers each with rapidly reduced pressure (and therefore vastly increase the IMFP).[87] Electrons eventually reach the analyzer at ultrahigh vacuum conditions. The use of differential pumping introduces a secondary technical concern: electrostatic lenses are required to focus photoelectrons through the apertures connecting the different stages. These must be spaced appropriately (i.e., have sufficiently sized gaps between elements) and lens tables must be used to limit electric potential differences in order to avoid large electric field gradients that cause gas discharging.[87]

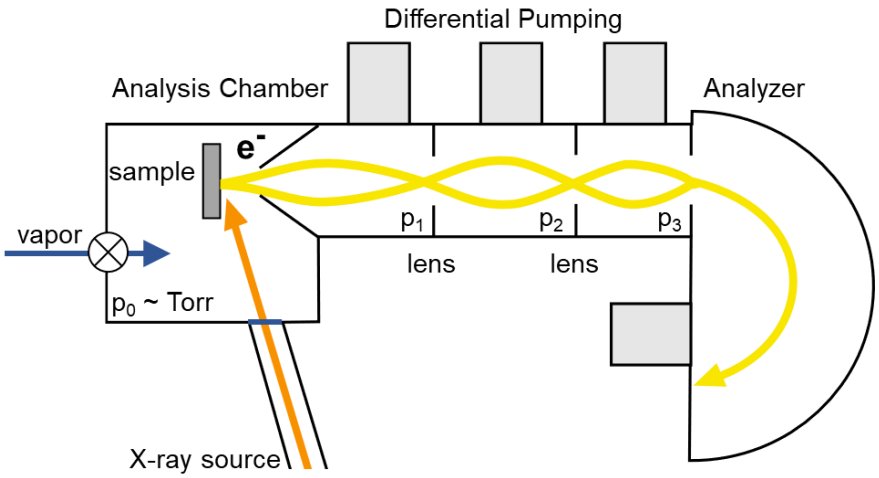

Figure 1-3. Differential pumping in APXPS allows the sample chamber to be maintained at higher pressures while electrons pass (guided by lenses) through multiple apertures with reduced pressures, until reaching the analyzer at ultrahigh vacuum conditions.

While the first laboratory APXPS units were built in the 1970s, synchrotron X-ray sources are particularly ideal for APXPS due to the high flux that minimizes the effects of attenuation by gas.[90] These sources also enable exposure to X-rays with tunable photon energy, which is useful for depth profiling experiments. Energy conservation (**Eqn 1.1**) stipulates that changing photon energy ($h\nu$) proportionally affects kinetic energy. X-rays with higher photon energies, for instance, increase the kinetic energy of photoelectrons and their inelastic mean free path, allowing for escape from deeper within the surface. Synchrotron APXPS allows for control over the measurement depth unparalleled by laboratory XPS, which use either Al K_α or Mg K_α as the X-ray source to produce photons at 1486.7 or 1253.7 eV, respectively. For laboratory XPS, a photoelectron's kinetic energy depends on the atomic core level (e.g. O 1s) from which it came, where higher binding energies result in electrons with lower kinetic energy that can only escape closer to the surface. Synchrotron APXPS systems enable alteration of X-ray photon energy to match photoelectron kinetic energy across all core levels, allowing the same depth to be sampled

regardless of the photoelectron's original electronic environment. Depth probing can also be performed by decreasing or increasing the photon energy of incoming X-rays to sample nearer or further from the surface, respectively. Soft X-ray APXPS ($h\nu < 2$ keV) is typically used to investigate the top few nanometers of surface in pressures up to 2-3 Torr,[91] while use of tender X-rays (2-10 keV) enables probing under fully hydrated conditions and through a solid-liquid interface, penetrating on the order of tens of nanometers into the film.[92] Synchrotron APXPS is thus convenient for measuring polymer surface chemistry over depths from ~1-30 nm and under tunable conditions from ultrahigh vacuum to 100% humidity at room temperature (20 Torr water vapor).

1.4.2 APXPS for polymer materials

Interactions with water critically affect polymer performance in underwater applications by influencing surface properties in the hydrated state and by forming a nanometers-thick hydration layer that mediates interactions with solutes.[93] Polymer coatings that are studied *ex situ* in XPS show surface chemistry that may not be representative of the interface present underwater. APXPS, by providing information on atomic concentration in water vapor pressures up to 20 Torr (100% humidity at room temperature) allows for an accurate understanding of polymer surface chemistry in relevant conditions. APXPS also enables fine control over the pressure in the analysis chamber to facilitate observation of restructuring. Depth profiling is also particularly useful for understanding polymer materials and their restructuring, as the relative changes in atomic composition can be used to formulate a representative model of the surface in the (surface-normal) z-direction.

In addition to determining water's effects on polymer surface chemistry, APXPS is useful for identifying and quantifying interactions between water and the surface. Amounts of adsorbed water can be determined quantitatively and thereafter serve as a metric for comparing atomic-level hydrophilicity. Chemical shifts in the O 1s core level can further elucidate the state in which water interacts with the surface: for many metal surfaces, adsorption is mediated first by chemical hydroxylation of the surface. These sites form strong hydrogen-bonding environments that then facilitate molecular water adsorption.[94] However, organic materials participate in molecular adsorption of water that is fully reversible, as demonstrated in an APXPS study comparing the hydrophilicity of organic functional groups on simple self-assembled monolayers (SAMs).[95] In this work, the amount of water that adsorbed to these materials varied depending on the hydrophilicity of the monolayer head groups; while the methyl-terminated SAM showed no water adsorption up to 1 Torr, alcohol- and carboxylic acid-terminated SAMs formed partial multilayer water films. The presence of hydrogen bonding sites for water at these two functional groups are presumed to be responsible for this adsorption, emphasizing the importance of chemical functionalities in membrane design. This has held true for measurements taken of polymeric thin films derived from poly(styrene sulfonate) and related polymers, which showed a dependence on both the types of secondary interactions experienced by the polymer and the counterion identity for the sulfonated polymers.[91] However, these materials were seen to experience water sorption: probing different depths had no effect on measured water content, and polymers are known to sorb water based on the thermodynamic mixing favorability.[96,97] APXPS of polymer materials can provide a useful comparison of chemical functionalities and their specific interactions with surface water,

and these quantitative predictions of water affinity enable more well-informed polymer materials design.

1.4.3 APXPS for water purification membranes

As water treatment processes are tuned to address more complex waters, interactions at solute–membrane interfaces that drive desired (water transport, contaminant rejection) and undesired (fouling) interactions must be understood to tailor future design. XPS has largely been used to understand fouling chemistry *ex situ*, limiting the information on direct functional group interactions that trigger undesirable adsorption. APXPS also shows significant potential for characterizing solute–solute, solute–membrane, and solute–water interactions on membrane interfaces and elucidating of fouling mechanisms. Fundamentally, small molecule solutes can be introduced in the vapor phase as a method of identifying solute affinity for the surface, both with and without water present.

Experiments have already been performed in environmental science that investigate affinity of organic molecules onto ice. Recently, specialized APXPS methods employed at synchrotron facilities have already been applied to explore the chemistry of electrochemically-controlled interfaces between solids and liquids.[92] Liquid cell designs for XPS measurements have incorporated Nafion membranes to separate the high pressure cell from the XPS chamber and to simultaneously serve as electrolyte. While this allowed oxygen evolution at an anode to be tracked, the membranes themselves were not further characterized.[98,99] These liquid cell designs could be leveraged to probe *in situ* solute transport through Nafion and other electropotential-based membrane systems used in water treatment (e.g., ion exchange membranes used in electrodialysis). APXPS is also useful for monitoring the electrical potentials that develop on surfaces, such as the electric double

layer.[100] Although the structural and chemical complexity of membrane–water interfaces makes these analyses more difficult, APXPS could be leveraged to measure potential development at the membrane–solution interface that would explain the partial exclusion of co-ions from absorbing into charged polymers. In turn, these experimental findings could be applied to the development of models that more accurately predict ion partitioning, among other transport properties, in ion exchange membranes.

1.5 Motivations and dissertation scope

Polymer surfaces are prevalent in underwater applications ranging from water filtration membranes to marine antifouling coatings. For each application, the ability of the surface to elicit appropriate responses from dissolved solutes, biomolecules, and larger particles and organisms determines the success of the final material. Historically, empirical results derived from chemically distinctive coatings and membranes have been used to guide the fields.[25,101] In order to improve the rate of advancement, design rules are essential but difficult to ascertain from polymers with larger degrees of dispersity. Leveraging sequence-defined materials enables control over both chemistry and molecular-scale spacing that has been shown to significantly impact interactions with water and marine organisms.[102–104] The ease of synthesis and diversity of chemical functionalities for polypeptoids makes them particularly desirable,[54] while incorporation into block copolymers makes polypeptoids feasible for larger-scale testing without compromising the impact of sequence control. Self-assembled monolayers also are useful for creating well-ordered surfaces required for highly controlled experiments. These densely packed

monomolecular layers enable study of singular functional group chemistries with negligible surface roughness.

In addition to creating sequence-controlled, highly tunable surfaces, advances in understanding the underwater polymer interface are essential. While much progress has been made in recent years, relatively few techniques provide chemical information on polymer surfaces in underwater conditions. Ambient pressure XPS (APXPS) presents the opportunity to gather quantitative information on both surface chemistry and water interactions in terms of adsorption and sorption. Furthermore, synchrotron radiation sources can provide depth profiling of polymer materials in both dry and hydrated conditions. This technique has primarily been used to study well-ordered inorganic surfaces, but investigation of organic and polymeric surfaces is becoming more prevalent.[91,105,106]

This thesis describes the creation and study of tunable water–polymer interfaces by pairing sequence-defined materials and controlled self-assembled monolayer surfaces with ambient pressure X-ray photoelectron spectroscopy (APXPS) and other surface-sensitive techniques. Combined, the ability to control the chemistries present at the surface and quantitatively characterize them presents an opportunity for development of essential design rules for applications such as marine antifouling and water purification membranes.

1.6 Permissions

Parts of this dissertation were reproduced in part with permissions from:

(1) Barry, M. E.; Davidson, E. C.; Zhang, C.; Patterson, A. L.; Yu, B.; Leonardi, A. K.; Duzen, N.; Malaviya, K.; Clarke, J. L.; Finlay, J. A.; Clare, A. S.; Chen, Z.; Ober, C. K.; Segalman, R. A. The role of hydrogen bonding in peptoid-based marine antifouling coatings. *Macromolecules* **2019**, 52 (3), 1287-1295.

(2) Barry, M. E.; Landsman, M. R.; Nomaan, S. M.; Aydogan Gokturk, P.; Cooper, C. M.; Kienzle, B. A., McKay, C.; L. E. Katz. Expanding the Use of Synchrotron Techniques for Water Treatment: From Minerals to Membranes. *Synchrotron Radiation News* **2020**, 33 (4), 3-12.

(3) Barry, M. E.; Gokturk, P. A.; DeStefano, A. J.; van Zoelen, W.; Leonardi, A. K.; Crumlin, A. J.; Segalman, R. A. Effects of amphiphilic polypeptoid side chains on hydrated polymer surface chemistry and hydrophilicity. *In preparation.*

1.7 References

(1) Schultz, M. P. Effects of Coating Roughness and Biofouling on Ship Resistance and Powering. *Biofouling* **2007**, *23* (5), 331–341. https://doi.org/10.1080/08927010701461974.

(2) Gu, Y.; Yu, L.; Mou, J.; Wu, D.; Xu, M.; Zhou, P.; Ren, Y. Research Strategies to Develop Environmentally Friendly Marine Antifouling Coatings. *Mar. Drugs* **2020**, *18* (7), 371. https://doi.org/10.3390/md18070371.

(3) Buskens, P.; Wouters, M.; Rentrop, C.; Vroon, Z. A Brief Review of Environmentally Benign Antifouling and Foul-Release Coatings for Marine Applications. *J. Coat. Technol. Res.* **2013**, *10* (1), 29–36. https://doi.org/10.1007/s11998-012-9456-0.

(4) Hellio, C.; Yebra, D. M. 1 - Introduction. In *Advances in Marine Antifouling Coatings and Technologies*; Hellio, C., Yebra, D., Eds.; Woodhead Publishing Series in Metals and Surface Engineering; Woodhead Publishing, 2009; pp 1–15. https://doi.org/10.1533/9781845696313.1.

(5) Lim, J. Y.; Tay, T. S.; Lim, C. S.; Lee, S. S. C.; Teo, S. L.-M.; Tan, K. S. Mytella Strigata (Bivalvia: Mytilidae): An Alien Mussel Recently Introduced to Singapore and Spreading Rapidly. *Molluscan Res.* **2018**, *38* (3), 170–186. https://doi.org/10.1080/13235818.2018.1423858.

(6) Sanpanich, K.; Wells, F. Mytella Strigata (Hanley, 1843) Emerging as an Invasive Marine Threat in Southeast Asia. *BioInvasions Rec.* **2019**, *8*. https://doi.org/10.3391/bir.2019.8.2.16.

(7) Gipperth, L. The Legal Design of the International and European Union Ban on Tributyltin Antifouling Paint: Direct and Indirect Effects. *J. Environ. Manage.* **2009**, *90*, S86–S95. https://doi.org/10.1016/j.jenvman.2008.08.013.

(8) Yang, W. J.; Neoh, K.-G.; Kang, E.-T.; Teo, S. L.-M.; Rittschof, D. Polymer Brush Coatings for Combating Marine Biofouling. *Prog. Polym. Sci.* **2014**, *39* (5), 1017–1042. https://doi.org/10.1016/j.progpolymsci.2014.02.002.

(9) Leonardi, A. K.; Ober, C. K. Polymer-Based Marine Antifouling and Fouling Release Surfaces: Strategies for Synthesis and Modification. *Annu. Rev. Chem. Biomol. Eng.* **2019**, *10* (1), 241–264. https://doi.org/10.1146/annurev-chembioeng-060718-030401.

(10) Lejars, M.; Margaillan, A.; Bressy, C. Fouling Release Coatings: A Nontoxic Alternative to Biocidal Antifouling Coatings. *Chem. Rev.* **2012**, *112* (8), 4347–4390. https://doi.org/10.1021/cr200350v.

(11) Gudipati, C. S.; Finlay, J. A.; Callow, J. A.; Callow, M. E.; Wooley, K. L. The Antifouling and Fouling-Release Perfomance of Hyperbranched Fluoropolymer (HBFP)−Poly(Ethylene Glycol) (PEG) Composite Coatings Evaluated by Adsorption of Biomacromolecules and the Green Fouling Alga Ulva. *Langmuir* **2005**, *21* (7), 3044–3053. https://doi.org/10.1021/la048015o.

(12) Sundaram, H. S.; Cho, Y.; Dimitriou, M. D.; Weinman, C. J.; Finlay, J. A.; Cone, G.; Callow, M. E.; Callow, J. A.; Kramer, E. J.; Ober, C. K. Fluorine-Free Mixed Amphiphilic Polymers Based on PDMS and PEG Side Chains for Fouling Release Applications. *Biofouling* **2011**, *27* (6), 589–602. https://doi.org/10.1080/08927014.2011.587662.

(13) Ma, W.; Rajabzadeh, S.; Shaikh, A. R.; Kakihana, Y.; Sun, Y.; Matsuyama, H. Effect of Type of Poly(Ethylene Glycol) (PEG) Based Amphiphilic Copolymer on Antifouling Properties of Copolymer/Poly(Vinylidene Fluoride) (PVDF) Blend

Membranes. *J. Membr. Sci.* **2016**, *514*, 429–439. https://doi.org/10.1016/j.memsci.2016.05.021.

(14) Quiñones-Pérez, M.; Cieza, R. J.; Ngo, B. K. D.; Grunlan, M. A.; Domenech, M. Amphiphilic Silicones to Reduce the Absorption of Small Hydrophobic Molecules. *Acta Biomater.* **2021**, *121*, 339–348. https://doi.org/10.1016/j.actbio.2020.11.041.

(15) Dimitriou, M. D.; Zhou, Z.; Yoo, H.-S.; Killops, K. L.; Finlay, J. A.; Cone, G.; Sundaram, H. S.; Lynd, N. A.; Barteau, K. P.; Campos, L. M.; Fischer, D. A.; Callow, M. E.; Callow, J. A.; Ober, C. K.; Hawker, C. J.; Kramer, E. J. A General Approach to Controlling the Surface Composition of Poly(Ethylene Oxide)-Based Block Copolymers for Antifouling Coatings. *Langmuir* **2011**, *27* (22), 13762–13772. https://doi.org/10.1021/la202509m.

(16) Martinelli, E.; Suffredini, M.; Galli, G.; Glisenti, A.; Pettitt, M. E.; Callow, M. E.; Callow, J. A.; Williams, D.; Lyall, G. Amphiphilic Block Copolymer/Poly(Dimethylsiloxane) (PDMS) Blends and Nanocomposites for Improved Fouling-Release. *Biofouling* **2011**, *27* (5), 529–541. https://doi.org/10.1080/08927014.2011.584972.

(17) Martinelli, E.; Sarvothaman, M. K.; Galli, G.; Pettitt, M. E.; Callow, M. E.; Callow, J. A.; Conlan, S. L.; Clare, A. S.; Sugiharto, A. B.; Davies, C.; Williams, D. Poly(Dimethyl Siloxane) (PDMS) Network Blends of Amphiphilic Acrylic Copolymers with Poly(Ethylene Glycol)-Fluoroalkyl Side Chains for Fouling-Release Coatings. II. Laboratory Assays and Field Immersion Trials. *Biofouling* **2012**, *28* (6), 571–582. https://doi.org/10.1080/08927014.2012.697897.

(18) Faÿ, F.; Hawkins, M. L.; Réhel, K.; Grunlan, M. A.; Linossier, I. Non-Toxic, Anti-Fouling Silicones with Variable PEO–Silane Amphiphile Content. *Green Mater.* **2016**, *4* (2), 53–62. https://doi.org/10.1680/jgrma.16.00003.

(19) Galhenage, T. P.; Webster, D. C.; Moreira, A. M. S.; Burgett, R. J.; Stafslien, S. J.; Vanderwal, L.; Finlay, J. A.; Franco, S. C.; Clare, A. S. Poly(Ethylene) Glycol-Modified, Amphiphilic, Siloxane–Polyurethane Coatings and Their Performance as Fouling-Release Surfaces. *J. Coat. Technol. Res.* **2017**, *14* (2), 307–322. https://doi.org/10.1007/s11998-016-9862-9.

(20) Tortajada, C.; Biswas, A. K. Achieving Universal Access to Clean Water and Sanitation in an Era of Water Scarcity: Strengthening Contributions from Academia. *Curr. Opin. Environ. Sustain.* **2018**, *34*, 21–25. https://doi.org/10.1016/j.cosust.2018.08.001.

(21) Smalley, R. E. Future Global Energy Prosperity: The Terawatt Challenge. *MRS Bull.* **2005**, *30* (6), 412–417. https://doi.org/10.1557/mrs2005.124.

(22) Landsman, M. R.; Sujanani, R.; Brodfuehrer, S. H.; Cooper, C. M.; Darr, A. G.; Justin Davis, R.; Kim, K.; Kum, S.; Nalley, L. K.; Nomaan, S. M.; Oden, C. P.; Paspureddi, A.; Reimund, K. K.; Rowles, L. S.; Yeo, S.; Lawler, D. F.; Freeman, B. D.; Katz, L. E. Water Treatment: Are Membranes the Panacea? *Annu. Rev. Chem. Biomol. Eng.* **2020**, *11* (1), null. https://doi.org/10.1146/annurev-chembioeng-111919-091940.

(23) Ulbricht, M. Advanced Functional Polymer Membranes. *Polymer* **2006**, *47* (7), 2217–2262. https://doi.org/10.1016/j.polymer.2006.01.084.

(24) Fane, A. G.; Wang, R.; Hu, M. X. Synthetic Membranes for Water Purification: Status and Future. *Angew. Chem. Int. Ed.* **2015**, *54* (11), 3368–3386. https://doi.org/10.1002/anie.201409783.

(25) Werber, J. R.; Osuji, C. O.; Elimelech, M. Materials for Next-Generation Desalination and Water Purification Membranes. *Nat. Rev. Mater.* **2016**, *1* (5), 1–15. https://doi.org/10.1038/natrevmats.2016.18.

(26) Elimelech, M.; Phillip, W. A. The Future of Seawater Desalination: Energy, Technology, and the Environment. *Science* **2011**, *333* (6043), 712–717. https://doi.org/10.1126/science.1200488.

(27) Sujanani, R.; Landsman, M. R.; Jiao, S.; Moon, J. D.; Shell, M. S.; Lawler, D. F.; Katz, L. E.; Freeman, B. D. Designing Solute-Tailored Selectivity in Membranes: Perspectives for Water Reuse and Resource Recovery. *ACS Macro Lett.* **2020**, *9* (11), 1709–1717. https://doi.org/10.1021/acsmacrolett.0c00710.

(28) Alzahrani, S.; Mohammad, A. W. Challenges and Trends in Membrane Technology Implementation for Produced Water Treatment: A Review. *J. Water Process Eng.* **2014**, *4*, 107–133. https://doi.org/10.1016/j.jwpe.2014.09.007.

(29) Mondal, S. Polymeric Membranes for Produced Water Treatment: An Overview of Fouling Behavior and Its Control. *Rev. Chem. Eng.* **2016**, *32* (6), 611–628. https://doi.org/10.1515/revce-2015-0027.

(30) She, Q.; Wang, R.; Fane, A. G.; Tang, C. Y. Membrane Fouling in Osmotically Driven Membrane Processes: A Review. *J. Membr. Sci.* **2016**, *499*, 201–233. https://doi.org/10.1016/j.memsci.2015.10.040.

(31) Zhang, H.; Geise, G. M. Modeling the Water Permeability and Water/Salt Selectivity Tradeoff in Polymer Membranes. *J. Membr. Sci.* **2016**, *520*, 790–800. https://doi.org/10.1016/j.memsci.2016.08.035.

(32) Miller, D. J.; Dreyer, D. R.; Bielawski, C. W.; Paul, D. R.; Freeman, B. D. Surface Modification of Water Purification Membranes. *Angew. Chem. Int. Ed.* **2017**, *56* (17), 4662–4711. https://doi.org/10.1002/anie.201601509.

(33) Park, H. B.; Kamcev, J.; Robeson, L. M.; Elimelech, M.; Freeman, B. D. Maximizing the Right Stuff: The Trade-off between Membrane Permeability and Selectivity. *Science* **2017**, *356* (6343). https://doi.org/10.1126/science.aab0530.

(34) Zhang, W.; Ding, L.; Luo, J.; Jaffrin, M. Y.; Tang, B. Membrane Fouling in Photocatalytic Membrane Reactors (PMRs) for Water and Wastewater Treatment: A Critical Review. *Chem. Eng. J.* **2016**, *302*, 446–458. https://doi.org/10.1016/j.cej.2016.05.071.

(35) Li, D.; Wang, H. Recent Developments in Reverse Osmosis Desalination Membranes. *J. Mater. Chem.* **2010**, *20* (22), 4551–4566. https://doi.org/10.1039/B924553G.

(36) Wang, Y.; Wang, T.; Su, Y.; Peng, F.; Wu, H.; Jiang, Z. Remarkable Reduction of Irreversible Fouling and Improvement of the Permeation Properties of Poly(Ether Sulfone) Ultrafiltration Membranes by Blending with Pluronic F127. *Langmuir* **2005**, *21* (25), 11856–11862. https://doi.org/10.1021/la052052d.

(37) Park, J. Y.; Acar, M. H.; Akthakul, A.; Kuhlman, W.; Mayes, A. M. Polysulfone-Graft-Poly(Ethylene Glycol) Graft Copolymers for Surface Modification of Polysulfone Membranes. *Biomaterials* **2006**, *27* (6), 856–865. https://doi.org/10.1016/j.biomaterials.2005.07.010.

(38) Rana, D.; Matsuura, T.; Narbaitz, R. M. Novel Hydrophilic Surface Modifying Macromolecules for Polymeric Membranes: Polyurethane Ends Capped by Hydroxy Group. *J. Membr. Sci.* **2006**, *282* (1), 205–216. https://doi.org/10.1016/j.memsci.2006.05.024.

(39) Hester, J. F.; Mayes, A. M. Design and Performance of Foul-Resistant Poly(Vinylidene Fluoride) Membranes Prepared in a Single-Step by Surface Segregation. *J. Membr. Sci.* **2002**, *202* (1), 119–135. https://doi.org/10.1016/S0376-7388(01)00735-9.

(40) Hester, J. F.; Banerjee, P.; Won, Y.-Y.; Akthakul, A.; Acar, M. H.; Mayes, A. M. ATRP of Amphiphilic Graft Copolymers Based on PVDF and Their Use as

Membrane Additives. *Macromolecules* **2002**, *35* (20), 7652–7661. https://doi.org/10.1021/ma0122270.

(41) Hamza, A.; Pham, V. A.; Matsuura, T.; Santerre, J. P. Development of Membranes with Low Surface Energy to Reduce the Fouling in Ultrafiltration Applications. *J. Membr. Sci.* **1997**, *131* (1), 217–227. https://doi.org/10.1016/S0376-7388(97)00050-1.

(42) Wang, J.; Zhang, S.; Wu, P.; Shi, W.; Wang, Z.; Hu, Y. In Situ Surface Modification of Thin-Film Composite Polyamide Membrane with Zwitterions for Enhanced Chlorine Resistance and Transport Properties. *ACS Appl. Mater. Interfaces* **2019**, *11* (12), 12043–12052. https://doi.org/10.1021/acsami.8b21572.

(43) Johnson, B. C.; Yilgör, İ.; Tran, C.; Iqbal, M.; Wightman, J. P.; Lloyd, D. R.; McGrath, J. E. Synthesis and Characterization of Sulfonated Poly(Acrylene Ether Sulfones). *J. Polym. Sci. Polym. Chem. Ed.* **1984**, *22* (3), 721–737. https://doi.org/10.1002/pol.1984.170220320.

(44) Guan, R.; Zou, H.; Lu, D.; Gong, C.; Liu, Y. Polyethersulfone Sulfonated by Chlorosulfonic Acid and Its Membrane Characteristics. *Eur. Polym. J.* **2005**, *41* (7), 1554–1560. https://doi.org/10.1016/j.eurpolymj.2005.01.018.

(45) Zhao, Y.; Zhang, Z.; Dai, L.; Mao, H.; Zhang, S. Enhanced Both Water Flux and Salt Rejection of Reverse Osmosis Membrane through Combining Isophthaloyl Dichloride with Biphenyl Tetraacyl Chloride as Organic Phase Monomer for Seawater Desalination. *J. Membr. Sci.* **2017**, *522*, 175–182. https://doi.org/10.1016/j.memsci.2016.09.022.

(46) Choi, W.; Gu, J.-E.; Park, S.-H.; Kim, S.; Bang, J.; Baek, K.-Y.; Park, B.; Lee, J. S.; Chan, E. P.; Lee, J.-H. Tailor-Made Polyamide Membranes for Water Desalination. *ACS Nano* **2015**, *9* (1), 345–355. https://doi.org/10.1021/nn505318v.

(47) Kim, K. S.; Lee, K. H.; Cho, K.; Park, C. E. Surface Modification of Polysulfone Ultrafiltration Membrane by Oxygen Plasma Treatment. *J. Membr. Sci.* **2002**, *199* (1), 135–145. https://doi.org/10.1016/S0376-7388(01)00686-X.

(48) Wavhal, D. S.; Fisher, E. R. Modification of Polysulfone Ultrafiltration Membranes by CO2 Plasma Treatment. *Desalination* **2005**, *172* (2), 189–205. https://doi.org/10.1016/j.desal.2004.06.201.

(49) Pedram, S.; Mortaheb, H. R.; Arefi-Khonsari, F. Plasma Treatment of Polyethersulfone Membrane for Benzene Removal from Water by Air Gap

Membrane Distillation. *Environ. Technol.* **2018**, *39* (2), 157–171. https://doi.org/10.1080/09593330.2017.1296896.

(50) McCloskey, B. D.; Park, H. B.; Ju, H.; Rowe, B. W.; Miller, D. J.; Chun, B. J.; Kin, K.; Freeman, B. D. Influence of Polydopamine Deposition Conditions on Pure Water Flux and Foulant Adhesion Resistance of Reverse Osmosis, Ultrafiltration, and Microfiltration Membranes. *Polymer* **2010**, *51* (15), 3472–3485. https://doi.org/10.1016/j.polymer.2010.05.008.

(51) Arena, J. T.; McCloskey, B.; Freeman, B. D.; McCutcheon, J. R. Surface Modification of Thin Film Composite Membrane Support Layers with Polydopamine: Enabling Use of Reverse Osmosis Membranes in Pressure Retarded Osmosis. *J. Membr. Sci.* **2011**, *375* (1), 55–62. https://doi.org/10.1016/j.memsci.2011.01.060.

(52) Kasemset, S.; Lee, A.; Miller, D. J.; Freeman, B. D.; Sharma, M. M. Effect of Polydopamine Deposition Conditions on Fouling Resistance, Physical Properties, and Permeation Properties of Reverse Osmosis Membranes in Oil/Water Separation. *J. Membr. Sci.* **2013**, *425–426*, 208–216. https://doi.org/10.1016/j.memsci.2012.08.049.

(53) Monroe, J. I.; Shell, M. S. Computational Discovery of Chemically Patterned Surfaces That Effect Unique Hydration Water Dynamics. *Proc. Natl. Acad. Sci.* **2018**, *115* (32), 8093–8098. https://doi.org/10.1073/pnas.1807208115.

(54) Zuckermann, R. N.; Kerr, J. M.; Kent, S. B. H.; Moos, W. H. Efficient Method for the Preparation of Peptoids [Oligo(N-Substituted Glycines)] by Submonomer Solid-Phase Synthesis. *J. Am. Chem. Soc.* **1992**, *114* (26), 10646–10647. https://doi.org/10.1021/ja00052a076.

(55) Zuckermann, R. N. Peptoid Origins. *Pept. Sci.* **2011**, *96* (5), 545–555. https://doi.org/10.1002/bip.21573.

(56) Vericat, C.; Vela, M. E.; Benitez, G.; Carro, P.; Salvarezza, R. C. Self-Assembled Monolayers of Thiols and Dithiols on Gold: New Challenges for a Well-Known System. *Chem. Soc. Rev.* **2010**, *39* (5), 1805–1834. https://doi.org/10.1039/B907301A.

(57) Gooding, J. J.; Mearns, F.; Yang, W.; Liu, J. Self-Assembled Monolayers into the 21st Century: Recent Advances and Applications. *Electroanalysis* **2003**, *15* (2), 81–96. https://doi.org/10.1002/elan.200390017.

(58) Fowkes, F. M. Dispersion Force Contributions to Surface and Interfacial Tensions, Contact Angles, and Heats of Immersion. In *Contact Angle, Wettability, and Adhesion*; Advances in Chemistry; American Chemical Society, 1964; Vol. 43, pp 99–111. https://doi.org/10.1021/ba-1964-0043.ch006.

(59) Jeffrey, G. A.; Saenger, W. The Importance of Hydrogen Bonds. In *Hydrogen Bonding in Biological Structures*; Springer Science & Business Media, 2012; pp 8–10.

(60) Lee, B. P.; Messersmith, P. B.; Israelachvili, J. N.; Waite, J. H. Mussel-Inspired Adhesives and Coatings. *Annu. Rev. Mater. Res.* **2011**, *41* (1), 99–132. https://doi.org/10.1146/annurev-matsci-062910-100429.

(61) Faghihnejad, A.; Feldman, K. E.; Yu, J.; Tirrell, M. V.; Israelachvili, J. N.; Hawker, C. J.; Kramer, E. J.; Zeng, H. Adhesion and Surface Interactions of a Self-Healing Polymer with Multiple Hydrogen-Bonding Groups. *Adv. Funct. Mater.* **2014**, *24* (16), 2322–2333. https://doi.org/10.1002/adfm.201303013.

(62) Ahn, B. K.; Lee, D. W.; Israelachvili, J. N.; Waite, J. H. Surface-Initiated Self-Healing of Polymers in Aqueous Media. *Nat. Mater.* **2014**, *13* (9), 867–872. https://doi.org/10.1038/nmat4037.

(63) Salmeron, M. From Surfaces to Interfaces: Ambient Pressure XPS and Beyond. *Top. Catal.* **2018**, *61* (20), 2044–2051. https://doi.org/10.1007/s11244-018-1069-0.

(64) Monroe, J.; Barry, M.; DeStefano, A.; Gokturk, P. A.; Jiao, S.; Robinson-Brown, D.; Webber, T.; Crumlin, E. J.; Han, S.; Shell, M. S. Water Structure and Properties at Hydrophilic and Hydrophobic Surfaces. *Annu. Rev. Chem. Biomol. Eng.* **2020**, *11* (1), null. https://doi.org/10.1146/annurev-chembioeng-120919-114657.

(65) Martinelli, E.; Agostini, S.; Galli, G.; Chiellini, E.; Glisenti, A.; Pettitt, M. E.; Callow, M. E.; Callow, J. A.; Graf, K.; Bartels, F. W. Nanostructured Films of Amphiphilic Fluorinated Block Copolymers for Fouling Release Application. *Langmuir* **2008**, *24* (22), 13138–13147. https://doi.org/10.1021/la801991k.

(66) Chen, L.; Xie, Z.; Gan, T.; Wang, Y.; Zhang, G.; Mirkin, C. A.; Zheng, Z. Biomimicking Nano-Micro Binary Polymer Brushes for Smart Cell Orientation and Adhesion Control. *Small* **2016**, *12* (25), 3400–3406. https://doi.org/10.1002/smll.201600634.

(67) Cheng, Q.; Li, M.; Yang, F.; Liu, M.; Li, L.; Wang, S.; Jiang, L. An Underwater PH-Responsive Superoleophobic Surface with Reversibly Switchable Oil-Adhesion. *Soft Matter* **2012**, *8* (25), 6740–6743. https://doi.org/10.1039/C2SM25421B.

(68) Cui, X.; Liu, J.; Xie, L.; Huang, J.; Liu, Q.; Israelachvili, J. N.; Zeng, H. Modulation of Hydrophobic Interaction by Mediating Surface Nanoscale Structure and Chemistry, Not Monotonically by Hydrophobicity. *Angew. Chem. Int. Ed.* **2018**, *57* (37), 11903–11908. https://doi.org/10.1002/anie.201805137.

(69) Stock, P.; Monroe, J. I.; Utzig, T.; Smith, D. J.; Shell, M. S.; Valtiner, M. Unraveling Hydrophobic Interactions at the Molecular Scale Using Force Spectroscopy and Molecular Dynamics Simulations. *ACS Nano* **2017**, *11* (3), 2586–2597. https://doi.org/10.1021/acsnano.6b06360.

(70) Li, H.; Zhang, W.; Xu, W.; Zhang, X. Hydrogen Bonding Governs the Elastic Properties of Poly(Vinyl Alcohol) in Water: Single-Molecule Force Spectroscopic Studies of PVA by AFM. *Macromolecules* **2000**, *33* (2), 465–469. https://doi.org/10.1021/ma990878e.

(71) Lyubchenko, Y. L.; Gall, A. A.; Shlyakhtenko, L. S.; Harrington, R. E.; Jacobs, B. L.; Oden, P. I.; Lindsay, S. M. Atomic Force Microscopy Imaging of Double Stranded DNA and RNA. *J. Biomol. Struct. Dyn.* **1992**, *10* (3), 589–606. https://doi.org/10.1080/07391102.1992.10508670.

(72) Lindsay, S. M.; Nagahara, L. A.; Thundat, T.; Knipping, U.; Rill, R. L.; Drake, B.; Prater, C. B.; Weisenhorn, A. L.; Gould, S. A. C.; Hansma, P. K. STM and AFM Images of Nucleosome DNA Under Water. *J. Biomol. Struct. Dyn.* **1989**, *7* (2), 279–287. https://doi.org/10.1080/07391102.1989.10507771.

(73) Salmeron, M.; Schlögl, R. Ambient Pressure Photoelectron Spectroscopy: A New Tool for Surface Science and Nanotechnology. *Surf. Sci. Rep.* **2008**, *63* (4), 169–199. https://doi.org/10.1016/j.surfrep.2008.01.001.

(74) Carrasco, J.; Hodgson, A.; Michaelides, A. A Molecular Perspective of Water at Metal Interfaces. *Nat. Mater.* **2012**, *11* (8), 667–674. https://doi.org/10.1038/nmat3354.

(75) Peng, J.; Guo, J.; Hapala, P.; Cao, D.; Ma, R.; Cheng, B.; Xu, L.; Ondráček, M.; Jelínek, P.; Wang, E.; Jiang, Y. Weakly Perturbative Imaging of Interfacial Water with Submolecular Resolution by Atomic Force Microscopy. *Nat. Commun.* **2018**, *9* (1), 122. https://doi.org/10.1038/s41467-017-02635-5.

(76) Leng, C.; Sun, S.; Zhang, K.; Jiang, S.; Chen, Z. Molecular Level Studies on Interfacial Hydration of Zwitterionic and Other Antifouling Polymers in Situ. *Acta Biomater.* **2016**, *40*, 6–15. https://doi.org/10.1016/j.actbio.2016.02.030.

(77) Chen, Z. Investigating Buried Polymer Interfaces Using Sum Frequency Generation Vibrational Spectroscopy. *Prog. Polym. Sci.* **2010**, *35* (11), 1376–1402. https://doi.org/10.1016/j.progpolymsci.2010.07.003.

(78) Jarisz, T.; Roy, S.; Hore, D. K. Surface Water as a Mediator and Reporter of Adhesion at Aqueous Interfaces. *Acc. Chem. Res.* **2018**, *51* (9), 2287–2295. https://doi.org/10.1021/acs.accounts.8b00258.

(79) Kondo, T.; Gemmei-Ide, M.; Kitano, H.; Ohno, K.; Noguchi, H.; Uosaki, K. Sum Frequency Generation Study on the Structure of Water in the Vicinity of an Amphoteric Polymer Brush. *Colloids Surf. B Biointerfaces* **2012**, *91*, 215–218. https://doi.org/10.1016/j.colsurfb.2011.11.012.

(80) Kitano, H.; Gemmei-Ide, M. Structure of Water in the Vicinity of Amphoteric Polymers as Revealed by Vibrational Spectroscopy. *J. Biomater. Sci. Polym. Ed.* **2010**, *21* (14), 1877–1893. https://doi.org/10.1163/092050610X488278.

(81) Kitano, H.; Sudo, K.; Ichikawa, K.; Ide, M.; Ishihara, K. Raman Spectroscopic Study on the Structure of Water in Aqueous Polyelectrolyte Solutions. *J. Phys. Chem. B* **2000**, *104* (47), 11425–11429. https://doi.org/10.1021/jp000429c.

(82) Arble, C.; Jia, M.; Newberg, J. T. Lab-Based Ambient Pressure X-Ray Photoelectron Spectroscopy from Past to Present. *Surf. Sci. Rep.* **2018**, *73* (2), 37–57. https://doi.org/10.1016/j.surfrep.2018.02.002.

(83) Andrade, J. D. X-Ray Photoelectron Spectroscopy (XPS). In *Surface and Interfacial Aspects of Biomedical Polymers: Volume 1 Surface Chemistry and Physics*; Andrade, J. D., Ed.; Springer US: Boston, MA, 1985; pp 105–195. https://doi.org/10.1007/978-1-4684-8610-0_5.

(84) Hollander, J. M.; Jolly, W. L. X-Ray Photoelectron Spectroscopy. *Acc. Chem. Res.* **1970**, *3* (6), 193–200. https://doi.org/10.1021/ar50030a003.

(85) Henke, B. L.; Gullikson, E. M.; Davis, J. C. X-Ray Interactions: Photoabsorption, Scattering, Transmission, and Reflection at E = 50-30,000 EV, Z = 1-92. *At. Data Nucl. Data Tables* **1993**, *54* (2), 181–342. https://doi.org/10.1006/adnd.1993.1013.

(86) Karslıoğlu, O.; Bluhm, H. Ambient-Pressure X-Ray Photoelectron Spectroscopy (APXPS). In *Operando Research in Heterogeneous Catalysis*; Frenken, J., Groot, I., Eds.; Springer Series in Chemical Physics; Springer International Publishing: Cham, 2017; pp 31–57. https://doi.org/10.1007/978-3-319-44439-0_2.

(87) Starr, D. E.; Liu, Z.; Hävecker, M.; Knop-Gericke, A.; Bluhm, H. Investigation of Solid/Vapor Interfaces Using Ambient Pressure X-Ray Photoelectron Spectroscopy. *Chem. Soc. Rev.* **2013**, *42* (13), 5833–5857. https://doi.org/10.1039/C3CS60057B.

(88) Qian, J.; Baskin, A.; Liu, Z.; Prendergast, D.; Crumlin, E. J. Addressing the Sensitivity of Signals from Solid/Liquid Ambient Pressure XPS (APXPS) Measurement. *J. Chem. Phys.* **2020**, *153* (4), 044709. https://doi.org/10.1063/5.0006242.

(89) Shavorskiy, A.; Karslioglu, O.; Zegkinoglou, I.; Bluhm, H. Synchrotron-Based Ambient Pressure X-Ray Photoelectron Spectroscopy. *Synchrotron Radiat. News* **2014**, *27* (2), 14–23. https://doi.org/10.1080/08940886.2014.889547.

(90) Gokturk, P. A.; Barry, M.; Segalman, R.; Crumlin, E. J. Directly Probing Polymer Thin Film Chemistry and Counterion Influence on Water Sorption. *ACS Appl. Polym. Mater.* **2020**, *2* (11), 4752–4761. https://doi.org/10.1021/acsapm.0c00756.

(91) Axnanda, S.; Crumlin, E. J.; Mao, B.; Rani, S.; Chang, R.; Karlsson, P. G.; Edwards, M. O. M.; Lundqvist, M.; Moberg, R.; Ross, P.; Hussain, Z.; Liu, Z. Using "Tender" X-Ray Ambient Pressure X-Ray Photoelectron Spectroscopy as A Direct Probe of Solid-Liquid Interface. *Sci. Rep.* **2015**, *5* (1), 9788. https://doi.org/10.1038/srep09788.

(92) Argyris, D.; Cole, D. R.; Striolo, A. Ion-Specific Effects under Confinement: The Role of Interfacial Water. *ACS Nano* **2010**, *4* (4), 2035–2042. https://doi.org/10.1021/nn100251g.

(93) Yamamoto, S.; Kendelewicz, T.; Newberg, J. T.; Ketteler, G.; Starr, D. E.; Mysak, E. R.; Andersson, K. J.; Ogasawara, H.; Bluhm, H.; Salmeron, M.; Brown, G. E.; Nilsson, A. Water Adsorption on α-Fe2O3(0001) at near Ambient Conditions. *J. Phys. Chem. C* **2010**, *114* (5), 2256–2266. https://doi.org/10.1021/jp909876t.

(94) Ketteler, G.; Ashby, P.; Mun, B. S.; Ratera, I.; Bluhm, H.; Kasemo, B.; Salmeron, M. In Situphotoelectron Spectroscopy Study of Water Adsorption on Model Biomaterial Surfaces. *J. Phys. Condens. Matter* **2008**, *20* (18), 184024. https://doi.org/10.1088/0953-8984/20/18/184024.

(95) G. Mikos, A.; A. Peppas, N. Flory Interaction Parameter χ for Hydrophilic Copolymers with Water. *Biomaterials* **1988**, *9* (5), 419–423. https://doi.org/10.1016/0142-9612(88)90006-3.

(96) Elbs, H.; Krausch, G. Ellipsometric Determination of Flory-Huggins Interaction Parameters in Solution. *Polymer* **2004**, *45* (23), 7935–7942. https://doi.org/10.1016/j.polymer.2004.09.021.

(97) Arrigo, R.; Hävecker, M.; Schuster, M. E.; Ranjan, C.; Stotz, E.; Knop-Gericke, A.; Schlögl, R. In Situ Study of the Gas-Phase Electrolysis of Water on Platinum by NAP-XPS. *Angew. Chem. Int. Ed.* **2013**, *52* (44), 11660–11664. https://doi.org/10.1002/anie.201304765.

(98) Streibel, V.; Hävecker, M.; Yi, Y.; Velasco Vélez, J. J.; Skorupska, K.; Stotz, E.; Knop-Gericke, A.; Schlögl, R.; Arrigo, R. In Situ Electrochemical Cells to Study the Oxygen Evolution Reaction by Near Ambient Pressure X-Ray Photoelectron Spectroscopy. *Top. Catal.* **2018**, *61* (20), 2064–2084. https://doi.org/10.1007/s11244-018-1061-8.

(99) Favaro, M.; Jeong, B.; Ross, P. N.; Yano, J.; Hussain, Z.; Liu, Z.; Crumlin, E. J. Unravelling the Electrochemical Double Layer by Direct Probing of the Solid/Liquid Interface. *Nat. Commun.* **2016**, *7* (1), 12695. https://doi.org/10.1038/ncomms12695.

(100) Kiil, S.; Yebra, D. M. 14 - Modelling the Design and Optimization of Chemically Active Marine Antifouling Coatings. In *Advances in Marine Antifouling Coatings and Technologies*; Hellio, C., Yebra, D., Eds.; Woodhead Publishing Series in Metals and Surface Engineering; Woodhead Publishing, 2009; pp 334–364. https://doi.org/10.1533/9781845696313.2.334.

(101) Calabrese, D. R.; Wenning, B.; Finlay, J. A.; Callow, M. E.; Callow, J. A.; Fischer, D.; Ober, C. K. Amphiphilic Oligopeptides Grafted to PDMS-Based Diblock Copolymers for Use in Antifouling and Fouling Release Coatings. *Polym. Adv. Technol.* **2015**, *26* (7), 829–836. https://doi.org/10.1002/pat.3515.

(102) Patterson, A. L.; Wenning, B.; Rizis, G.; Calabrese, D. R.; Finlay, J. A.; Franco, S. C.; Zuckermann, R. N.; Clare, A. S.; Kramer, E. J.; Ober, C. K.; Segalman, R. A. Role of Backbone Chemistry and Monomer Sequence in Amphiphilic Oligopeptide- and Oligopeptoid-Functionalized PDMS- and PEO-Based Block Copolymers for Marine Antifouling and Fouling Release Coatings. *Macromolecules* **2017**, *50* (7), 2656–2667. https://doi.org/10.1021/acs.macromol.6b02505.

(103) Barry, M. E.; Davidson, E. C.; Zhang, C.; Patterson, A. L.; Yu, B.; Leonardi, A. K.; Duzen, N.; Malaviya, K.; Clarke, J. L.; Finlay, J. A.; Clare, A. S.; Chen, Z.; Ober, C. K.; Segalman, R. A. The Role of Hydrogen Bonding in Peptoid-Based Marine

Antifouling Coatings. *Macromolecules* **2019**, *52* (3), 1287–1295. https://doi.org/10.1021/acs.macromol.8b02390.

(104) Buechner, C.; Gericke, S. M.; Trotochaud, L.; Karslıoğlu, O.; Raso, J.; Bluhm, H. Quantitative Characterization of a Desalination Membrane Model System by X-Ray Photoelectron Spectroscopy. *Langmuir* **2019**, *35* (35), 11315–11321. https://doi.org/10.1021/acs.langmuir.9b01838.

(105) Gericke, S. M.; Mulhearn, W. D.; Goodacre, D. E.; Raso, J.; Miller, D. J.; Carver, L.; Nemšák, S.; Karslıoğlu, O.; Trotochaud, L.; Bluhm, H.; Stafford, C. M.; Buechner, C. Water-Polyamide Chemical Interplay in Desalination Membranes Explored by Ambient Pressure X-Ray Photoelectron Spectroscopy. *Phys. Chem. Chem. Phys.* **2020**, *22* (27), 15658–15663. https://doi.org/10.1039/D0CP01842B.

Chapter 2
The role of hydrogen bonding in peptoid-based marine antifouling coatings[1]

The benefits of incorporating amphiphilic properties into antifouling and fouling-release coatings are well-established. Use of sequence-defined peptides and peptoids in these coatings allows precise control over the spacing and chemistry of the amphiphilic groups, but amphiphilic peptoids have generally outperformed analogous peptides for reasons attributed to differences in backbone structure. The present work demonstrates that the superior properties of peptoids relative to peptides are primarily attributable to a lack of hydrogen bond donors rather than to their secondary structure. A new amphiphilic peptoid was designed containing functional groups similar to those typically found on a hydrogen-bonding peptide backbone. This peptoid and a non-hydrogen-bonding peptoid analogue were incorporated as side chains in PDMS-based polymer scaffolds. Bioassays with the soft algal fouling organisms *Ulva linza* and *Navicula incerta* indicate that hydrogen bonding largely determines the differences seen between similar peptide and peptoid

[1]Emily Davidson designed and synthesized the peptoid sequences with support from Anastasia Patterson and Beihang Yu. Chengcheng Zhang and Ketaki Malaviya performed SFG and contact angle measurements, respectively, and Amanda Leonardi and Nilay Duzen synthesized the PDMS-based copolymer.

species, while sum frequency generation vibrational spectroscopy suggests that the presence of hydrogen bond donors enhances interfacial water structuring. This reduced initial *U. linza* adhesion, but attached algae were more strongly bound by hydrogen bonding interactions. Consequently, amphiphilic peptoid materials lacking hydrogen bond donors are better suited to resist marine fouling, with enhanced release of *U. linza* and similar performance against *N. incerta* relative to hydrogen-bonding analogues.

This chapter was reproduced with permission from: Barry, M. E.; Davidson, E. C.; Zhang, C.; Patterson, A. L.; Yu, B.; Leonardi, A. K.; Duzen, N.; Malaviya, K.; Clarke, J. L.; Finlay, J. A.; Clare, A. S.; Chen, Z.; Ober, C. K.; Segalman, R. A. The role of hydrogen bonding in peptoid-based marine antifouling coatings. *Macromolecules* **2019**, 52 (3), 1287-1295. Copyright 2019 American Chemical Society.

2.1 Introduction

Marine fouling, caused by the attachment of a broad range of organisms to marine structures including ships' hulls and offshore rigs, begins soon after exposure to an oceanic environment. The surface initially experiences biomolecule deposition, but this is quickly followed by colonization with unicellular organisms such as bacteria, algae (often predominantly diatoms), fungi and protozoa. Simultaneously, larger organisms may begin to attach, including hard calcareous fouling organisms such as tubeworms and barnacles and larger algae including species of *Ulva*. The presence of these organisms dramatically increases surface roughness and reduces hydrodynamic efficiency for ocean-going vessels.[1-4] Fouling by soft algal slimes requires ship power output to be increased over 20% to maintain cruising speed, and even moderate settlement of calcareous fouling organisms

can double the power necessary for transport.[5] Coatings containing biocides, such as copper or tri-*n*-butyltin (TBT), have historically been used to limit the settlement and growth of fouling organisms.[2, 6] However, organotins have since been banned by the International Maritime Organization due to their toxicity to marine life,[2, 7] and other metal-containing biocides are already heavily regulated due to environmental risks.[2, 8] As a result, there is significant interest in developing biocide-free antifouling materials.[6, 9]

Nontoxic fouling-resistant coatings interfere with the adhesion of fouling organisms via two mechanisms. Antifouling materials, such as those incorporating poly(ethylene oxide) PEO or zwitterions, operate by preventing initial adhesion of the organisms.[10-12] In contrast, organisms can attach to fouling-release materials, such as those containing fluoropolymers and polydimethylsiloxane (PDMS), but only weakly; the polymer's low modulus and low surface energy enhance removal of fouling organisms by hydrodynamic forces.[2-3, 13] Many different materials have been tested, but siloxane coatings containing silicone oil lubricants in particular have shown excellent fouling-release properties.[14-15] Another approach is to include amphiphilic groups in the coatings where it has been shown that the combination of hydrophilic and hydrophobic components at the surface can be particularly effective in minimizing permanent attachment.[16-18] A wide variety of chemical structures have been used in these amphiphilic materials and can be found in a number of reviews.[3, 11, 19-20] However, comparison of the functional groups that provide these amphiphilic materials with their antifouling properties is difficult, as amphiphilic materials are known to induce varying responses depending on the length scale of the hydrophilic and hydrophobic components as well as the components' chemical identities.[21-23]

The incorporation of unique amphiphilic groups into surface-active block copolymers (SABCs) is an effective framework for studying the antifouling and fouling-release properties of selected chemistries.[22, 24-26] Chemical functionalities can be attached via click chemistry as side chain substituents in a block copolymer, allowing for direct comparison of a number of functional groups on a single, unchanging polymer scaffold. Full coatings can also be produced that consist of a thin layer of SABC above commercially-available polystyrene-*b*-poly(ethylene/butylene)-*b*-polystyrene (SEBS), allowing for surface chemistries to be varied without compromising mechanical stability or altering the polymer modulus. Perhaps most importantly, minimal amounts of surface-active functionalities incorporated into only the top layer of the coating can significantly alter surface properties and antifouling characteristics. This system has been used to independently investigate the roles played by amphiphile chemistry,[26] moiety patterning,[22] and block copolymer framework identity[24] on antifouling and fouling-release profiles.

Precise control over the length scale for a wide range of modular amphiphilic components can be attained in these SABCs with the use of peptoids, sequence-defined peptidomimetic *N*-substituted glycine oligomers. An iterative synthesis of sub-monomer units allows for control of monomer type in defined sequences along the peptoid chain.[27-28] Because the formation of the amide group in each peptoid monomer is divided into two reactions, virtually any primary amine can be incorporated into the chain, with a higher yield per reaction that allows for polymeric chain lengths and increased (gram-scale) batch size, relative to peptides. Furthermore, *N*-substitution in peptoids results in a tertiary amide that inherently lacks hydrogen bond donors, unlike the secondary amides present in

peptides, and eliminates the chirality of the backbone α-carbon that enables secondary structure in peptides (**Figure 2-1**).

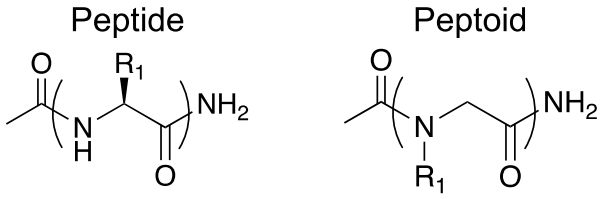

Figure 2-1. Peptoid *N*-substitution changes the backbone structure relative to peptides, eliminating backbone chirality as well as the amide hydrogen bond donor.

SABCs leveraging amphiphilic peptoids as side chains have been shown to reduce fouling through both antifouling and fouling-release methods.[21, 23] However, amphiphilic peptides have not demonstrated the same degree of success for marine fouling applications: peptide side chains on modified poly(dimethylsiloxane) (PDMS) block copolymer coatings have been shown to have higher attachment of *Navicula incerta* and significantly reduced surface-release efficacy for *Ulva linza* relative to coatings modified with analogous peptoid side chains.[23] Despite their similar chemical structure (**Figure A1** in Appendix A), the peptide-containing samples also demonstrated significantly reduced *U. linza* settlement. Because analogous pendant groups were used for the peptoid and peptide side chains, the contrasting antifouling behavior was attributed to differences between the peptide and peptoid backbones.

To better understand the role of hydrogen bonding in antifouling and fouling-release performance, a new hydrophilic peptoid monomer has been developed that contained a hydrogen-bond-donating amide group added to the hydrophilic moiety from previously-tested amphiphilic peptoids.[23] Amphiphilic peptoids containing either this hydrogen-bonding monomer or a non-hydrogen-bonding analogue were incorporated into

PDMS-based SABCs (**Figure 2-2**) to determine the effects of hydrogen bonding on the attachment and release of fouling algae. Further surface characterization performed via sum-frequency generation (SFG) vibrational spectroscopy suggests a competing hydration-based mechanism for differences in performance.

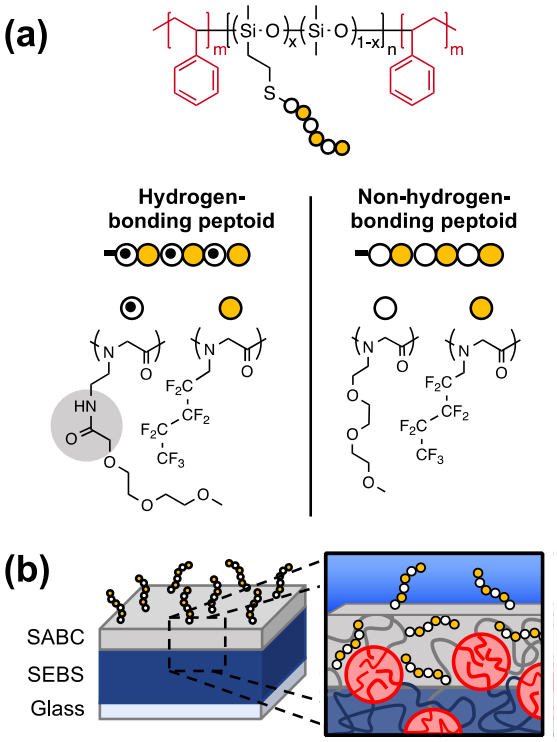

Figure 2-2. (a) Analogous hydrogen-bonding or non-hydrogen-bonding pendant groups were incorporated into amphiphilic peptoid side chains on a PDMS-based surface-active block copolymer (SABC). **(b)** Samples consisted of a spray-coated SABC on a spin-coated SEBS underlayer to form the final coating. Annealing enabled diffusion between polystyrene microphase-segregated spheres in both layers, lending mechanical stability to the final coating.

2.2 Experimental Methods

2.2.1 Materials

All materials were purchased from Sigma-Aldrich and used as received, unless otherwise noted. Polystyrene-*block*-poly(ethylene-*ran*-butylene)-*block*-polystyrene (SEBS, MD6945) and maleic anhydride-grafted SEBS (MA-SEBS, FG1901X) were generously provided by Kraton Polymers. Hexamethylcyclotrisiloxane (D3) and 1,3,5-trivinyl-1,3,5-trimethylcyclotrisiloxane (V3) were purchased from Gelest. Boc-ethylene

diamine, Boc-ethanolamine, and *S*-trityl-3-mercaptopropionic acid were purchased from Oakwood Chemicals. Basic alumina and 2,2-dimethoxy-2-phenylacetophenone (DMPA) were obtained from Acros Organics, and triethylene glycol monomethyl ether was purchased from Fluka Analytical. Bromoacetic acid was purchased from Alfa Aesar and dichloromethane was purchased from Fisher Scientific. Dimethylformamide (DMF) was purchased from VWR, *N,N'*-diisopropylcarbodiimide was purchased from Chem-Impex, and Rink amide MBHA resin (0.80 mmol/g) was purchased from Millipore Sigma. 1*H*,1*H*-perfluoropentylamine was purchased from Manchester Organics, and triisopropylsilane (TIS) was purchased from TCI. Dry tetrahydrofuran used in synthesis was purified by solvent columns (PureSolv) from Innovative Technology, Inc.

Tetrahydrofuran (THF), styrene, and 1,3,5-trivinyl-1,3,5-trimethylcyclotrisiloxane (V3) for anionic polymerization of polystyrene-*block*-poly(dimethylsiloxane-*ran*-vinylmethylsiloxane)-*block*-polystyrene (PS-*b*-P(DMS/VMS)-*b*-PS) were dried by stirring over ground calcium hydride (CaH_2), then distilled and degassed by a freeze–pump–thaw process. Hexamethylcyclotrisiloxane (D3) was dried by stirring in benzene over CaH_2, distilled, and then sublimed into a flask containing benzene and a living anionic polystyrene polymerization, polymerized with *sec*-butyl lithium. Continued stirring further dried the D3 until the solution was colorless, after which the benzene was distilled and the D3 sublimed into a clean flask. D3 concentration in benzene was determined by ^{1}H-NMR. Dichlorodimethylsilane and chlorotrimethylsilane were purified by distillation and degassed by a freeze–pump–thaw process.

2.2.2 PS-b-P(DMS/VMS)-b-PS synthesis

PS-*b*-P(DMS/VMS)-*b*-PS synthesis followed an established procedure previously reported.[23] In brief, polystyrene was polymerized with *sec*-butyl lithium and chain-extended with distributed polydimethylsiloxane and polyvinylmethylsiloxane. A triblock architecture was made by coupling active chain ends together. The final molecular weight of the polymer was determined by GPC, while 1H-NMR verified vinyl content. Further details can be found in Appendix A.

2.2.3 Synthesis of triethylene glycol amine

The non-H-bonding submonomer (**Figure 2-2a**) was synthesized by a series of displacements on triethylene glycol monomethyl ether ($mPEG_3$-OH). First, $mPEG_3$-OH (88.7 g, 540 mmol) and *N*,*N*-diisopropylethylamine (DIEA; 83.7 g, 648 mmol) were combined in 160 mL of dry tetrahydrofuran (THF), then cooled to 0 °C and purged with N_2 for 15 minutes. Mesyl chloride (74.3 g, 649 mmol) was added dropwise and left to stir overnight to form the mesylated triethylene glycol amine intermediate. The white filtrate was removed and the reaction solution filtered through silica to remove unreacted starting materials. THF was then removed via rotary evaporation and the product redissolved in dimethylsulfoxide. Potassium phthalimide (120 g, 648 mmol) was added and allowed to react overnight. The phthalimide-protected triethylene glycol amine product was extracted into ether and purified using a basic alumina column with ethyl acetate as the eluent. Solvent was removed by rotary evaporation, yielding a viscous yellow liquid.

The final submonomer product was obtained by deprotecting the phthalimide group with excess butylamine. A portion of the phthalimide $mPEG_3$ (5.83 g, 19.9 mmol) was dissolved in 60 mL of ethanol. Butylamine (3.93 mL, 39.8 mmol) was added and the

reaction was stirred overnight at 70 °C. The solids were removed by filtration, and ethanol and excess butylamine were then evaporated under reduced pressure at room temperature. The crude product was redissolved in chloroform and extracted into 0.6 M aqueous HCl. The amine was then neutralized with 0.5 M NaOH, extracted back into chloroform, and dried with $MgSO_4$. Rotary evaporation then yielded the pure submonomer product, confirmed by ^{1}H-NMR and UPLC-MS. Notably, this synthesis route avoids the use of either sodium azide or hydrazine.

2.2.4 Synthesis of amide-linked triethylene glycol amine

The hydrogen-bond-donating submonomer (**Figure 2-2a**) was synthesized using DIC-mediated coupling of a triethylene glycol carboxylic acid and Boc-protected diamine. 2-[2-(2-Methoxyethoxy)ethoxy]acetic acid ($mPEG_3$-COOH; 80.9 g, 421 mmol) was dissolved in 500 mL DMF, then *N,N'*-diisopropylcarbodiimide (DIC; 71.1 mL, 454 mmol) was added and allowed to stir for 30 minutes. *N*-Boc-ethylenediamine (87.3 g, 545 mmol) in 300 mL DMF was then added. The reaction was purged with N_2 and allowed to run overnight. DMF was removed via centrifugal evaporation and solid DIC byproducts were filtered out. The Boc-protected amide-linked $mPEG_3$ amine product was purified using an alumina plug with ethyl acetate as eluent.

The protected amide-linked amine was deprotected using trifluoracetic acid (TFA). 10 g of protected amine (31 mmol) was dissolved in 60 mL DCM. TFA (40 mL, 522 mmol) was added dropwise and stirred for 2.5 hours, at which time thin layer chromatography confirmed complete removal of the protecting group. DCM and TFA were then removed under reduced pressure. The deprotected amide-linked amine was next dissolved in water and washed three times with DCM and once with ether. Water was removed using rotary

evaporation. The charged terminal amine was then neutralized by dissolving the deprotected amine product (6 g, 27 mmol) in 1 M DMF solution (27 mL), and slowly adding 1:1 NaOH:H_2O (w/v) solution, stirring until neutral pH was reached.[29] The submonomer identity was confirmed via UPLC-MS before the neutralized 1 M DMF solution was used in peptoid synthesis.

2.2.5 Peptoid synthesis

Peptoids were synthesized on a Prelude synthesizer (Protein Technologies) according to published solid-phase submonomer synthesis procedures using Rink amide MBHA resin.[21, 23, 27] Two sequences of hexamer peptoids were made, one with three alternating 1*H*,1*H*-perfluoropentylamine submonomers and three triethylene glycol submonomers, while the other contained alternating fluorinated submonomers and amide-linked triethylene glycol submonomers. The *N*-terminus of the peptoid chain was capped with *S*-trityl-3-mercaptopropionic acid that, upon cleavage and deprotection with trifluoroacetic acid, yielded a thiol-terminated oligomer capable of attachment to the PDMS-based polymer via a radical mediated thiol–ene "click" reaction. The cleaved peptoids were dissolved in a 1:1 acetonitrile:water (v/v) solution and washed with hexanes, then lyophilized to yield the pure peptoid product as confirmed by UPLC-MS (**Figure A2**). Further synthetic details can be found in Appendix A.

2.2.6 Click attachment to polymer scaffold

Thiol-terminated peptoids were incorporated into the siloxane triblock copolymer via radical mediated thiol–ene "click" chemistry as previously reported.[23] Triblock copolymer (0.95 g, 0.3 mmol vinyl groups) was dissolved in 10 mL of dichloromethane, to which either the H-bonding peptoid (2.3 g, 1.3 mmol) or non-H-bonding peptoid (2.2 g,

1.4 mmol) were added. After adding 65 mg of 2,2-dimethoxy-2-phenyl acetophenone (DMPA), the solution was sparged with N_2 for 30 min, then irradiated with 365 nm UV light while stirring for 3 h. The peptoid-modified PDMS triblock copolymer was then precipitated into methanol, filtered, and dried under vacuum. ^{1}H NMR verified a 75% reduction of vinyl peaks for both materials, likely limited by steric hindrance associated with substituting three sites per V3 monomer unit with peptoid side chains (**Figure A5**).

2.2.7 Slide preparation for biofouling assays

Coated slides for *U. linza* and *N. incerta* assays were prepared as previously reported.[23] Microscope glass slides (3 x 1 in) were cleaned using nanostrip for 30 minutes, then rinsed sequentially with deionized water and anhydrous ethanol. After drying, the clean glass slides were aminosilane-treated by soaking overnight in dilute 3-(aminopropyl)trimethoxysilane solution (3.5% in anhydrous ethanol (v/v)) with a catalytic amount of acetic acid. The slides were then sequentially rinsed with anhydrous ethanol and water, then cured in vacuum at 120 °C for 4 h. Immediately after curing, the slides were spin-coated with an initial SEBS/MA-SEBS solution (7% SEBS (w/v) and 2% MA-SEBS (w/v) in toluene) at 500 rpm for 5 s, followed by 2500 rpm for 30 s. Curing at 120 °C under vacuum for 24 h enabled the maleic anhydride groups on the polymer backbone to react with amine groups on the functionalized glass surface, improving adhesion strength between the polymer and glass. An additional SEBS solution (12% SEBS in toluene (w/v)) was then applied via spin-coating three times (2500 rpm, 30 s). The 1 mm thick coating was then annealed under vacuum at 120 °C for 24 h. H-bonding, non-H-bonding, and unfunctionalized PDMS-based SABC solutions (5% w/v in 20:1 DCM:toluene (v/v)) were spray-coated (Badger model 250 airbrush) on SEBS-coated slides to form a top layer tens

of microns thick. Annealing at 60 °C for 6 h and then 120 °C for 24 h allowed for diffusion of the microphase-segregating PS groups between layers, improving mechanical stability.

2.2.8 Prism preparation for SFG study

For SFG testing, optically clear CaF_2 prisms were cleaned via ozone treatment and spin-coated with sample solutions to sufficient thickness to ensure sample signal solely came from the material–environment interface, determined experimentally to be at least 50 nm (**Figure A7**). Due to solubility differences, the unfunctionalized PDMS-based SABC solution (2.5 wt% in cyclohexane) was applied once (1500 rpm, 45 s) while the H-bonding and non-H-bonding SABCs (1 wt% in cyclopentanone) were applied twice (1000 rpm, 2 min). Thickness was confirmed via ellipsometry on corresponding silicon substrates to be between 50 and 200 nm.

2.2.9 ^{1}H NMR

All ^{1}H NMR spectra were obtained using a Varian VNMRS 600 MHz spectrometer in $CDCl_3$ solution.

2.2.10 GPC

GPC was performed on a Waters ambient temperature GPC equipped with a Waters 410 differential refractive index detector and a Waters 486 UV-Vis detector. Samples were eluted at 1.0 mL/min at 40 ^{o}C, using THF as an eluent. Narrowly dispersed polystyrene standards were used for calibration.

2.2.11 UPLC-MS

Mass data for all samples were obtained using a Waters Acquity H-class Ultra High Pressure Liquid Chromatography (UPLC) system coupled with a Waters Xevo G2-XS

Time-of-Flight Mass Spectrometer. Time-of-flight mass spectrometry was obtained in positive electrospray ionization (ESI^+) mode. Liquid chromatography separations used gradients from H_2O to ACN with 0.1% TFA on a BEH C_{18} column.

2.2.12 Water contact angle

Water contact angles were measured using the captive bubble method. Sample slides were suspended in Milli-Q water with the coated side facing down. A 22-gauge stainless steel needle was used to release a bubble that was trapped against the coated face of the sample. This provided contact angle measurements under full immersion, which more closely replicates the underwater conditions experienced by antifouling materials. For each material, the contact angle was measured in triplicate (in different locations) for three separate slides. To characterize film restructuring underwater, contact angle measurements were taken immediately after submersion, after 5 h, and then every 24 h over the course of 7 days. All measurements were collected using the ramé-hart model 100-00 goniometer.

2.2.13 Ulva linza *bioassays*

Before performing *U. linza* biofouling assays, nine coated slides for each material were equilibrated for 72 hours in 0.22 μm-filtered artificial seawater (ASW, Tropic Marin) in individual wells of quadriPERM dishes (Sarstedt). Zoospores were obtained from mature plants according to a standard method,[30] then suspended in a solution of filtered ASW at a concentration of 1×10^5 mL^{-1}. 10 mL of the suspension was added to each well of the quadriPERM dishes and allowed to settle in darkness for 45 min at 20 °C. Unsettled spores were then removed by gently washing in filtered ASW. Three slides were set aside, fixed using 2.5% glutaraldehyde in ASW, and analyzed to determine spore settlement

density using a Zeiss Axioskop 2 fluorescence microscope. Leica LASX image analysis software was used to count 30 fields of view of 0.15 mm^2 on each slide.

The spores on the remaining six slides were cultured for 7 days in an illuminated incubator using nutrient-supplemented ASW to produce sporelings (young plants). Sporeling biomass was determined *in situ* by chlorophyll fluorescence measurements using a Tecan fluorescence plate reader (GENios Plus), and quantified in terms of relative fluorescence units (RFU) determined as the mean of 70 point fluorescence readings taken from the central portion of each slide.

Sporeling attachment strength was assessed by determining biomass removal after using a water jet to spray the surface with an impact pressure of 55 kPa.[31] The biomass remaining on the sample was again quantified using the fluorescence plate reader, and the percentage removal calculated from the difference in biomass RFU before and after exposure.

2.2.14 Navicula incerta *bioassays*

Before performing *N. incerta* assays, six coated slides for each material were equilibrated for 72 hours in 0.22 μm filtered ASW in individual wells of quadriPERM dishes. *N. incerta* cells were cultured for 3 days, then diluted to produce a suspension with chlorophyll *a* content of approximately 0.25 μg mL^{-1}. Ten mL of the suspension was then added to each quadriPERM well and left to settle for 2 h at 20 °C. Unbound cells were removed by shaking on an orbital shaker at 60 rpm for 5 minutes, followed by rinsing in seawater. Three slides were set aside, fixed in 2.5% glutaraldehyde in ASW, air dried, and

then analyzed via transmitted light microscopy to quantify initial attachment density. Manual counts were made for 15 fields of view of 0.15 mm^2 per slide.

Diatom attachment strength was determined for the remaining three slides by quantifying removal after exposure to a shear stress of 28 Pa in a specially-designed water channel.[32] The diatoms were fixed by immersing the slides in glutaraldehyde solution (2.5% (v/v) in ASW) and cells counted using transmitted light microscopy as before.

2.2.15 Statistical Analysis

U. linza settlement and *N. incerta* initial attachment data are presented as means with 95% confidence intervals and were analyzed via one-way ANOVA to identify statistically significant differences between groups ($p<0.05$), followed by a post hoc pairwise Tukey comparison test. Percent removal for *U. linza* and *N. incerta* is presented as means within 95% confidence intervals and the statistical tests previously mentioned were used to analyze the arcsine transform of fractional removal data.

2.2.16 SFG Testing

Sum-frequency generation (SFG) theory, experimental details, and data analysis have been extensively reported,[33-42] and spectra of the coated prisms were collected in air and water according to previously reported methods.[36-42] SFG data collection used two input laser beams, a visible beam and an infrared beam, both with a diameter of approximately 0.5 mm. The visible beam, with a fixed wavelength at 532 nm, was generated by doubling the frequency of a 20 ps pulse width output from an EKSPLA Nd:YAG laser. The IR beam with wavenumber tunability from 1000 to 4300 cm^{-1} was produced using an EKSPLA optical parametric generation/amplification and difference

frequency generation system with LBO and $AgGaS_2$ crystals. These two input beams penetrated the prism and then reached the polymer coating surfaces that were in contact with either air or water, superimposed on each other spatially and temporally to generate the sum frequency (SF) signal. This signal was collected using a photomultiplier and net intensity normalized by measuring the input visible and IR intensities according to the back reflections of the two beams using the focus lenses.

2.3 Results and Discussion

The hydrogen-bonding (H-bonding) peptoid and its non-hydrogen-bonding (non-H-bonding) peptoid analogue were individually incorporated into triblock SABCs consisting of a PDMS-based midblock with polystyrene (PS) end blocks (**Figure 2-2a**). Each sample consisted of a SABC topcoat above a layer of a SEBS thermoplastic elastomer to provide a consistent modulus in the material and improve the coating's mechanical stability. Annealing enabled the microphase-separated PS end blocks to diffuse between the SABC and SEBS layers, forming physical anchors that prevent delamination (**Figure 2-2b**). The samples were evaluated for fouling resistance and release using *U. linza* and *N. incerta* bioassays and were characterized using captive bubble water contact angle measurements and sum-frequency generation. In addition to the H-bonding and non-H-bonding peptoid samples, the unfunctionalized PDMS-based polymer scaffold served as a control to identify the effects of amphiphilicity on surface properties and fouling.

The H-bonding amphiphilic peptoid was designed to act as a hydrogen-bonding peptide mimic without the structural effects caused by chirality. Because the peptoid backbone innately lacks hydrogen bonding, a secondary amide (the source of hydrogen-

bonding in the peptide backbone) was added along the side chain in the ether-based hydrophilic monomer. The amphiphilic peptoid was made by alternating this hydrogen-bonding monomer with a hydrophobic peptoid monomer containing fluoralkyl functionality.

The surface activity of both amphiphilic peptoid side chains was confirmed using captive bubble contact angle goniometry, chosen over conventional contact angle goniometry to better mimic the underwater environment experienced by surfaces exposed to biofouling organisms. The H-bonding and non-H-bonding peptoid materials both demonstrated increased hydrophilicity relative to the unfunctionalized PDMS-based control (**Figure A6**). Notably, the contact angle of the two peptoid-containing samples approached similar values over extended time underwater, suggesting the equilibrated surfaces maintained comparable surface energy and hydrophilicity on a macroscopic scale.

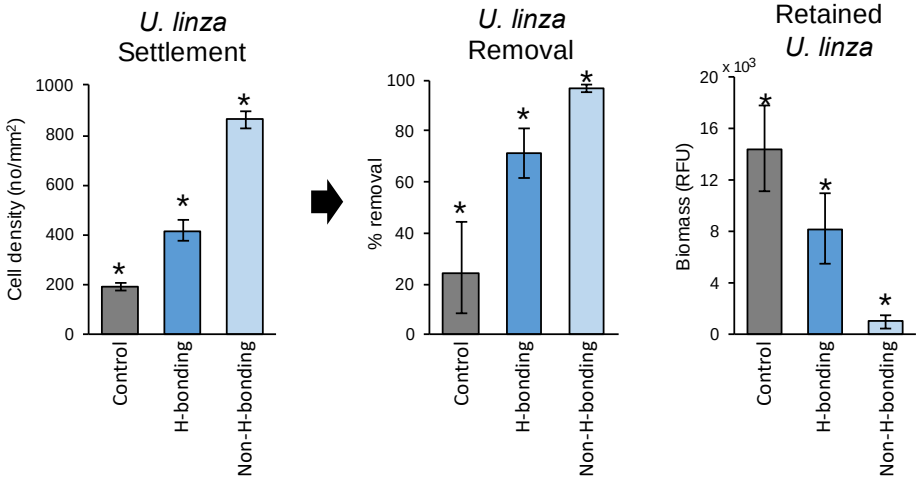

Figure 2-3. Biofouling assay settlement and release data for *U. linza* indicate the non-H-bonding sample had higher settlement relative to its H-bonding analogue and the unfunctionalized PDMS control, but superior removal rates resulted in fewer retained sporelings relative to the H-bonding and unfunctionalized PDMS materials. All samples differ significantly (*$p<0.05$). Error bars indicate 95% confidence limits.

Despite their similar hydrophilicity, the peptoid materials differed greatly in antifouling and fouling-release properties in *U. linza* bioassays (**Figure 2-3**). The settlement of *U. linza* spores was much higher on the non-H-bonding peptoid than on either the PDMS-based scaffold control or the H-bonding surface ($F_{2,267} = 421.7$; $p<0.05$). When subjected to a water jet with impact pressure of 55 kPa, the same non-H-bonding surface demonstrated nearly perfect removal, releasing over 97% of the sporelings present on its surface ($F_{2,15} = 40.9$; $p<0.05$). The 7-day-old sporelings were particularly weakly attached to this coating as a result of the chemistry and spacing of its hydrophilic and hydrophobic functionalities. The extremely high level of removal resulted in a far cleaner surface than those of the other two materials ($F_{2,15} = 27.9$; $p<0.05$; **Figure 2-3**).

U. linza tends to attach strongly to hydrophilic materials such as glass.[43-44] The findings of this study suggest that attachment of spores of *U. linza* to surfaces may be strongly influenced by hydrogen bonding. The introduction of hydrogen bonding in the H-bonding peptoid did not alter macroscale hydrophilicity relative to its non-H-bonding analogue (see **Figure A6** in Appendix A for contact angle comparisons) but did increase the attachment strength of *U. linza* sporelings. The H-bonding peptoid surface retained over 28% of sporelings, leaving nearly eight times the fouling present on the non-H-bonding peptoid film. Although the H-bonding peptoid surface showed lower settlement compared with the non-H-bonding peptoid film, its reduced fouling-release properties made it less useful for practical applications.

While the PDMS-based scaffold control had lower settlement than either amphiphilic peptoid sample, adhered sporelings were more strongly bound and the surface retained the most fouling after removal. As has been seen before,[23] modification with

amphiphilic peptoids appears to improve fouling-release properties, though the extent of success varied. We consequently conclude that the non-H-bonding sample better resists permanent *U. linza* attachment compared with both its H-bonding analogue and the PDMS control.

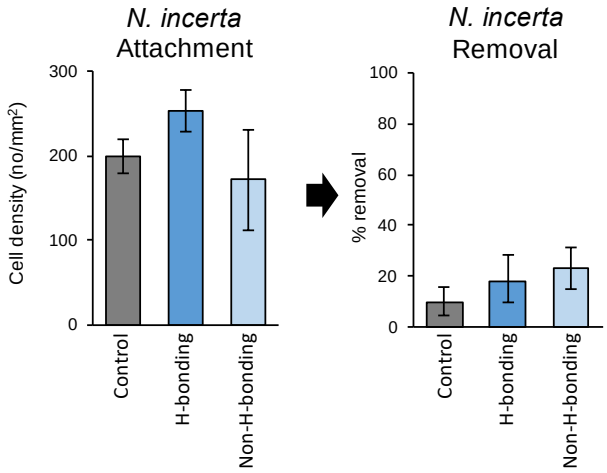

Figure 2-4. Fouling results for *Navicula incerta* indicate minimal effects due to the presence of amphiphilic peptoid chains; the PDMS scaffold dominated behavior. Error bars indicate 95% confidence limits.

In contrast to the results for *U. linza,* hydrogen bonding did not appear to drive or hinder fouling by *N. incerta* relative to the effects of the scaffold material (**Figure 2-4**). Initial attachment was lower on the non-H-bonding surface than on the H-bonding one, but neither were significantly different to the PDMS scaffold ($F_{2,132} = 4.3$; $p<0.05$). There was no difference in removal from the three surfaces when exposed to a shear stress of 28 Pa ($F_{2,132} = 1.3$; $p>0.05$) and fouling release was relatively low under this flow regime. Previous work has indicated that the initial attachment of diatoms depends largely on the properties of the SABC into which the peptoid side chains are incorporated. This has been demonstrated in the superior performance of poly(ethylene oxide)-based peptoid coatings compared to their PDMS-based counterparts.[23] As a result, the similarities between samples can be attributed to the scaffold polymer rather than the H-bonding and non-H-bonding peptoid side chains.

The results for *U. linza* and *N. incerta* correlate with those seen in previous experiments using peptides and peptoids;[23] while settlement of *U. linza* spores was higher on the non-H-bonding peptoids in both studies, the same coatings showed superior fouling-release efficacy and ultimately better resistance to permanent adhesion. Because the H-bonding and non-H-bonding materials all maintained similar macroscale hydrophilicity, the presence of peptide-like hydrogen bond donors must result in a microscale physicochemical change that substantially alters the underwater interface and its interactions with fouling organisms.

The chemical structure of surfaces can be investigated using sum frequency generation (SFG) vibrational spectroscopy, a second-order nonlinear optical spectroscopic technique.[33-35, 45-49] The surface sensitivity of the SFG spectroscopy comes from its selection rule, wherein only a medium with no inversion symmetry can generate SFG signal. Because symmetry is broken at interfaces but not in the bulk, SFG signals can be generated with surface specificity in the topmost surface layer.[50] SFG has been developed into a powerful tool to investigate many surfaces and interfaces, including polymer surfaces in water.[36-42]

SFG surface analysis of the H-bonding and non-H-bonding peptoid materials underwater indicates that water binding strength may be responsible for the observed differences in fouling behavior for *U. linza* (**Figure 2-5**).

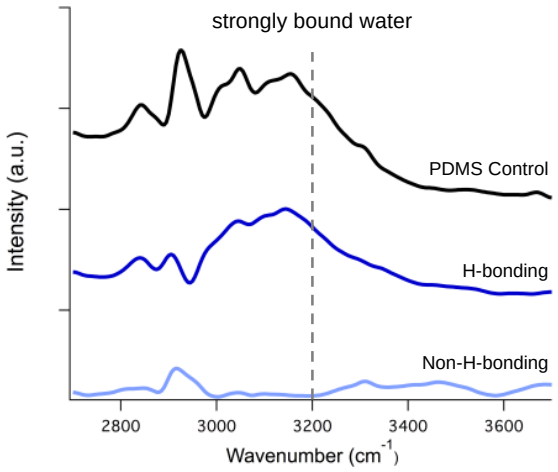

Figure 2-5. SFG spectra taken underwater show varying intensities for strong water bonding at 3200 cm^{-1} as indicated by the dashed line. The H-bonding sample and PDMS control both show highly ordered water at the interface, while the non-H-bonding sample shows little ordering. Spectra are vertically offset for clarity, and smoothed with 5-point averaging.

Strongly hydrophilic or hydrophobic surfaces can induce the organization of water molecules near the surface into strongly ordered structures, where interfacial water molecules align and therein emit strong SFG signals.[51-53] This tightly bound, strongly ordered water is visible as broad peaks centered near 3200 cm^{-1} for the H-bonding peptoid and the PDMS-based control (lacking peptoid side chains), but not for the non-H-bonding peptoid. These findings could explain the reduced settlement of *U. linza* on the H-bonding peptoid, as tightly bound water partially shields the surface from spores. However, upon displacement of the water followed by *U. linza* settlement and growth, stronger interactions between the organism and the surface are high enough to resist removal. Conversely, the non-H-bonding peptoid that lacked water structuring showed higher *U. linza* settlement, but the sporelings were only weakly bound to the surface as indicated by its 97% fouling release.

The formation of a structured water layer for the H-bonding peptoid material, but not for its non-H-bonding analogue, seems to be due primarily to hydrogen bond donation rather than differences in surface energy; contact angle results indicate similar

hydrophilicity for both peptoid materials, but greater hydrophobicity for the non-functionalized control (**Figure A6**), and SFG spectroscopy indicates that when immersed in water both peptoid chains were present at the coating surface (**Figure A8**). Many antifouling coatings rely on the presence of a hydration layer to prevent settlement of proteins or cells. Zwitterionic materials in particular have been shown to induce water structuring, which prevents settlement of fouling species.[54] However, for the peptoid-based materials that target both antifouling and fouling release properties, the moderately improved strength of the hydration layer may come at the cost of increased affinity for some fouling species such as *U. linza*.

Interestingly, the hydrophobic PDMS control showed high ordering of water despite lacking hydrophilic groups, but similar hydrophobic surfaces have already been shown to enhance water ordering in SFG measurements.[51, 55] Furthermore, the effects of this ordering are similar to those for the H-bonding material: fouling results for *U. linza* show similarly low settlement as well as poor fouling release. Prior work has shown that these amphiphilic peptoid side chains are most successful when used to strengthen the antifouling mechanism of the host polymer. The incorporation of the H-bonding peptoid amphiphile into a PDMS-based scaffold polymer, which is designed for fouling release rather than fouling resistance, reduced *U. linza* settlement at the expense of release. The presence of the non-H-bonding amphiphile, despite having a higher spore settlement density than its H-bonding analogue, enhanced fouling release of *U. linza* sporelings from the PDMS-based scaffold to over 97%. Therefore, the non-H-bonding amphiphile can be considered the superior candidate for resisting fouling algae on fouling-release coatings such as PDMS.

2.4 Conclusions

Peptoid-based materials have shown promise as marine antifouling coatings due to their versatility, leveraging control over a large number of chemical functionalities as well as their positions relative to each other. Despite their similar attributes, peptide-containing materials have failed to match the success of their peptoid analogues.[23] The primary cause of this difference was suspected to have been related to the hydrogen bond donor present in the secondary amide on the peptide backbone, but peptide chirality also has been known to play a role in cell attachment and could not be overlooked.[5, 56] The development of a hydrogen-bonding peptoid that inherently lacks chirality (and therein secondary structure) allowed this study to focus on the role hydrogen bonding plays in the attachment and release of fouling algae. Results of the biofouling assays carried out with the H-bonding and non-H-bonding peptoids have indicated that hydrogen bonding, rather than secondary structure, largely determined the differences seen between similar peptide and peptoid coating components.

Further characterization of the surface with SFG suggested that H-bonding peptoids are surrounded by a highly-ordered water layer that reduced the settlement density of spores of *U. linza*. However, the attachment strength of the sporelings was stronger on these surfaces than on the non H-bonding surfaces, which proved to be the better fouling-release surface and had a cleaner surface after exposure to hydrodynamic removal forces. This suggests that once a spore penetrated the water layer and adhered to the material, its attachment strength was enhanced by the hydrogen bonds present at the surface. Many antifouling coatings are understood to function by the formation of a hydration layer (e.g. PEO-based materials); maximizing hydrophilicity without the use of hydrogen bond

donors would be expected to improve the combined fouling resistance and release of algal species such as *U. linza*. In contrast, the adhesion of diatoms to the peptoid-containing coatings did not appear to be affected by hydrogen bonding and it is likely that attachment was largely determined by the PDMS scaffold polymer. Future studies should be performed to verify whether these findings could be extrapolated to coatings designed primarily according to antifouling (rather than fouling-release) mechanisms.

2.5 Acknowledgements

The authors gratefully acknowledge financial support by the Office of Naval Research (ONR) from **Awards N00014-17-1-2047**, **N00014-13-1-0633**, **N00014-13-1-0634**, **N00014-16-1-3115**, **N00014-16-1-2960**, **N00014-16-1-2988**, and **N00014-16-1-3125**. M.E.B and A.L.P gratefully acknowledge the National Science Foundation (NSF) for graduate fellowships. The authors also made use of facilities through the Molecular Foundry, a Lawrence Berkeley National Laboratory User Facility supported by the Office of Science, Office of Basic Energy Sciences, U.S. Department of Energy, under Contract DE-AC02-05CH11231. The authors thank Rachel Behrens for assistance with mass spectrometry and gratefully acknowledge the use of shared experimental facilities supported by the NSF MRSEC Program under Awards No. DMR-1720256 and DMR-1719875, members of the NSF-funded Materials Research Facilities Network at UC Santa Barbara and Cornell, respectively.

2.6 Appendix A

2.6.1 Peptoid and peptide structure comparison

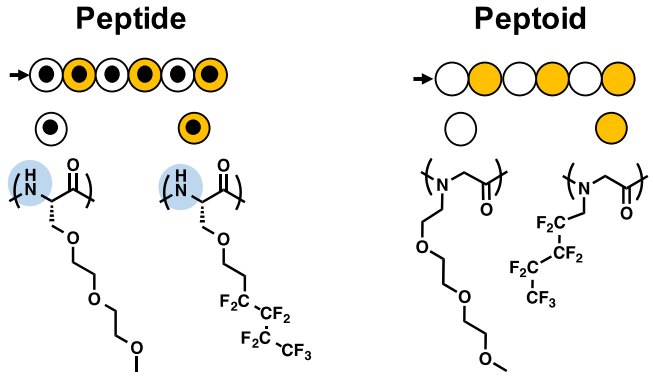

Figure A1. Previous work by Patterson, et al[23] compared analogous peptide and peptoid side chains. Peptides contain hydrogen bond acceptors (blue) as well as a chiral carbon center that enables secondary structure, features not present in the analogous peptoids.

2.6.2 Peptoid synthesis

Synthesis was conducted with slight modifications to published procedures[21, 23, 27] on a Prelude synthesizer (Protein Technologies, Inc.). Rink amide MBHA resin (0.80 mmol g^{-1} loading) was deprotected with a 4-methylpiperidine solution (20% (v/v) in DMF) for 20 minutes, stirring by bubbling with N_2 and immediately followed by DMF washing. The free amine chain end was acylated using 1.0 mL of bromoacetic acid (0.6 M in DMF) and 0.15 mL of N,N-diisopropylcarbodiimide (DIC) solution (59% (v/v) in DMF) for 20 min. The reagents were then removed and the resin was washed with DMF.

Nucleophilic displacement of the bromide chain with submonomers was performed for 1 h in all cases. Displacement with 2-[2-(methoxyethyl)ethoxy]ethanamine and the amide-linked triethylene glycol amine were done at room temperature on the Prelude synthesizer, but displacement with 1H,1H-perfluoropentylamine necessitated stirring at 50°C (in vials). After the monomer solution was drained from the resin using the Prelude, the resin was again washed with DMF before repeating acylation and displacement according to the desired sequences (**Figure A2**). Both peptoid sequences were functionalized with a thiol endgroup using S-trityl-3-mercaptopropionic acid and N,N'-diisopropylcarbodiimide (DIC) (both 0.4 M and 59% v/v respectively in DMF). 2 mL of solution per 50µmol peptoid were added, bubbled with N_2 for 30 minutes, and washed with DMF.

Peptoid chains were cleaved from the resin using a trifluoroacetic acid (TFA) cleavage cocktail (47.5% TFA, 47.5% DCM, 2.5% water, 2.5% triisopropylsilane (TIPS); 50 mL per 350 µmol peptoid) for 10 minutes, cleaving the peptoids from the resin and deprotecting the thiol. The cocktail was then evaporated on a Genevac EZ-2 Elite centrifugal evaporator.

The cleaved peptoids were dissolved in 1:1 acetonitrile/water mixtures, lyophilized, then redissolved in 1:1 acetonitrile/water and washed with hexanes to remove TIPS. The second lyophilization yielded pure peptoid products.

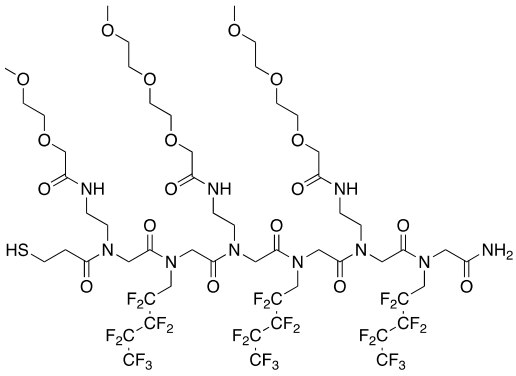

H-bonding peptoid

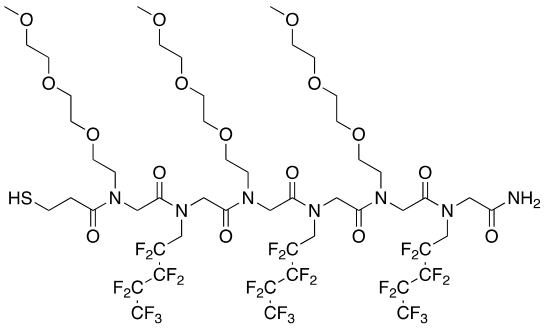

non-H-bonding peptoid

	Exact Mass (g/mol)	
	Theoretical	Measured
H-bonding peptoid	1752.48	1752.57
non-H-bonding peptoid	1581.42	1581.45

Figure A2. Full structures of synthesized peptoids.

2.6.3 PS-P(DMS/VMS)-PS synthesis

Synthesis of the PDMS-based triblock copolymer followed previously described protocols.[21, 23, 27] Anionic polymerization of dried styrene was performed under inert atmosphere in benzene using *sec*-butyl lithium as initiator. Chain-extending siloxane polymerization was initiated by the addition of D3 to the active reaction mixture. After 24 hours when the color of the living styrene anion had completely disappeared, dry THF was added to promote the polymerization. After another 2 hours, V3 in THF was added via syringe pump over 48 hours. The reaction was then allowed to continue for 24 hours.

During the reaction, aliquots were analyzed via GPC and ^{1}H-NMR until reaching the desired conversion. The reaction was terminated by coupling active chain ends using dichlorodimethylsilane in THF and stirring for 16 hours, after which excess coupling agent was added continuously over 24 hours to ensure completion. The final triblock product was precipitated in a 90/10 (v/v) mixture of methanol and water, filtered, and dried. Final molecular weight of the polymer was determined by GPC, while ^{1}H-NMR verified vinyl content.

Sample	M_n (kg/mol)	Đ
PS endblock	6.8†	1.03
PS-P(DMS/VMS) uncoupled diblock	45.9†	1.20
PS-P(DMS/VMS)-PS coupled triblock	6.8–78.2–6.8	1.26

†versus polystyrene standards (Cornell)

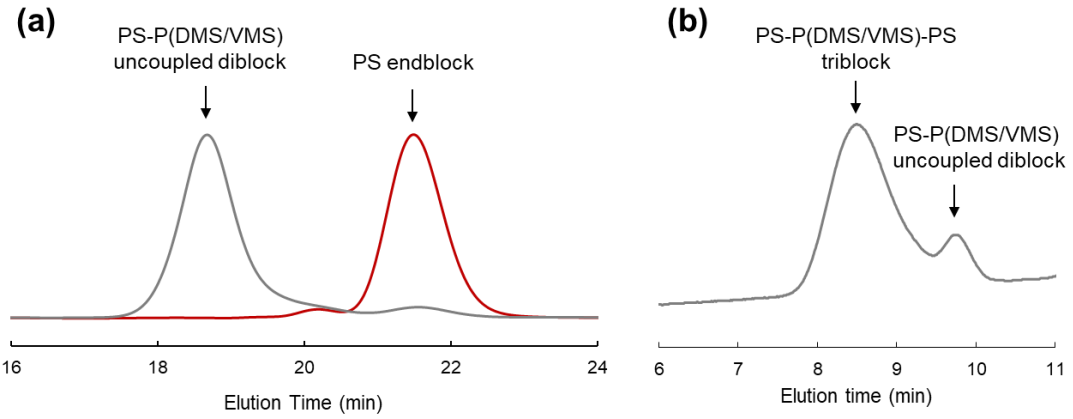

Figure A3. GPC traces for (a) uncoupled diblock and PS precursor (Cornell), and (b) final PS-P(DMS/VMS)-PS triblock copolymer after diblock coupling (UCSB).

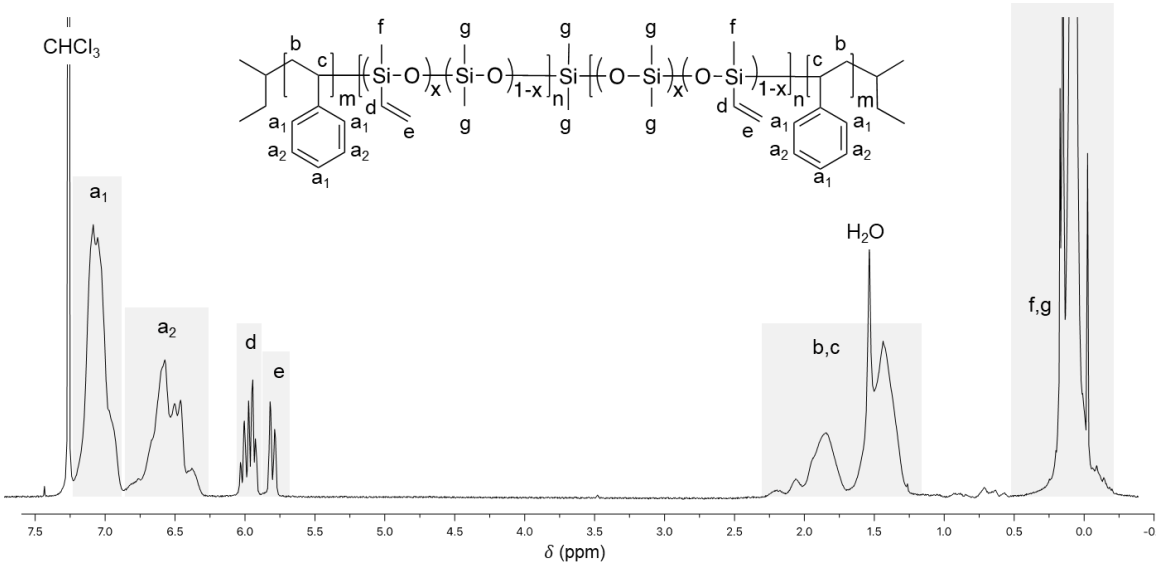

Figure A4. ^{1}H-NMR spectrum of the PS-P(DMS/VMS)-PS triblock copolymer.

2.6.4 Thiol–ene "click" of peptoid SABCs

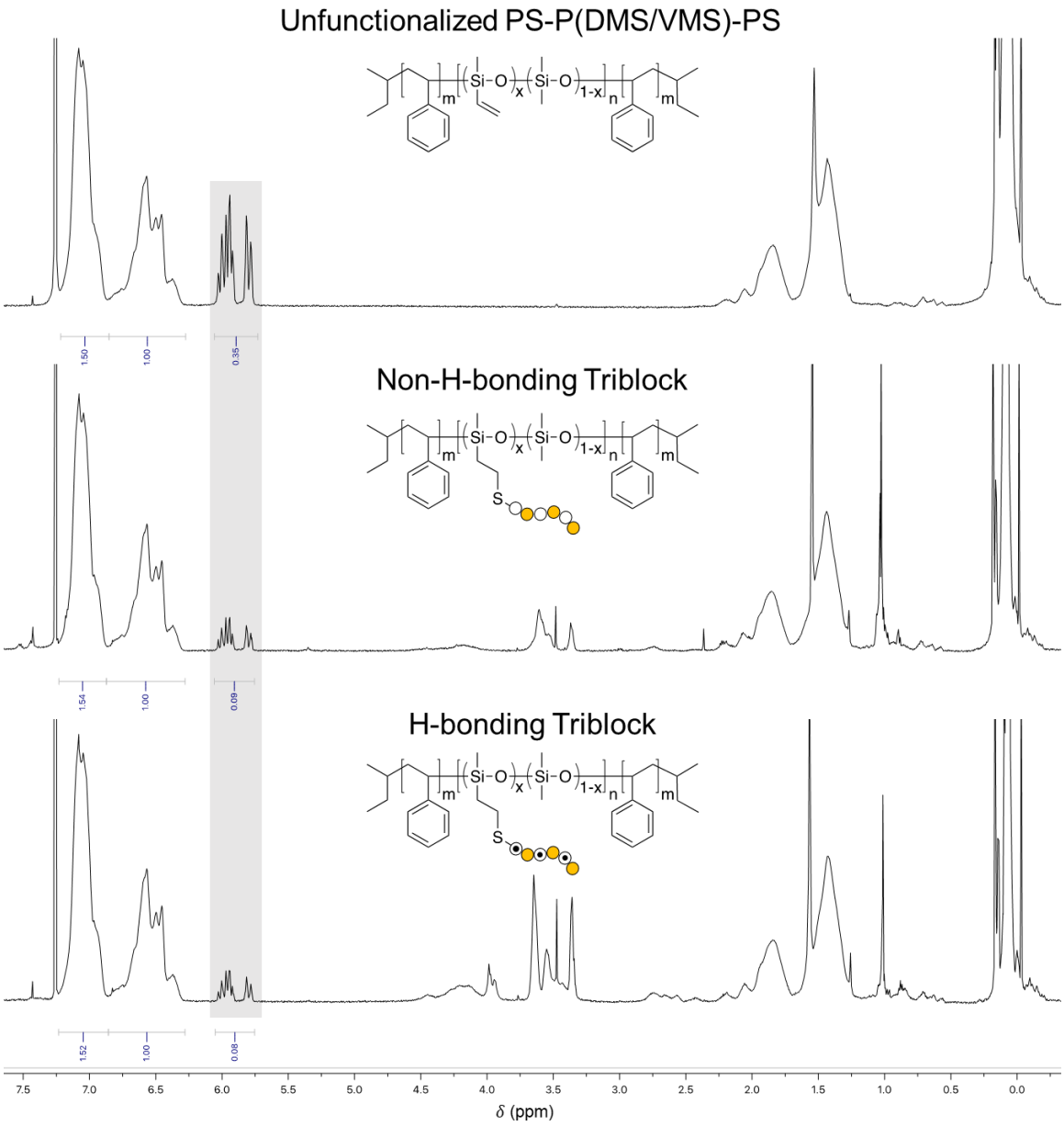

Figure A5. Changes in magnitude for vinyl protons relative to aromatic protons in ^{1}H-NMR indicate successful attachment of peptoid side chains. Steric hindrance associated with attachment limited completion to approximately 75%. Click completion was also associated with a change in solubility that precluded GPC measurements.

2.6.5 Captive bubble contact angle goniometry

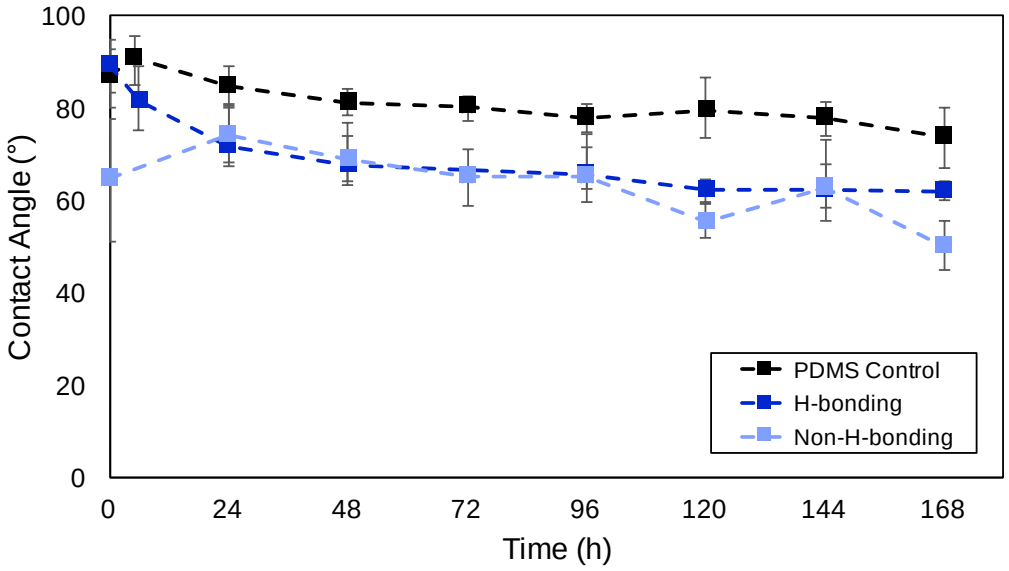

Figure A6. Contact angle goniometry indicates similar hydrophilicity for the H-bonding and non-H-bonding peptoid materials, while the control PDMS triblock copolymer has a slightly higher angle.

2.6.6 Supplemental SFG spectra

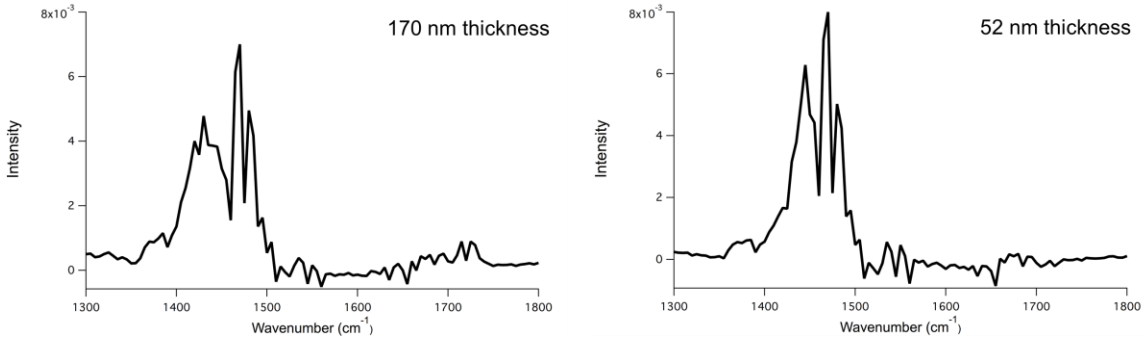

Figure A7. Representative SFG signals in air for two spin-coated H-bonding films show nearly identical signals despite differences in film thickness, indicating 52 nm is sufficiently thick.

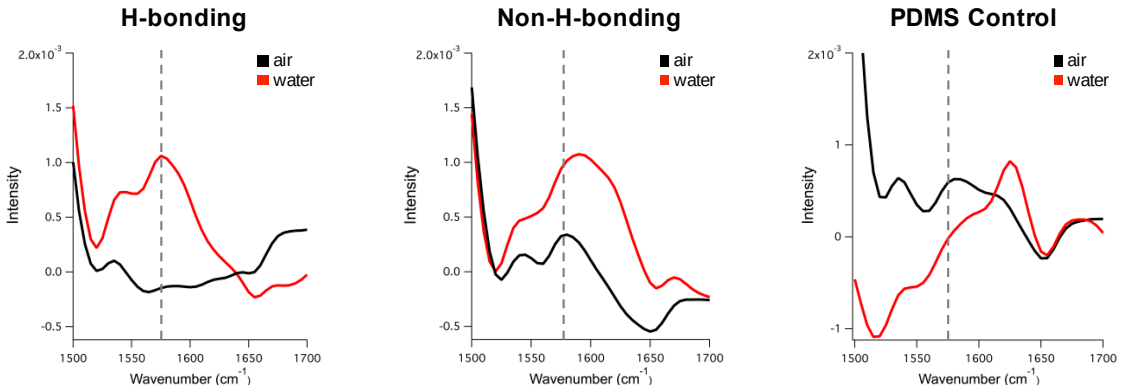

Figure A8. The presence of a broad amide bend peak near 1575 cm^{-1} underwater indicates the restructuring of peptoid side chains to the surface. Therefore, the lack of water structuring for the non-H-bonding film cannot be attributed to a lack of peptoid at the surface.

2.7 References

(1) Unabia, C. R. C.; Hadfield, M. G., Role of bacteria in larval settlement and metamorphosis of the polychaete Hydroides elegans. *Marine Biology* **1999,** *133* (1), 55-64. https://doi.org/10.1007/s002270050442

(2) Chambers, L. D.; Stokes, K. R.; Walsh, F. C.; Wood, R. J. K., Modern approaches to marine antifouling coatings. *Surf Coat Tech* **2006,** *201* (6), 3642-3652. https://doi.org/10.1016/j.surfcoat.2006.08.129

(3) Callow, J. A.; Callow, M. E., Trends in the development of environmentally friendly fouling-resistant marine coatings. *Nat Commun* **2011,** *2*, 244. https://doi.org/10.1038/ncomms1251

(4) Schultz, M. P.; Walker, J. M.; Steppe, C. N.; Flack, K. A., Impact of diatomaceous biofilms on the frictional drag of fouling-release coatings. *Biofouling* **2015,** *31* (9-10), 759-73. https://doi.org/10.1080/08927014.2015.1108407

(5) Schultz, M. P., Effects of coating roughness and biofouling on ship resistance and powering. *Biofouling* **2007,** *23* (5-6), 331-41. https://doi.org/10.1080/08927010701461974

(6) Banerjee, I.; Pangule, R. C.; Kane, R. S., Antifouling coatings: recent developments in the design of surfaces that prevent fouling by proteins, bacteria, and marine organisms. *Adv Mater* **2011,** *23* (6), 690-718. https://doi.org/10.1002/adma.201001215

(7) Lejars, M.; Margaillan, A.; Bressy, C., Fouling release coatings: a nontoxic alternative to biocidal antifouling coatings. *Chem Rev* **2012,** *112* (8), 4347-90. https://doi.org/10.1021/cr200350v

(8) Finnie, A. A.; Williams, D. N., Paint and Coatings Technology for the Control of Marine Fouling. *Biofouling* **2010,** *18*.

(9) Hellio, C.; Maréchal, J. P.; Da Gama, B. A. P.; Pereira, R. C.; Clare, A. S., Natural Marine Products with Antifouling Activities. In *Advances in Marine Antifouling Coatings and Technologies*, Hellio, C.; Yebra, D., Eds. Woodhead Publishing: 2009; pp 572-622. https://doi.org/10.1533/9781845696313.3.572

(10) Callow, J. A.; Callow, M. E., Trends in the Development of Environmentally Friendly Fouling-Resistant Marine Coatings. *Nature Communications* **2011,** *2*, 244. https://doi.org/10.1038/ncomms1251

(11) Yang, W. J.; Neoh, K. G.; Kang, E. T.; Teo, S. L. M.; Rittschof, D., Polymer brush coatings for combating marine biofouling. *Progress in Polymer Science* **2014,** *39* (5), 1017-1042. https://doi.org/10.1016/j.progpolymsci.2014.02.002

(12) Ekblad, T.; Bergstrom, G.; Ederth, T.; Conlan, S. L.; Mutton, R.; Clare, A. S.; Wang, S.; Liu, Y.; Zhao, Q.; D'Souza, F.; Donnelly, G. T.; Willemsen, P. R.; Pettitt, M. E.; Callow, M. E.; Callow, J. A.; Liedberg, B., Poly(ethylene glycol)-containing hydrogel surfaces for antifouling applications in marine and freshwater environments. *Biomacromolecules* **2008,** *9* (10), 2775-83. https://doi.org/10.1021/bm800547m

(13) Dobretsov, S.; Thomason, J. C., The development of marine biofilms on two commercial non-biocidal coatings: a comparison between silicone and fluoropolymer technologies. *Biofouling* **2011,** *27* (8), 869-80. https://doi.org/10.1080/08927014.2011.607233

(14) Amini, S.; Kolle, S.; Petrone, L.; Ahanotu, O.; Sunny, S.; Sutanto, C. N.; Hoon, S.; Cohen, L.; Weaver, J. C.; Aizenberg, J.; Vogel, N.; Miserez, A., Preventing Mussel Adhesion Using Lubricant-Infused Materials. *Science* **2017,** *357* (6352), 668-673. https://doi.org/10.1126/science.aai8977

(15) Hoipkemeier-Wilson, L.; Schumacher, J. F.; Carman, M. L.; Gibson, A. L.; Feinberg, A. W.; Callow, M. E.; Finlay, J. A.; Callow, J. A.; Brennan, A. B., Antifouling potential of lubricious, micro-engineered, PDMS elastomers against zoospores of the green fouling alga Ulva (Enteromorpha). *Biofouling* **2004,** *20* (1), 53-63. https://doi.org/10.1080/08927010410001662689

(16) Martinelli, E.; Gunes, D.; Wenning, B. M.; Ober, C. K.; Finlay, J. A.; Callow, M. E.; Callow, J. A.; Di Fino, A.; Clare, A. S.; Galli, G., Effects of surface-active block copolymers with oxyethylene and fluoroalkyl side chains on the antifouling performance of silicone-based films. *Biofouling* **2016,** *32* (1), 81-93. https://doi.org/10.1080/08927014.2015.1131822

(17) Hawkins, M. L.; Fay, F.; Rehel, K.; Linossier, I.; Grunlan, M. A., Bacteria and diatom resistance of silicones modified with PEO-silane amphiphiles. *Biofouling* **2014,** *30* (2), 247-58. https://doi.org/10.1080/08927014.2013.862235

(18) Gudipati, C. S.; Finlay, J. A.; Callow, J. A.; Callow, M. E.; Wooley, K. L., The antifouling and fouling-release performance of hyperbranched fluoropolymer (HBFP)-poly(ethylene glycol) (PEG) composite coatings evaluated by adsorption of biomacromolecules and the green fouling alga Ulva. *Langmuir* **2005,** *21* (7), 3044-53. https://doi.org/10.1021/la048015o

(19) Hellio, C.; Yebra, D., *Advances in Marine Antifouling Coatings and Technologies*. Elsevier: 2009.

(20) Krishnan, S.; Weinman, C. J.; Ober, C. K., Advances in polymers for anti-biofouling surfaces. *Journal of Materials Chemistry* **2008,** *18* (29), 3405-3413. https://doi.org/10.1039/b801491d

(21) van Zoelen, W.; Buss, H. G.; Ellebracht, N. C.; Lynd, N. A.; Fischer, D. A.; Finlay, J.; Hill, S.; Callow, M. E.; Callow, J. A.; Kramer, E. J.; Zuckermann, R. N.; Segalman, R. A., Sequence of Hydrophobic and Hydrophilic Residues in Amphiphilic Polymer Coatings Affects Surface Structure and Marine Antifouling/Fouling Release Properties. *ACS Macro Letters* **2014,** *3* (4), 364-368. https://doi.org/10.1021/mz500090n

(22) Calabrese, D. R.; Wenning, B.; Finlay, J. A.; Callow, M. E.; Callow, J. A.; Fischer, D.; Ober, C. K., Amphiphilic Oligopeptides Grafted to PDMS-Based Diblock Copolymers for Use in Antifouling and Fouling Release Coatings. *Polymers for Advanced Technologies* **2015,** *26* (7), 829-836. https://doi.org/doi:10.1002/pat.3515

(23) Patterson, A. L.; Wenning, B.; Rizis, G.; Calabrese, D. R.; Finlay, J. A.; Franco, S. C.; Zuckermann, R. N.; Clare, A. S.; Kramer, E. J.; Ober, C. K.; Segalman, R. A., Role of Backbone Chemistry and Monomer Sequence in Amphiphilic Oligopeptide- and Oligopeptoid-Functionalized PDMS- and PEO-Based Block Copolymers for Marine Antifouling and Fouling Release Coatings. *Macromolecules* **2017,** *50* (7), 2656-2667. https://doi.org/10.1021/acs.macromol.6b02505

(24) Calabrese, D. R.; Wenning, B. M.; Buss, H.; Finlay, J. A.; Fischer, D.; Clare, A. S.; Segalman, R. A.; Ober, C. K., Oligopeptide-Modified Hydrophobic and Hydrophilic Polymers as Antifouling Coatings. *Green Materials* **2017,** *5* (1), 31-43. https://doi.org/10.1680/jgrma.17.00006

(25) Weinman, C. J.; Finlay, J. A.; Park, D.; Paik, M. Y.; Krishnan, S.; Sundaram, H. S.; Dimitriou, M.; Sohn, K. E.; Callow, M. E.; Callow, J. A.; Handlin, D. L.; Willis, C. L.; Kramer, E. J.; Ober, C. K., ABC triblock surface active block copolymer with grafted ethoxylated fluoroalkyl amphiphilic side chains for marine antifouling/fouling-release applications. *Langmuir* **2009,** *25* (20), 12266-74. https://doi.org/10.1021/la901654q

(26) Krishnan, S.; Ayothi, R.; Hexemer, A.; Finlay, J. A.; Sohn, K. E.; Perry, R.; Ober, C. K.; Kramer, E. J.; Callow, M. E.; Callow, J. A.; Fischer, D. A., Anti-biofouling properties of comblike block copolymers with amphiphilic side chains. *Langmuir* **2006,** *22* (11), 5075-86. https://doi.org/10.1021/la052978l

(27) Zuckermann, R. N.; Kerr, J. M.; Kent, S. B. H.; Moos, W. H., Efficient Method for the Preparation of Peptoids [Oligo(N-Substituted Glycines)] by Submonomer Solid-Phase Synthesis. *Journal of the American Chemical Society* **1992,** *114* (26), 10646-10647. https://doi.org/10.1021/ja00052a076

(28) Zuckermann, R. N., Peptoid origins. *Biopolymers* **2011,** *96* (5), 545-55. https://doi.org/10.1002/bip.21573

(29) Figliozzi, G. M.; Goldsmith, R.; Ng, S. C.; Banville, S. C.; Zuckermann, R. N., Synthesis of N-substituted Glycine Peptoid Libraries. In *Methods in Enzymology*, Academic Press: 1996; Vol. 267, pp 437-447. https://doi.org/10.1016/S0076-6879(96)67027-X

(30) Sundaram, H. S.; Cho, Y.; Dimitriou, M. D.; Weinman, C. J.; Finlay, J. A.; Cone, G.; Callow, M. E.; Callow, J. A.; Kramer, E. J.; Ober, C. K., Fluorine-free mixed amphiphilic polymers based on PDMS and PEG side chains for fouling release applications. *Biofouling* **2011,** *27* (6), 589-602. https://doi.org/10.1080/08927014.2011.587662

(31) Finlay, J. A.; Callow, M. E.; Ista, L. K.; Lopez, G. P.; Callow, J. A., The influence of surface wettability on the adhesion strength of settled spores of the green alga enteromorpha and the diatom amphora. *Integr Comp Biol* **2002,** *42* (6), 1116-22. https://doi.org/10.1093/icb/42.6.1116

(32) Schultz, M. P.; Finlay, J. A.; Callow, M. E.; Callow, J. A., A turbulent channel flow apparatus for the determination of the adhesion strength of microfouling organisms. *Biofouling* **2000,** *15* (4), 243-+. https://doi.org/10.1080/08927010009386315

(33) Perry, A.; Neipert, C.; Space, B.; Moore, P. B., Theoretical modeling of interface specific vibrational spectroscopy: methods and applications to aqueous interfaces. *Chem Rev* **2006,** *106* (4), 1234-58. https://doi.org/10.1021/cr040379y

(34) Chen, Z.; Shen, Y. R.; Somorjai, G. A., Studies of polymer surfaces by sum frequency generation vibrational spectroscopy. *Annu Rev Phys Chem* **2002,** *53* (1), 437-65. https://doi.org/10.1146/annurev.physchem.53.091801.115126

(35) Shen, Y. R., Optical Second Harmonic Generation at Interfaces. *Annual Review of Physical Chemistry* **1989,** *40* (1), 327-350. https://doi.org/10.1146/annurev.pc.40.100189.001551

(36) Chen, C.; Wang, J.; Chen, Z., Surface restructuring behavior of various types of poly(dimethylsiloxane) in water detected by SFG. *Langmuir* **2004,** *20* (23), 10186-93. https://doi.org/10.1021/la049327u

(37) Hankett, J. M.; Liu, Y. W.; Zhang, X. X.; Zhang, C.; Chen, Z., Molecular level studies of polymer behaviors at the water interface using sum frequency generation vibrational spectroscopy. *J Polym Sci Pol Phys* **2013,** *51* (5), 311-328. https://doi.org/10.1002/polb.23221

(38) Hankett, J. M.; Lu, X.; Liu, Y.; Seeley, E.; Chen, Z., Interfacial molecular restructuring of plasticized polymers in water. *Phys Chem Chem Phys* **2014,** *16* (37), 20097-106. https://doi.org/10.1039/c4cp03206c

(39) Wang, J.; Paszti, Z.; Even, M. A.; Chen, Z., Measuring polymer surface ordering differences in air and water by sum frequency generation vibrational spectroscopy. *J Am Chem Soc* **2002,** *124* (24), 7016-23. https://doi.org/10.1021/ja012387r

(40) Wang, J.; Woodcock, S. E.; Buck, S. M.; Chen, C.; Chen, Z., Different surface-restructuring behaviors of poly(methacrylate)s detected by SFG in water. *J Am Chem Soc* **2001,** *123* (38), 9470-1. https://doi.org/10.1021/ja0164071

(41) Leng, C.; Sun, S.; Zhang, K.; Jiang, S.; Chen, Z., Molecular level studies on interfacial hydration of zwitterionic and other antifouling polymers in situ. *Acta Biomater* **2016,** *40*, 6-15. https://doi.org/10.1016/j.actbio.2016.02.030

(42) Liu, X.; Leng, C.; Yu, L.; He, K.; Brown, L. J.; Chen, Z.; Cho, J.; Wang, D., Ion-specific oil repellency of polyelectrolyte multilayers in water: molecular insights into the hydrophilicity of charged surfaces. *Angew Chem Int Ed Engl* **2015,** *54* (16), 4851-6. https://doi.org/10.1002/anie.201411992

(43) Callow, J. A.; Callow, M. E.; Ista, L. K.; Lopez, G.; Chaudhury, M. K., The influence of surface energy on the wetting behaviour of the spore adhesive of the marine alga Ulva linza (synonym Enteromorpha linza). *J R Soc Interface* **2005,** *2* (4), 319-25. https://doi.org/10.1098/rsif.2005.0041

(44) Thome, I.; Pettitt, M. E.; Callow, M. E.; Callow, J. A.; Grunze, M.; Rosenhahn, A., Conditioning of surfaces by macromolecules and its implication for the settlement of zoospores of the green alga Ulva linza. *Biofouling* **2012,** *28* (5), 501-10. https://doi.org/10.1080/08927014.2012.689288

(45) Jung, S. Y.; Lim, S. M.; Albertorio, F.; Kim, G.; Gurau, M. C.; Yang, R. D.; Holden, M. A.; Cremer, P. S., The Vroman effect: a molecular level description of fibrinogen displacement. *J Am Chem Soc* **2003,** *125* (42), 12782-6. https://doi.org/10.1021/ja037263o

(46) Lutz, H.; Jaeger, V.; Schmuser, L.; Bonn, M.; Pfaendtner, J.; Weidner, T., The Structure of the Diatom Silaffin Peptide R5 within Freestanding Two-Dimensional

Biosilica Sheets. *Angew Chem Int Ed Engl* **2017,** *56* (28), 8277-8280. https://doi.org/10.1002/anie.201702707

(47) Samson, J. S.; Scheu, R.; Smolentsev, N.; Rick, S. W.; Roke, S., Sum frequency spectroscopy of the hydrophobic nanodroplet/water interface: Absence of hydroxyl ion and dangling OH bond signatures. *Chemical Physics Letters* **2014,** *615*, 124-131. https://doi.org/10.1016/j.cplett.2014.09.034

(48) Tan, J.; Zhang, B.; Luo, Y.; Ye, S., Ultrafast Vibrational Dynamics of Membrane-Bound Peptides at the Lipid Bilayer/Water Interface. *Angew Chem Int Ed Engl* **2017,** *56* (42), 12977-12981. https://doi.org/10.1002/anie.201706996

(49) Ding, B.; Jasensky, J.; Li, Y.; Chen, Z., Engineering and Characterization of Peptides and Proteins at Surfaces and Interfaces: A Case Study in Surface-Sensitive Vibrational Spectroscopy. *Acc Chem Res* **2016,** *49* (6), 1149-57. https://doi.org/10.1021/acs.accounts.6b00091

(50) Raschke, M. B.; Shen, Y. R., Nonlinear optical spectroscopy of solid interfaces. *Curr Opin Solid St M* **2004,** *8* (5), 343-352. https://doi.org/10.1016/j.cossms.2005.01.002

(51) Gragson, D. E.; Richmond, G. L., Probing the structure of water molecules at an oil/water interface in the presence of a charged soluble surfactant through isotopic dilution studies. *J Phys Chem B* **1998,** *102* (3), 569-576. https://doi.org/10.1021/jp972444w

(52) Uosaki, K.; Yano, T.; Nihonyanagi, S., Interfacial water structure at as-prepared and UV-Induced hydrophilic TiO2 surfaces studied by sum frequency generation spectroscopy and quartz crystal microbalance. *J Phys Chem B* **2004,** *108* (50), 19086-19088. https://doi.org/10.1021/jp045173f

(53) Du, Q.; Freysz, E.; Shen, Y. R., Surface vibrational spectroscopic studies of hydrogen bonding and hydrophobicity. *Science* **1994,** *264* (5160), 826-8. https://doi.org/10.1126/science.264.5160.826

(54) Leng, C.; Han, X. F.; Shao, Q.; Zhu, Y. H.; Li, Y. T.; Jiang, S. Y.; Chen, Z., In Situ Probing of the Surface Hydration of Zwitterionic Polymer Brushes: Structural and Environmental Effects. *J Phys Chem C* **2014,** *118* (29), 15840-15845. https://doi.org/10.1021/jp504293r

(55) Strazdaite, S.; Versluis, J.; Backus, E. H.; Bakker, H. J., Enhanced ordering of water at hydrophobic surfaces. *J Chem Phys* **2014,** *140* (5), 054711. https://doi.org/10.1063/1.4863558

(56) Ochsenhirt, S. E.; Kokkoli, E.; McCarthy, J. B.; Tirrell, M., Effect of RGD secondary structure and the synergy site PHSRN on cell adhesion, spreading and specific integrin engagement. *Biomaterials* **2006,** *27* (20), 3863-74. https://doi.org/10.1016/j.biomaterials.2005.12.012

Chapter 3
Effects of amphiphilic polypeptoid side chains on hydrated polymer surface chemistry and hydrophilicity[2]

Polymers are commonly used in applications requiring long-term exposure to water and aqueous mixtures including as water purification membranes, marine antifouling coatings, and medical implants. Because polymer surfaces restructure in response to the surrounding environment, *in situ* characterization is crucial for providing an accurate understanding of the surface chemistry in use conditions. To investigate the effects of surface-active side chains on polymer surface chemistry and resultant interactions with interfacial water (i.e., water sorption), we present synchrotron APXPS studies performed on PEO- and PDMS-based polymer surfaces modified with amphiphilic polypeptoid side chains previously demonstrated to be efficacious in marine fouling prevention and removal. The polymer backbone and environmental conditions were found to affect polypeptoid surface presentation: the PEO-peptoid copolymers showed significant polypeptoid content in both vacuum and hydrated conditions due to fluorinated polypeptoid monomers that drive

[2] Pinar Aydogan Gokturk assisted in APXPS measurements, Audra DeStefano and Amanda Leonardi synthesized the PDMS-based sample, and Wendy van Zoelen designed the polypeptoid sequence and synthesized the PEO-based sample.

surface segregation under vacuum, while the modified PDMS-based copolymer showed increased polypeptoid content in hydrated conditions due to hydrophilicity of the ether monomers and polypeptoid backbone. Polypeptoids were found to bind approximately 2.8 water molecules per monomer unit in both copolymers, and the PEO-peptoid surface showed substantial water sorption that suggests a surface with a less well-defined water/polymer interface typical of antifouling polymers. This work suggests that side chains are ideal for tuning water affinity without altering the base polymer composition, provided that surface-driving groups are present to ensure activity at the interface. These types of systematic modifications will allow for novel polymers that maximize bound water at the surface and can deliver surface-active groups to the surface to improve effectiveness of polymer materials.

3.1 Introduction

Polymers used in underwater environments in applications ranging from water filtration to medical implants must elicit appropriate responses at interfaces with complex aqueous mixtures containing ionic and organic solutes. Among these challenges, marine fouling, or the undesirable settlement and colonization of marine organisms onto manmade surfaces, is a problem that affects all ocean-going vessels and begins nearly immediately upon immersion. After initial conditioning, bacteria and microalgae settle and form a biofilm that facilitates further fouling by larger species, including mussels, barnacles, and algae.[1–3] These larger foulers particularly disrupt the hydrodynamic efficiency of ships (dramatically increasing costs for transport) and require frequent cleaning, with an estimated cost of $150 billion USD annually for the worldwide marine industry.[4] Further

environmental concerns arise when fouled ships transport non-native species to local ecosystems, as has been observed with the marine mussel *Mytella strigata* in southeast Asia.[5,6]

For both marine antifouling and other underwater applications, non-toxic polymer surfaces represent an environmentally benign solution to fouling by reducing the favorability of solute or biomolecule adsorption or the adhesion of larger organisms.[7] For these materials, accurate characterization of the underwater surface is essential for designing novel effective coatings. Many antifouling polymers are designed to interact cooperatively with water at the surface to preclude settlement-mediating interactions with solutes or biomolecules. Hydrophilic chemistries are integral to this class of materials, with the majority of them containing poly(ethylene oxide) (PEO), though alternatives such as zwitterionic polymers, polysaccharides, and hydrogels are being pursued.[2,8–10] Conversely, low surface energy coatings, such as those made from polydimethylsiloxane (PDMS) and fluoropolymers,[2,8,11] reduce the favorability of adhesion to the surface. For marine antifouling applications, these "fouling release" coatings leverage hydrodynamic shear forces to release weakly adhered organisms.

Amphiphilic materials that incorporate both hydrophilic and hydrophobic chemistries are known to be particularly effective at preventing fouling, yet are also likely to surface reconstruct significantly from the dry conditions in which they are normally processed to aqueous marine or biological conditions, making design and characterization of real coatings a challenge.[12–15] These coatings often involve modification of rubbery PEO-based[16–18] and siloxane[19–23] polymers to form heterogeneous surfaces with domains on the micro- or nano-scale that prevent wide-scale settlement. While fluorinated, siloxane,

and ether chemistries are prevalent in amphiphilic coatings,[24–26] other modifiers range from hydrophilic to charged chemistries such as polyvinylpyrrolidone[27] and zwitterions.[28,29] Sequence-controlled chemistries impart additional ability to control the length scale of amphiphilicity. Polypeptoids are a structural analog of peptides with functional groups linked to the backbone via the amide nitrogen rather than the alpha carbon. Like peptides, they can be synthetically produced, and their submonomer synthesis allows for incorporation of a wider array of functional chemistries at significantly increased scale (gram scale).[30,31] Polypeptoids, which have improved stability against proteolysis relative to peptides, are also biocompatible and known to resist protein adsorption and cell attachment in medical applications.[32,33] Polypeptoids with fluorinated and ether-containing monomers have shown significant resistance to diatom and algae settlement when incorporated into PEO and PDMS block copolymers.[18,34] Further studies comparing hydrogen bonding and non-hydrogen bonding amphiphilic polypeptoids suggest that this performance is due to a combination of hydrophilicity with a the lack of hydrogen bond donors in the polypeptoid backbone.[35] Clearly, even minor changes in surface chemistry may affect a material's ability to prevent fouling.

Surface characterization is thus critical for identifying the relationship between the surface chemistry that is presented in the marine environment and fouling properties. Because rubbery polymer surfaces restructure quickly in response to the surrounding environment, *in situ* characterization is crucial for providing an accurate understanding of the surface chemistry in ambient conditions.[8,36] Water interactions are also known to directly affect adsorption and adhesion, but are challenging to characterize particularly at heterogeneous surfaces.[37] Contact angle goniometry and atomic force microscopy are

useful for qualifying surface energy and topography but lack chemical resolution. Vibrational spectroscopy techniques, particularly sum-frequency generation (SFG), have been useful for identifying chemical functionalities at the surface in conditions ranging from ambient to underwater, with the further ability of identifying hydrogen-bonded water at the interface.[13,36,38] SFG has shown that the relative surface coverage of hydrophilic monomers in amphiphilic polypeptoid-containing surfaces depends on the sequence and hydrophobic monomer content of the polypeptoids.[13] Furthermore, polypeptoid-containing surfaces were found to instigate ordering of strongly hydrogen-bonded water when hydrogen bond donors were present,[35] and that this ordering correlates with low contact angles.[13] However, techniques that quantitatively indicate surface composition, such as X-ray photoelectron spectroscopy (XPS), Auger Electron Spectroscopy (AES), and near edge X-ray absorption fine structure (NEXAFS) are usually performed *ex situ* in high vacuum conditions.[39]

Ambient pressure X-ray photoelectron spectroscopy (APXPS), like conventional XPS, provides quantitative information on surface chemistry but also allows for *in situ* measurements with water vapor.[40–42] Further, synchrotron X-ray sources for APXPS enable exposure to X-rays with tunable photon energy; depth profiling can be performed by decreasing or increasing the photon energy of incident X-rays to probe nearer or further from the surface, respectively. Soft X-ray ($h\nu$ < 2 keV) APXPS is thus useful for probing the top few nanometers of surface under pressures of up to 2-3 Torr.[43] Tender X-ray APXPS, which typically leverages X-rays between 2-7 keV, enables probing on the order of tens of nanometers into the film and through a denser vapor phase.[44] Several end stations

are equipped to perform experiments at 20 Torr water vapor pressure, at which point water vapor reaches saturation and condenses or a liquid phase of water can be maintained.[43,44]

APXPS has grown from characterizing surface chemistry and interactions for applications like catalysis and surface science[45–47] to include fields such as electrochemistry,[44,48,49] environmental science,[45,50–52] biology,[53,54] and polymer and membrane sciences.[43,55,56] It has shown potential for characterizing water interactions with the surfaces of varying materials, but nearly all studies have been performed on crystalline, well-defined substrates with minimal restructuring capability. For instance, water adsorption and dissociation has been explored on metal and oxide surfaces such as copper,[41,57] silver,[58] TiO_2,[41,42] SiO_2,[51] Al_2O_3,[59] and MgO.[60] Molecular adsorption of water is known to occur on organic surfaces, from alcohol and carboxylic acid-terminated self-assembled monolayers to highly crosslinked model layer-by-layer polyamide membranes.[53,55,56] Unsurprisingly, polymer surfaces interact differently with water, with large degrees of water uptake seen on poly(sodium styrene sulfonate) films with varying counterions.[43] Notably, water mixing was observed throughout the probed polymer interface, rather than isolated in multilayers above the substrate. This suggests that water sorption into hydrophilic polymer coatings may resemble wet conditions, and as such serve as a useful method for characterizing coating surface chemistry and affinity for water *in situ* for underwater applications including marine antifouling.

In this work, we investigated the effects of incorporating amphiphilic (polypeptoid) side chains into hydrophilic and hydrophobic block copolymers on (1) surface chemistry and its dependence on atmosphere conditions, and (2) water interactions and sorption that alter the polymer/water interface, using APXPS at soft and tender regimes in conditions

ranging from ultrahigh vacuum to 20 Torr water vapor (100% humidity at room temperature). These polymer coatings, shown in **Figure 3-1**, have identical polypeptoid side chain chemistry and inert end blocks that act as physical anchors, but different hydrophobic and hydrophilic middle blocks that are commonly used for fouling release and antifouling coatings, respectively. A previous study has shown that incorporating polypeptoids into PEO-based and PDMS-based copolymers enhances their inherent antifouling and fouling release performance, but more strongly improves the dominant mechanism (e.g. fouling release in PDMS-based copolymers);[34] this suggests that interactions with surface water may also be significant and differ between all materials. Soft X-ray APXPS was used to probe changes in surface chemistry as a function of depth in moderately humid conditions, while tender X-ray XPS enabled measurements taken in 100% relative humidity inside the analysis chamber. Exposure to 20 Torr water vapor resulted in water sorption for both the PEO-peptoid and PDMS-peptoid copolymers, with the former showing substantial amounts of water sorbed. The amphiphilic polypeptoids were seen to hierarchically surface segregate in the PEO-based copolymer, with the fluorinated chemistry arranged closest to the surface, while the PDMS-based copolymer showed polypeptoid restructuring between vacuum and hydrated conditions.

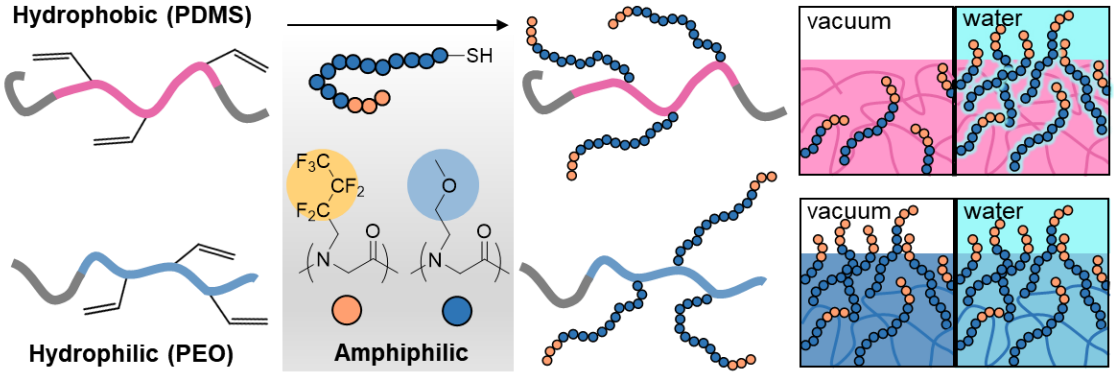

Figure 3-1. Hydrophobic PDMS-based and hydrophilic PEO-based block copolymers modified with an amphiphilic polypeptoid sequence were previously shown to be efficacious for algae and diatom fouling prevention.[18] The two modified surfaces were hypothesized to show contrasting responses in both vacuum and hydrated conditions, where the hydrophobic PDMS matrix buries polypeptoid signal except underwater, and the amphiphilic polypeptoid remains at the PEO surface both in vacuum and underwater.

3.2 Experimental Methods

3.2.1 Materials

All materials were purchased from Sigma Aldrich and used as received, unless noted otherwise. Hexamethylcyclotrisiloxane (D3) and 1,3,5-trivinyl-1,3,5-trimethylcyclotrisiloxane (V3) were purchased from Gelest. 2,2,3,3,4,4,4-Heptafluorobutylamine was purchased from Matrix Scientific, while 2-Methoxyethylamine was purchased from TCI. Bromoacetic acid was purchased from Alfa Aesar, and dichloromethane was purchased from Fisher Scientific. Dimethylformamide (DMF) was purchased from VWR, N,N′-diisopropylcarbodiimide was purchased from Chem-Impex, and Rink amide MBHA resin was purchased from MilliporeSigma. Polystyrene-block-poly- (ethylene-ran-butylene)-block-polystyrene (SEBS, MD6945) and

maleic anhydride-grafted SEBS (MA-SEBS, FG1901X) were generously provided by Kraton Polymers for use as a tie layer.

3.2.2 Polypeptoid synthesis

Polypeptoid synthesis was performed on a Prelude synthesizer (Protein Technologies) according to published solid phase submonomer synthesis procedures using Rink amide MBHA resin.[34,35,18] The selected sequence contained three 2,2,3,3,4,4,4-heptafluorobutylamine submonomers and twelve 2-methoxyethylamine submonomers, and was terminated with S-trityl-3-mercaptopropionic acid. This group was deprotected during cleavage with trifluoroacetic acid to yield a thiol-terminated polypeptoid for attachment to the block copolymers via a radical mediated thiol−ene "click" reaction. The cleaved polypeptoids were dissolved in a 1:1 acetonitrile:water (v/v) solution and lyophilized to yield the polypeptoid product as confirmed by MALDI. Further synthetic details can be found in Appendix B.

3.2.3 PDMS block copolymer synthesis

PS-*b*-P(DMS-*co*-VMS)-*b*-PS synthesis followed a previously-reported procedure.[34,35] In brief, polystyrene was polymerized with sec-butyllithium and followed with chain extension of a siloxane block consisting of distributed dimethylsiloxane and vinylmethylsiloxane monomers. A triblock architecture was made by coupling active chain ends together. The final molecular weight of the polymer was determined by GPC, while 1 H NMR verified vinyl content. The copolymer consisted of two 7 kDa PS end blocks with a 70 kDa P(DMS-*co*-VMS) midblock, with 3.6 mol% VMS.

3.2.4 PEO block copolymer synthesis

The PS-*b*-P(EO-*stat*-AGE) synthesis has been previously reported.[18] Alcohol-terminated polystyrene was grown anionically in cyclohexane with *sec*-butyllithium, terminated with ethylene oxide and quenched with isopropyl alcohol. The polymer was precipitated, filtered, dried under vacuum, and characterized with size-exclusion chromatography and 1 H NMR before being used as a macroinitiator for anionic copolymerization of ethylene oxide and allyl glycidyl ether in THF. The resulting polymer consisted of 22.3 kDa PS and 46 kDa P(EO-*stat*-AGE) blocks, with 2.9 mol% AGE.

3.2.5 Polymer functionalization

Thiol-terminated polypeptoids were attached to the PEO- and PDMS-based block copolymers via radical-mediated thiol−ene "click" chemistry. Approximately 100 mg of triblock copolymer was dissolved in either DMF (0.5 mL) for the PEO-based copolymer or DCM (4 mL) for the PDMS-based copolymer. 3 equivalents of polypeptoid and 0.4 equivalents of 2,2-dimethoxy-2-phenylacetophenone (DMPA) were each added. The reaction solution was first purged with inert gas and then irradiated with 365 nm UV light for 3 h. The functionalized PDMS-based copolymer was precipitated into acetonitrile, filtered, and dried. The functionalized PEO-based copolymer was suspended in 1:5 acetonitrile:water, then concentrated in an Amicon Ultra centrifugal filter unit (30 kDa, Millipore) to remove residual DMF. The polymer was then resuspended in 1:6 acetonitrile:water and lyophilized. Click completion was verified in NMR by the reduction of vinyl and allyl functional groups for the PDMS- and PEO-based copolymers, respectively.

3.2.6 PEO-peptoid thin film preparation

85 nm thin films were spin coated on gold-coated silicon wafers (100 nm, Sigma Aldrich). Before application of the polymer, the wafer substrate was washed with isopropanol, blow dried with nitrogen, and then exposed to UV-ozone for three minutes. The polypeptoid-modified PEO-based copolymer solution (2 wt%, 1:1 toluene/MEK) was applied to the gold via spin coating (1500 rpm, 60 s). The film thickness was verified with ellipsometry, then annealed at 120 ºC under ultrahigh vacuum for at least 16 hours to reach thermodynamic equilibrium.

3.2.7 PDMS-peptoid thin film preparation

Samples for soaking were prepared by spin coating onto a tie layer as used in marine antifouling studies covalently bound to a p-doped silicon wafer (0.001-0.005 Ω-cm). The wafer substrate was first treated with UV-ozone for five minutes, then exposed to a 3-(aminopropyl)trimethoxysilane solution (5.1 wt%, anhydrous ethanol) with a catalytic amount of acetic acid to provide amine-functionalized reactive sites. After rinsing with ethanol and water, the wafer was cured under vacuum at 120 °C for 4 h and then spin coated with an 85 nm tie layer solution (8.1 wt% SEBS and 2.3 wt% MA-SEBS in toluene). Crosslinking of the maleic anhydride on the tie layer and amine-functionalized silicon occurred at 120 °C under vacuum for 24 h. The PDMS-peptoid solution (0.4 wt%, cyclopentanone) was then spin coated (2500 rpm, 45 s) to a thickness of 70 nm. Annealing at 120 °C for 22 h allowed polystyrene end blocks of both the top and tie layers to form physical crosslinks, linking the PDMS-peptoid layer to the substrate. The final samples contained ~160 nm polymer layers covalently bound to conductive silicon, and XPS quantification of the surface indicated no tie layer was visible during measurements.

3.2.8 in situ *APXPS measurements*

All XPS measurements were conducted at the Advanced Light Source (ALS) of the Lawrence Berkeley National Laboratory with 100 eV pass energy. Tender APXPS was performed at Beamline 9.3.1 using 4 keV X-rays, while Soft APXPS was performed at Beamline 9.3.2 with X-ray photon energy ranging from 355-850 eV. Because the polymer films are ~100 and ~160 nm thick, no contributions from the substrate were detected during soft or tender APXPS measurements. Polymer charging was minimized by preparing thin films on conductive substrates (gold for the PEO-peptoid, p^+-Si for the PDMS-peptoid to enable soaking). Energy calibration for the PEO-peptoid was established using the N 1s amide centered at 400.2 eV,[61] while the PDMS-peptoid was calibrated using the O 1s silicon-character oxygen at 532 eV typically used for siloxanes.[62] The polymer materials exhibited beam-induced damage on the order of a few minutes, so rastering methods were used during data acquisition to minimize damage. Spectra were collected in 2-3 minutes in a single position before movement, and were found to be consistent from position to position. Summation of these spectra was done to improve the signal-to-noise ratio on tender APXPS measurements.

For all *in situ* measurements, Millipore water (18.2 MΩ) was added to a glass bulb and degassed by three freeze−pump−thaw cycles before introduction into the analysis chambers. Using a precision leak valve, pressures of up to 800 mTorr were added to the analysis chamber at Beamline 9.3.2 and up to 20 Torr at Beamline 9.3.1. After introduction of water to the chamber, samples were equilibrated for at least 15 minutes before data collection. No changes were seen thereafter over several hours, indicating equilibrium was sufficiently established. All fitting procedures were performed using Casa XPS software

using Shirley background subtraction and 70/30 symmetrical Gaussian/Lorentzian product function line shapes for surface components.

The PEO-peptoid sample on gold showed polypeptoid at levels similar to those previously seen in coatings for marine antifouling studies (**Figure 3-2b**).[18,34] However, PDMS-peptoid samples spin coated on gold never showed any surface polypeptoid content. Because polypeptoids incorporated into PDMS surfaces are known to bury under vacuum conditions,[34] the PDMS-peptoid thin film was modified to enable measurements of a soaked film and to be more representative of the original marine antifouling coatings: prior to spin coating the PDMS-peptoid, a thin underlayer of polystyrene-*b*-poly-(ethylene-*ran*-butylene)-*b*-polystyrene (SEBS) and maleic anhydride-grafted SEBS was covalently attached to an amine-functionalized conductive p^+-Si substrate. This underlayer did not contribute to XP spectra due to the ~80 nm thickness of the PDMS-peptoid overlayer. Data collected from soaked and pristine samples on p^+-Si were nearly identical in composition, so pristine PDMS-peptoid surfaces are used hereafter (**Figure B3**).

3.3 Results and Discussion

PDMS- and PEO-based materials are commonly modified to elicit desirable properties in applications ranging from marine antifouling to medical implants. Further, we have previously shown that PDMS and PEO coatings functionalized with polypeptoids are particularly efficacious for the prevention of diatom and algae settlement in a marine environment, yet the details of surface presentation *in situ* were unknown and critical to understanding the structure-property relationships in antifouling coating design.[18,34,35] Polypeptoid-containing PDMS-based and PEO-based surfaces were thus prepared and characterized using APXPS to understand polypeptoid surface segregation in contrasting copolymers commonly used for marine antifouling applications. The polypeptoids contain three surface-active fluorinated monomers present at the distal end of the chain that facilitate surface segregation of even low loadings of polypeptoid during vacuum annealing, which is particularly important for the PEO-based copolymers that would otherwise be buried under the polystyrene anchor groups.[18] The hydrophilic polypeptoid backbone and ether-containing monomers render the side chains amphiphilic to keep the polypeptoids at the surface in hydrated conditions.

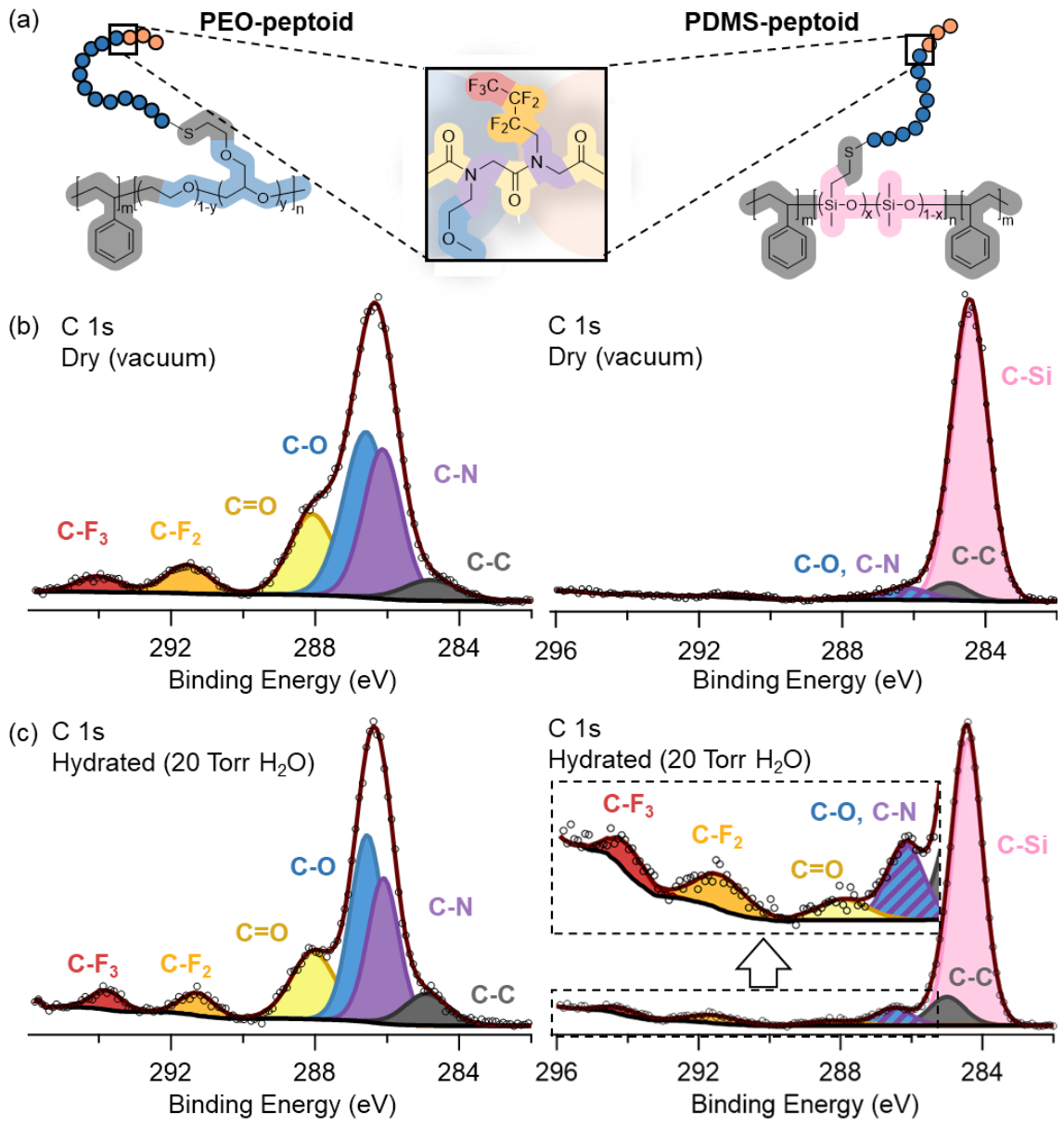

Figure 3-2. (a) Chemical structure of polypeptoid-modified PS-P(EO-*stat*-AGE) and PS-P(DMS-*co*-VMS) using 4 keV X-rays. (b) Under vacuum conditions, polypeptoid components contribute significantly to the PEO-based system but not the PDMS-based one. (c) Hydration at 20 Torr water vapor induces restructuring of the PDMS-peptoid surface, while only small changes in polypeptoid content are seen in the PEO-peptoid surface. A vertical zoom is used to clarify polypeptoid components on the PDMS-peptoid hydrated spectrum.

Amphiphilic polypeptoids were seen to behave differently in PDMS- and PEO-based polymer matrices under both vacuum and hydrated conditions as shown in tender

APXPS (**Figure 3-2**). Under vacuum conditions, the incorporation of the amphiphilic polypeptoid into the PEO-based copolymer completely alters the chemistry of the polymer surface to consist mostly of the polypeptoid side chains with minor amounts of PEO. The low surface energy of the fluorinated functional groups enables polypeptoid enrichment of the surface, displacing the polystyrene (PS) end blocks that would have otherwise populated the interface, as indicated by the large contributions from polypeptoid components of fluorine-, oxygen-, and nitrogen-character carbon as well as a reduction in aliphatic carbon from the PS end blocks. (Locations of all components and core levels can be found in Appendix B at **Figure B1**). Polypeptoids persisted at the polymer surface at full hydration for the PEO-based system. Hydration was reached using ambient pressure experiments conducted in 20 Torr water vapor, representing 100% relative humidity at room temperature. Under these conditions, water condensed onto the surface is in thermodynamic equilibrium with its vapor state. All polypeptoid components remained within a few percent of their vacuum-conditioned values, indicating minimal effects of hydration on surface presentation.

On the other hand, the PDMS-peptoid surface shows polypeptoids restructure between vacuum and hydrated conditions. Initially, very little polypeptoid is visible, indicating fluorinated groups cannot drive surface segregation as they did in the PEO-based system. The majority of signal is derived from the PDMS component, which is known to have a low surface energy that facilitates its organization at the polymer/vacuum interface during exposure to air or vacuum. However, the addition of 20 Torr water vapor induces rise of polypeptoid components in the C 1s spectrum. While the fluorinated carbon components become visible, the hydrophilic polypeptoid backbone likely drives

restructuring toward the water/polymer surface. The timescale of rearrangement for these polypeptoid-modified materials occurs relatively quickly: PDMS-peptoid that was soaked for 3 days prior to analysis at 20 Torr water vapor showed similar surface composition to the unsoaked sample described above that was exposed to 20 Torr water vapor for 2.5 hours prior to measurement (**Figure B3**). All polypeptoid restructuring at the surface happened within these two hours, and previous contact angle measurements suggest that polypeptoids can restructure at the surface within seconds to minutes.[13]

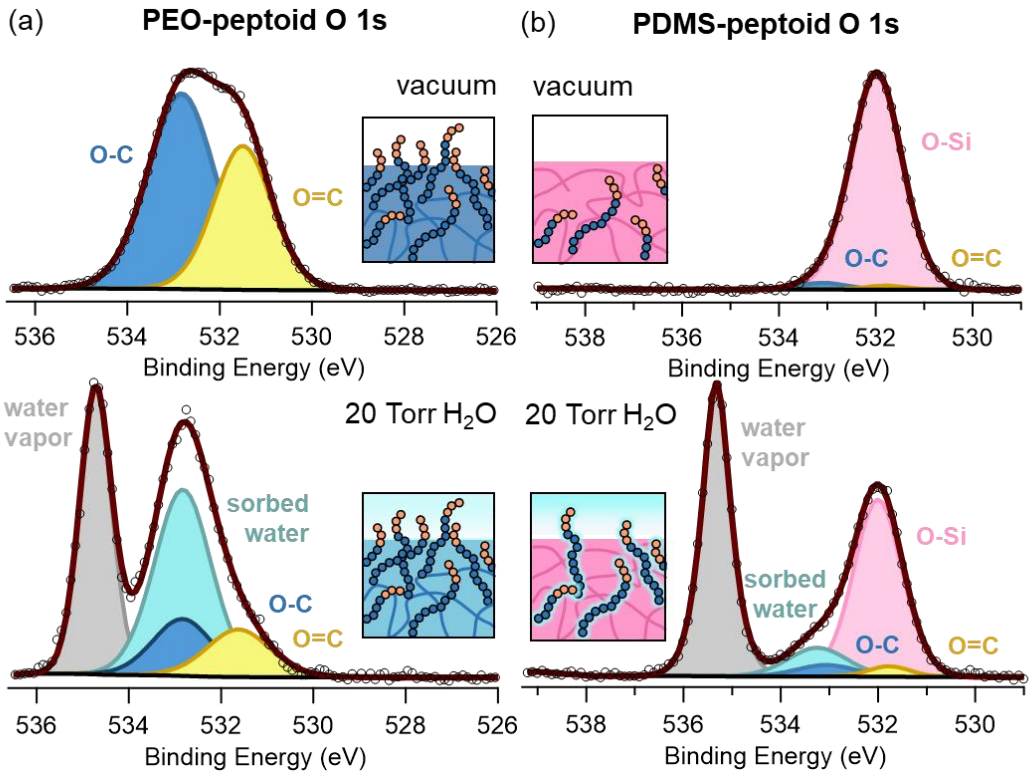

Figure 3-3. O 1s spectra of PEO- and PDMS-peptoid copolymers using 4 keV X-rays. (a) In addition to ether and carbonyl polypeptoid components as seen as UHV, 20 Torr spectra show large amounts of sorbed water indicative of a diffuse PEO-peptoid/water interface. (b) Addition of 20 Torr water vapor both increases polypeptoid components and instigates sorption of a small amount of water into the surface.

Both of the polypeptoid-containing surfaces induce sorption at 100% humidity (**Figure 3-3**). The PEO-peptoid surface in particular shows significant water sorption due to the hydrophilicity of both the PEO and polypeptoid backbone, while the PDMS-peptoid sample sorbs much smaller amounts of water under the same conditions. For the latter, the presence of water is notably correlated with an increase in polypeptoid peak composition. The addition of water incentivizes restructuring of the polypeptoid to the surface, which in turn facilitates increased water sorption. These events must be considered in tandem when evaluating large scale changes in material behavior, particularly for fouling applications: differences in the settlement of marine organisms may come from changes in surface chemistry as well as changes in water affinity.

The distribution of water within the polymer surface is also not homogeneous: water sorption as observed on the amphiphilic PDMS-peptoid surface is associated exclusively with the polypeptoid. An unmodified PDMS prepolymer sorbs no water (**Figure B4**), while a free polypeptoid surface indicates 2.8 water molecules per averaged peptoid monomer (derived from an observed 1.5 water : peptoid oxygen ratio as described in the SI). Given the amphiphilic polypeptoid is composed of fluorinated and ether monomers, this value is likely indicative of either 2 or 3 water molecules bound by each monomer. This suggests that slight adjustments in polypeptoid functional group content could enable control over the degree to which the surface binds water.

Polypeptoid water affinity was not seen to differ when incorporated as side chains in the PDMS-peptoid. When sorbed water in the PDMS-peptoid surface is only considered to come from the polypeptoid components, 2.8 waters are bound per peptoid monomer, which is similar to previously seen water concentrations for pure polypeptoid surfaces.

This also indicates that the amount of water bound to the PDMS-peptoid surface is directly proportional to the amount of polypeptoids; no reservoirs of free water (unaffiliated with the polypeptoid) were observed within the surface. It is worth noting that these findings do not verify or discount the possibility of a skin layer of peptoids directly at the polymer-water interface, which would contribute minimally to these XPS spectra that receive signal ~30 nm into the surface. However, sum frequency generation and marine antifouling experiments suggest amphiphilic polypeptoids restructure at this top surface based on substantial changes in surface hydrophilicity and algal adhesion resistance, respectively.[34,35]

For the PEO-peptoid sample, both PEO and polypeptoid components associate with water and make it necessary to identify the depth-dependent composition of the material in order to relate the surface chemistry with the amounts of sorbed water. This composition is not uniform, as the polypeptoids in the PEO-based copolymer were designed to be present at the surface in vacuum conditions courtesy of the surface-driving fluorine components. XPS taken at synchrotron light sources can characterize surface composition in the z-direction via depth profiling. Changing the incident X-ray photon energy causes emitted photoelectrons travel with different kinetic energy and therefore different inelastic mean free paths (IMFPs). Total probing depth is typically represented as 3 times the IMFP, with the majority of signal coming from the top of the surface and reduced contributions below. Tuning the photon energy from 335 to 850 eV changes the depth probed from ~2.1 nm to ~5.7 nm for a C 1s photoelectron in poly(ethylene oxide).[63]

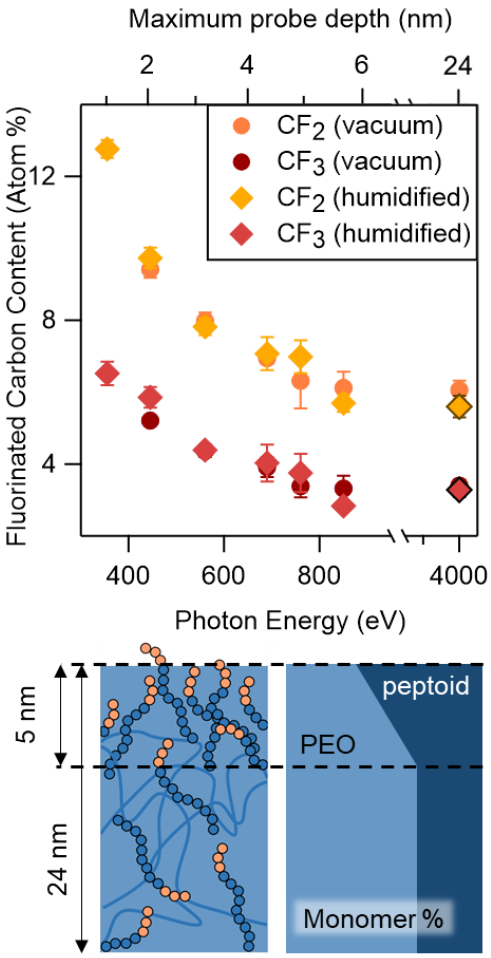

Figure 3-4. Top: Depth profiling of polypeptoid-modified PS-P(EO-*stat*-AGE) shows escalating fluorinated carbon content from polypeptoid monomers as probing depth decreases, with no effect seen when 800 mTorr water vapor is added to the system. Fluorocarbons measured using 4 keV X-rays are comparable in number to those measured with 850 eV photons at vacuum and 500 mTorr water vapor. Bottom: Schematic of polypeptoid content and organization at the surface. Signal from lower photon energies (which reduces probing depth) has increased contributions from surface-driven polypeptoid fluorinated groups. A linear model shown to the right was leveraged for characterizing sorbed water distribution.

Fluorinated carbon content in the C 1s was found to depend significantly on the probing depth (incoming photon energy), with increasing overexpression at the most surface-sensitive low photon energies (**Figure 3-3**). A fully saturated, but homogeneous, polypeptoid surface would be expected to have 3.6% and 7.2% of its carbons be primary and secondary fluorocarbons, respectively, based on the molecular formula. This is reached at ~5 nm depth, then greatly surpassed: not only are polypeptoids saturated at the interface, but the fluorinated monomers are located closest to the surface. This arrangement does not change with the addition of a small amount of water vapor to the chamber (5% humidity), and no water adsorption was observed. At the highest photon energies, primary and

secondary fluorocarbon content is reduced to approximately 3% and 6%, respectively. This content does not significantly change between probing depths of 5.7 and 24 nm (photon energies of 850 and 4000 eV), likely due to the high contribution of buried polypeptoids within the bulk polymer to the overall signal. The differences seen between experiments with low and moderate probing depths further highlight the importance of surface sensitivity in characterizing the surface presentation of polymer chemistries, as slight polypeptoid enrichment is detected at the highest photon energies while full saturation is suggested with more surface-sensitive low energy X-rays. APXPS with tunable synchrotron radiation is particularly well-suited for quantitatively identifying changes in surface chemistry with depth on the order of nanometers, providing more a complete understanding of the organization of the surface within the top 20 nm (**Figure 3-3**).

Leveraging the surface composition gained via depth profiling allows further insight into the ways in which water sorbed into the PEO-peptoid water/polymer interface is shared between both PEO and polypeptoid monomers. Accounting for enhanced polypeptoid content in the top 5 nm and bulk polypeptoid content below, and given the 1.9 water molecules per PEO monomer anticipated for the polymer backbone and the 2.8 waters per polypeptoid monomer (**Figure B4**), the PEO-peptoid surface should have ~1.7 water molecules per polymer oxygen as described in the SI. This matches the experimentally derived surface water/polymer oxygen ratio of 1.7:1 in the O 1s spectrum (**Figure 3-3a**), corroborating both the depth profile of the surface and amount of bound water by the polypeptoid and PEO components.

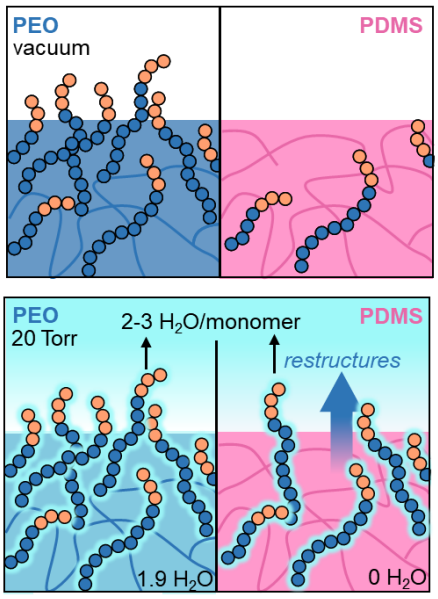

Figure 3-5. Polypeptoid surface presentation and effects on water affinity for PEO- and PDMS-based copolymers. Polypeptoids are drawn to the surface under vacuum by their fluorinated monomers (orange) in PEO, while their hydrophilic backbone and ether monomers (blue) instigate restructuring under hydrated conditions in PDMS. Polypeptoid components retain their affinity for water (averaged 2.8 water molecules per monomer) in both PDMS and PEO copolymers.

Overall, the water affinity of the amphiphilic polypeptoids remains constant regardless of the polymer system in which they are incorporated at 2.8 waters per monomer (**Figure 3-5**). The polymer components similarly contributed water affinity additively, with PDMS not participating in water sorption and PEO facilitating further water sorption. The amount of sorbed water is also directly proportional to polymer chemical content, suggesting that sorbed water interacts primarily with the polymer rather than other sorbed water molecules. Furthermore, this work indicates that water interactions in these polymers can be finely tuned by manipulating side chain chemistry or changing overall polypeptoid content. Ensuring surface presentation of the side chains is therefore the more significant challenge, one which requires knowledge of relevant functional group chemistries that enhance surface segregation in a given polymer system. While the fluorinated monomer chemistries enabled significant surface enrichment of polypeptoid side chains in the PEO-peptoid polymer, they were less effective in the PDMS-based system. Instead, the hydrophilic polypeptoid backbone enabled some restructuring to occur upon exposure to water. Ambient pressure XPS enables quantitative *in situ* characterization of the changes

in surface composition under different stages of hydration, and as such would be useful for identification of potential surface segregating groups and the conditions that trigger restructuring.

3.4 Conclusions

To investigate *in situ* surface composition of polymers for applications like marine antifouling, the surface composition of polypeptoid-modified PEO-based and PDMS-based block copolymers was analyzed via APXPS from ultrahigh vacuum conditions through 100% humidity at room temperature. Amphiphilic polypeptoids were seen at the surface under hydrated conditions for both polymers, but were present due to different driving forces. For the PDMS-based system, the hydrophilic polypeptoid backbone facilitated restructuring under humid conditions, while the PEO-based one relied on surface-active fluorinated polypeptoid monomers to drive organization under vacuum while annealing.

Polypeptoid side chains also modified polymer interactions with water, increasing the number of water molecules by virtue of each monomer's ability to bind between 2-3 water molecules. For the PDMS-peptoid, all surface water was likely affiliated with the polypeptoid chain, based on the polypeptoid and water content that matched ratios for pure polypeptoid surfaces. For the PEO-peptoid surface, both the PEO backbone and polypeptoid side chains sorbed water, with an increased concentration of polypeptoids detected via depth profiling at the upper surface. In both cases, all sorbed water was directly associated with specific polymer components rather than present in a subsurface water

phase. The total water content can be tuned by modifying the side chain chemistry or stoichiometry, though surface-driving groups must always be present in order to ensure the side chain is present at the interface. Through these types of systematic modifications, novel coatings can be efficiently designed to maximize bound water at the surface for antifouling purposes or deliver surface-active groups to the surface.

3.5 Acknowledgements

The authors gratefully acknowledge financial support by the Office of Naval Research (ONR) from Awards N00014-17-1-2047 for materials synthesis and structural characterization. P.A.G. and E.J.C. were fully and partially, respectively, supported by the Center for Materials for Water and Energy Systems (M-WET), an Energy Frontier Research Center funded by the U.S. Department of Energy (DOE), Office of Science, Basic Energy Sciences (BES), under Award #DE-SC0019272. E.J.C. was partially supported by an Early Career Award in the Condensed Phase and Interfacial Molecular Science Program, in the Chemical Sciences Geosciences and Biosciences Division of the Office of Basic Energy Sciences of the DOE under contract DE-AC02-05CH11231. M.E.B. gratefully acknowledges the National Science Foundation for a graduate fellowship under Award #DGE 1650114, while A.J.D acknowledges support from the National Defense Science and Engineering Graduate Fellowship Program. This research used resources of the Advanced Light Source and the Molecular Foundry, which are DOE Office of Science User Facilities supported by the Office of Science, Office of Basic Energy Sciences, of the U.S. Department of Energy, under Contract DE-AC02-05CH11231.

3.6 Appendix B

3.6.1 Polymer spectral components

Because of the complexity of the PEO-peptoid C 1s spectrum, the polypeptoid N 1s amide (N-C = 400.2 eV) was used to calibrate core level positions.[61] For the PDMS-peptoid, the typical calibration of the siloxane oxygen (O-Si = 532.0 eV)[62] was used due to the minimal polypeptoid content under dry conditions. O 1s carbonyl and ether components at 531.7 eV and 533.0 eV, respectively, are representative of literature values for peptides and PEO.[61,62] Primary and secondary fluorinated hydrocarbons are visible at 294.0 eV and 291.5 eV, with their F 1s counterparts at 689.4 eV. Carbonyl and ether-character carbon are at 288.1 and 286.7 eV, respectively, while nitrogen-bond carbon is at 286.1 eV. Minor amounts of aliphatic carbon from the side chain linker and polymer backbone can be seen at 285.1-285.2 eV (PEO-peptoid) and 285.0 eV (PDMS-peptoid). For the PDMS-peptoid, silicon-bond oxygen is present at 532.0 eV and silicon-bond carbon is present at 284.4 eV.

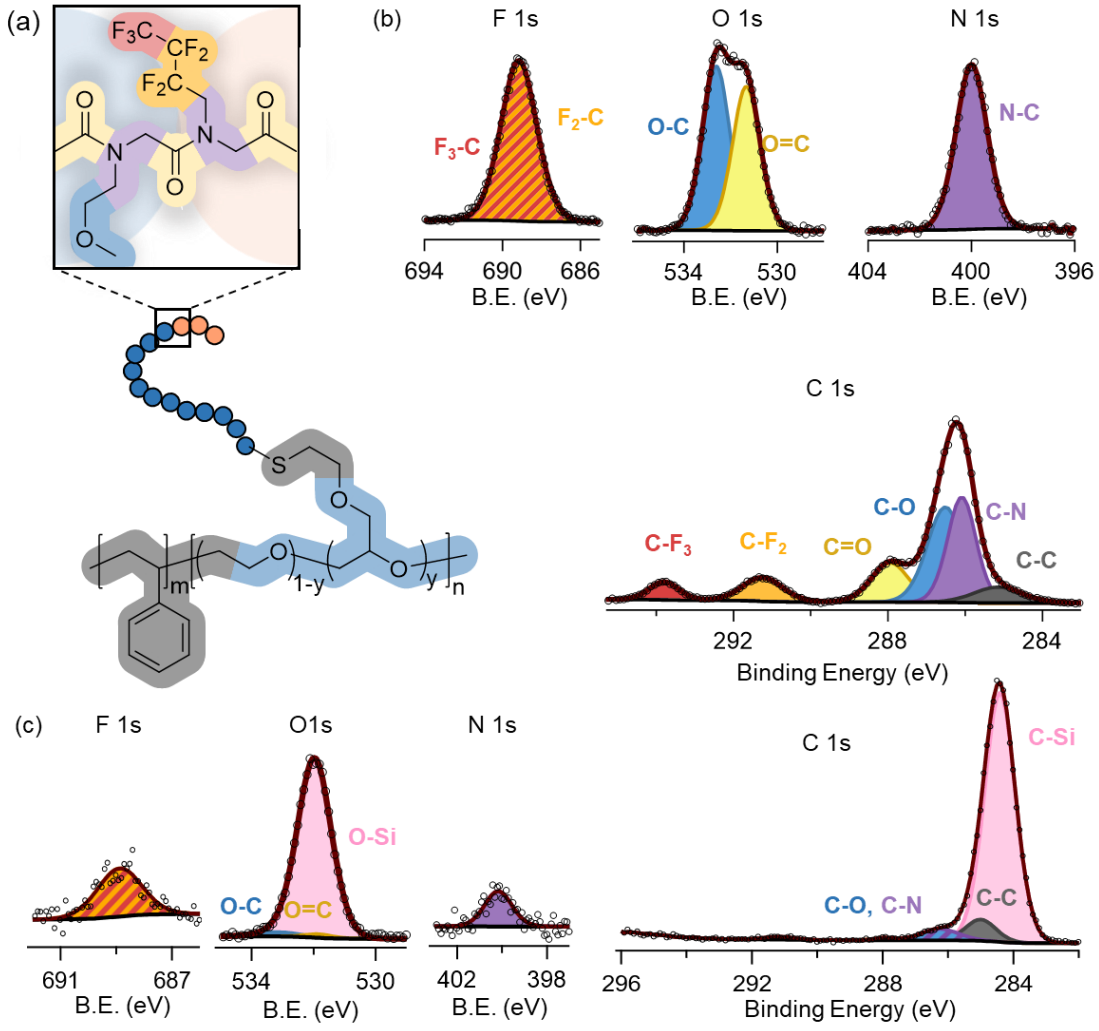

Figure B1. APXPS surface presentation of polypeptoid-modified PEO- and PDMS-based copolymers. (a) Representative chemical environments for the PEO-peptoid surface. (b) Relevant core levels for the PEO-peptoid surface, which is heavily composed of polypeptoid side chains. Measured under UHV with 150 eV photoelectrons. (c) The PDMS-peptoid surface is mostly comprised of the siloxane polymer backbone. XP spectra were collected under 2 Torr Ar with 4 keV photoelectrons.

3.6.2 Core level quantification

The amphiphilic polypeptoids contain a wide number of heteroatoms, such as the nitrogen- and fluorine- containing functional groups, that provide a number of non-carbon core levels to evaluate polypeptoid content at the surface. However, as seen in **Figure 3-2**, this diversity increases the number of species present in the carbon core levels. Cross-comparison between core levels is necessary for verification of functional group quantities (e.g., between O 1s and C 1s for ether or carbonyl components).

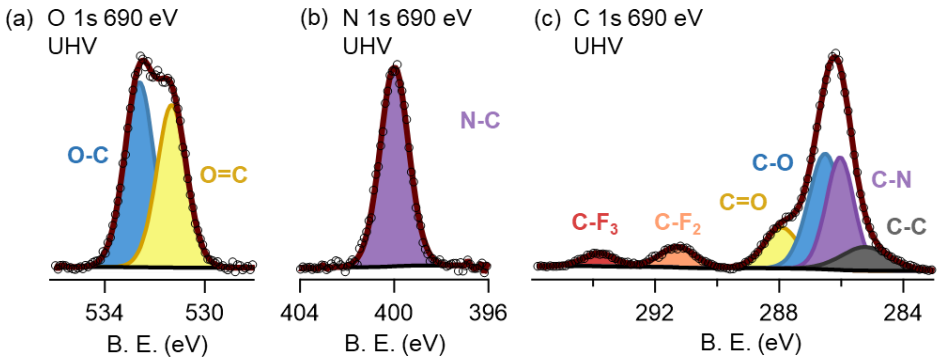

Figure B2. Ultrahigh vacuum spectra of the PS-PEO-peptoid copolymer surface at a single position. Large amounts of carbonyl-character oxygen in the O 1s core level (a) and amide nitrogen in the N 1s core level (b) indicate polypeptoids are present in high quantities at the surface. These correlate quantitatively with their carbon neighbors in the C 1s spectrum (c), matched by color and label.

Figure B2 depicts XP spectra of the PEO-peptoid surface at a single position. Quantification of the oxygen, nitrogen, and carbon core levels is consistent (**Table S2**), lending credibility to the fitting in the convolved, low-binding energy region of the C 1s spectrum: the total electron counts were found to be similar between oxygen and nitrogen species and their neighboring carbon equivalents in the C 1s spectrum (matched by color in **Figure B2**). Component intensity of X-ray photoelectron spectra is quantitatively related to the atomic density n, photoelectron cross section σ, electron inelastic mean free path l, and sample thickness d, as indicated in **Equation B1**.[57,64] For emitted electrons that are not elastically scattered, i.e., travel in a straight line, we can approximate the detected intensity by integrating over the exponential escape probability:

$$I_1 \approx n_1\sigma_1 \int_0^d \exp\left(-\frac{z}{l_1}\right) dz = \varphi_1\, n_1\sigma_1 l_1 [1 - \exp\left(-\frac{d}{l_1}\right)] \qquad \text{(Eqn. B1)}$$

For a sample with a single layer significantly thicker than the electron inelastic mean free path, the ratio between intensities (measured as region or component areas) can be simplified to:

$$\frac{I_1}{I_2} = \frac{n_1\sigma_1 l_1}{n_2\sigma_2 l_2} \cdot \frac{1 - \exp\left(-\frac{d}{l_1}\right)}{1 - \exp\left(-\frac{d'}{l_2}\right)} = \frac{n_1\sigma_1 l_1}{n_2\sigma_2 l_2} \qquad \text{(Eqn. B2)}$$

The unknown intensity of a C 1s component can thus be solved for given the known heteroatom intensity and spectroscopic parameters. **Table 1** depicts the values used to approximate the polymer component intensities in C 1s spectra. The relative atomic density of heteroatom and carbon pairs was determined according to the copolymer molecular

formula. The resulting predictions were used to verify accuracy of C 1s fits within ~10% error.

Table B1. Parameter values for verification of C 1s spectral components.

	Relative density	σ (690 eV)	l (690 eV)	σ (4 keV)	l (4 keV)
O 1s		0.320 Mb	8.8 Å	$2.11 \cdot 10^{-3}$ Mb	92.1 Å
O-C	$n_{O-C} = (1/2)n_{C-O}$				
O=C	$n_{O=C} = n_{C=O}$				
N 1s		0.208 Mb	12.8 Å	$1.21 \cdot 10^{-3}$ Mb	95.0 Å
N-C	$n_{N-C} = n_{C-N}$				
F 1s		--	--	$3.26 \cdot 10^{-3}$ Mb	88.6 Å
F-C	$n_{F-C} = (7/3)n_{C-F}$				
C 1s		0.121 Mb	16.3 Å	$6.57 \cdot 10^{-4}$ Mb	97.5 Å

Table B2. Representative prediction and verification of C 1s fits based on heteroatom core levels. Listed spectra are from high vacuum conditions at 690 eV at the same position.

	Heteroatom fit	RSF	Predicted C 1s	C 1s fit	Percent difference
N-C	825,848	1.49	1,230,771	1,288,201	4.6%
O=C	923,930	0.704	650,655	582,487	11.1%
O-C	1,071,817	1.41	1,507,478	1,576,313	4.5%

3.6.3 Soaked and unsoaked PDMS-peptoid samples

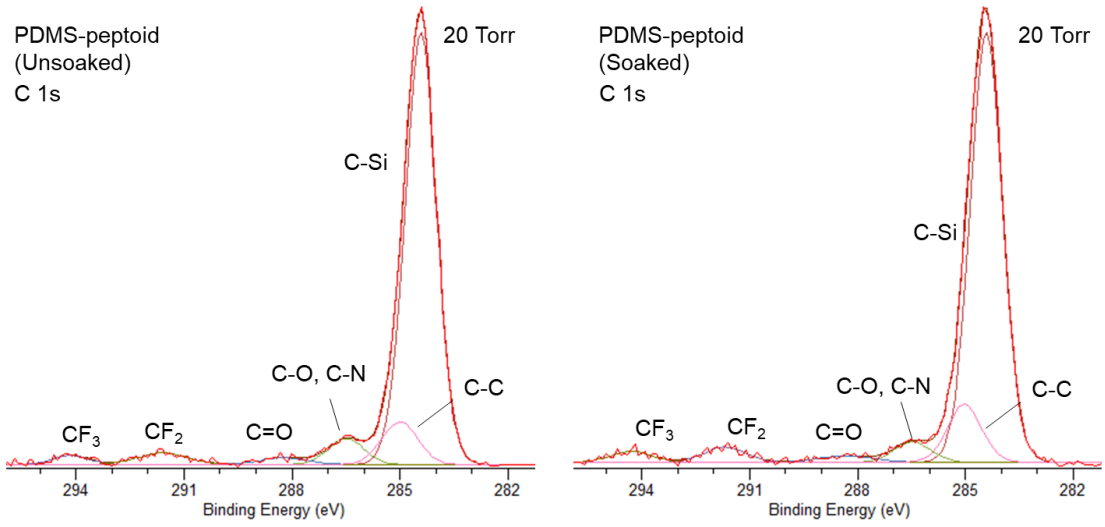

Figure B3. Carbon 1s spectra show similar composition between soaked and unsoaked samples.

3.6.4 Polypeptoid-modified polymer component spectra

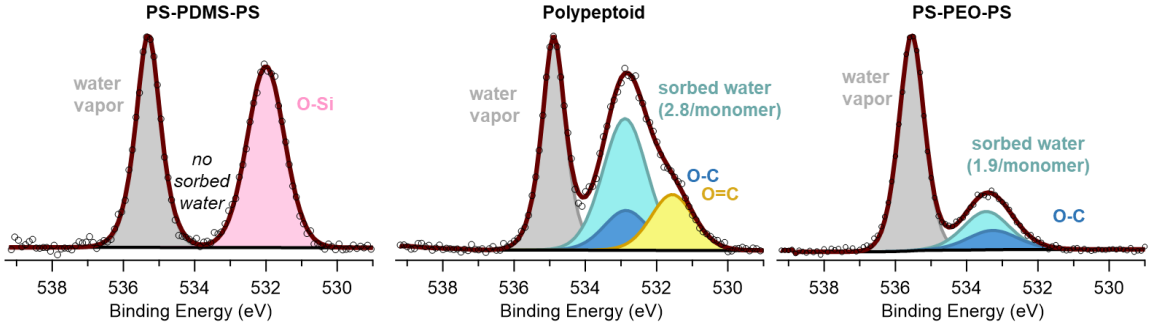

Figure B4. Water sorption onto PDMS, polypeptoid, and PEO surfaces show different water affinities in terms of sorption.

3.6.5 Quantification of water content

Because the PDMS-peptoid water content is contained only within the polypeptoid, the carbonyl and ether oxygen components were used within the O 1s to identify the ratio between sorbed water and polypeptoid oxygen (1.54). The oxygen content of a polypeptoid monomer averages to 1.86 O per polypeptoid monomer (1 per fluorinated, 2 per ether), and therefore sorbed water exists at a ratio of 2.83 water per polypeptoid monomer. The amounts of sorbed water in polypeptoid and PS-PEO-PS surfaces were found using the same methods.

Quantification of water content in the PEO-peptoid surface requires untangling of the z-dependent surface composition. Depth profiling indicates larger amounts of polypeptoid within the top 5 nm of the surface. By linearly fitting the excess fluorinated carbon content, estimates of the polypeptoid and PEO monomer fractions were made for the skin and bulk regions. A linear fit was chosen as the simplest gradient estimate since all measurements are also affected by the exponentially decaying depth-dependent signal intensity (in addition to the depth-dependent composition).

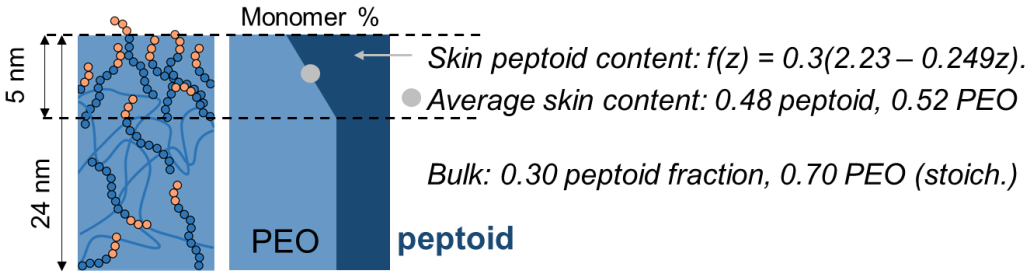

The amount of bound water per monomer differs for the PEO (w_{PEO}= 1.9) and polypeptoid (w_{pep}= 2.80) components. Therefore, the estimated net amount of water per monomer depends on the relative fractions in the skin and bulk layers:

$$W_{skin} = 0.48w_{pep} + 0.52w_{PEO} = \textbf{2.33 water molecules/polymer monomer}$$

$$W_{bulk} = 0.30w_{pep} + 0.70w_{PEO} = \textbf{2.17 water molecules/polymer monomer}$$

The model can be verified by comparing the amount of sorbed water relative to the polymer in the O 1s spectrum with the model prediction. The amount of oxygen molecules per monomer differs between the skin and bulk layers due to changes in polypeptoid content. Given an average of 1.86 O per polypeptoid monomer (1 per fluorinated, 2 per ether) and 1.03 per polymer backbone (1 per EO, 2 per AGE), the skin and bulk consist of 1.43 and 1.28 oxygen atoms per polymer monomer, respectively. Dividing W_{skin} and W_{bulk} by each layer's oxygen content per monomer yields the ratio of water molecules per polymer oxygen.

It is important to note that the skin layer contributes approximately ~48.9% of total signal from the polymer surface. Thus, weighting both layers' water composition yields an estimate of 1.66 water molecules per polymer oxygen for the O 1s spectrum, a value that is close to the 1.7 ratio found experimentally.

3.6.6 Polypeptoid synthesis

Solid-phase synthesis was conducted with minimal modifications to published procedures[23, 27] on a Prelude synthesizer (Protein Technologies, Inc.).[18,34,35] Rink amide resin (0.40 mmol g^{-1} loading) was first deprotected with 20% 4-methylpiperidine solution in dimethylformamide (DMF) for 20 minutes, before washing in DMF. The free amine chain end was acylated with 0.6 M bromoacetic acid and 0.4 M N,N-diisopropylcarbodiimide (DIC) in DMF for 20 min. Following washing in DMF, nucleophilic displacement of the bromine was performed with either 2-methoxyethylamine or 1H,1H-heptafluorobutylamine to yield ether or fluorinated peptoid monomers, respectively. A concentration of 1 M in DMF was used for both 2-methoxyelthylamine and 2,2,3,3,4,4,4-heptafluorobutylamine. The heptafluorobutylamine additions proceeded for 3 hours at 50 °C and the methoxyethylamine additions proceeded for 1 hour at room temperature. After the monomer solution was drained from the resin using the Prelude, the resin was again washed with DMF before repeating additions. The polypeptoid was functionalized with a thiol endgroup using S-trityl-3-mercaptopropionic acid and N,N'-diisopropylcarbodiimide (DIC) (both 0.4 M in DMF). 2 mL of solution per 50μmol peptoid were added, bubbled with N_2 for 30 minutes, and washed with DMF.

Polypeptoids were cleaved from the solid support using a cocktail of trifluoroacetic acid : dicholoromethane : triisopropylsilane: water (47.5 : 47.5 : 2.5 : 2.5, v/v/v/v) for 20 minutes, a process which simultaneously deprotected the thiol. The resin was filtered and rinsed with dichloromethane and the collected solution was dried under vacuum and lyophilized

from water and acetonitrile (1 : 1, v/v). MALDI was performed to confirm the completion of the synthesis.

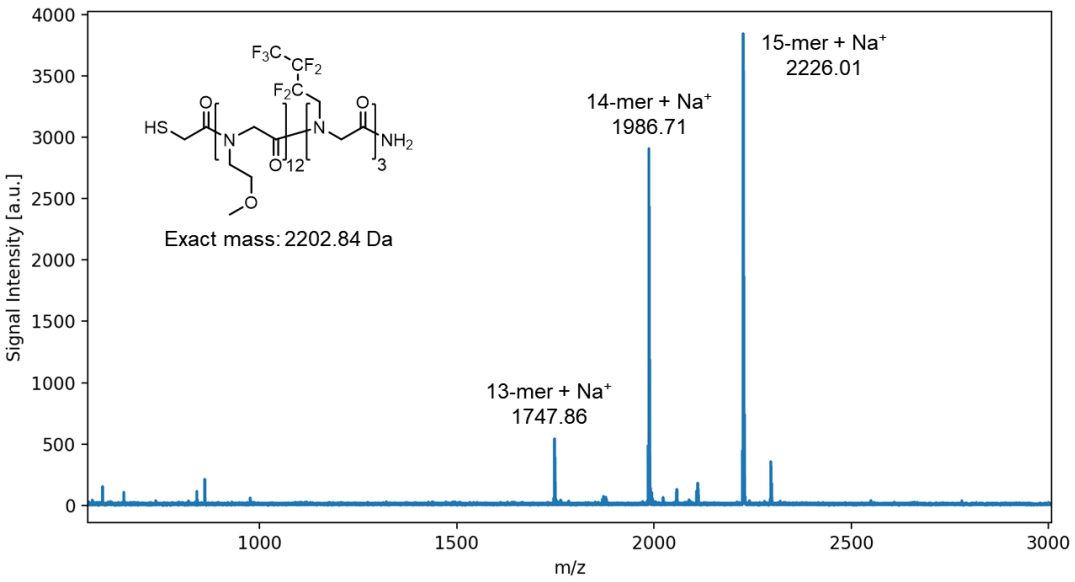

Figure B4. MALDI trace of the synthesized polypeptoid. The desired 15-mer polypeptoid was shown to be a majority product, with a detected mass of 2226.01 Da ($+Na^+$). A moderate amount of 14-mers was also detected containing two of three fluorinated monomers, and a small amount of 13-mers with only one fluorinated monomer.

3.6.7 Click efficacy

a) PEO-peptoid click attachment

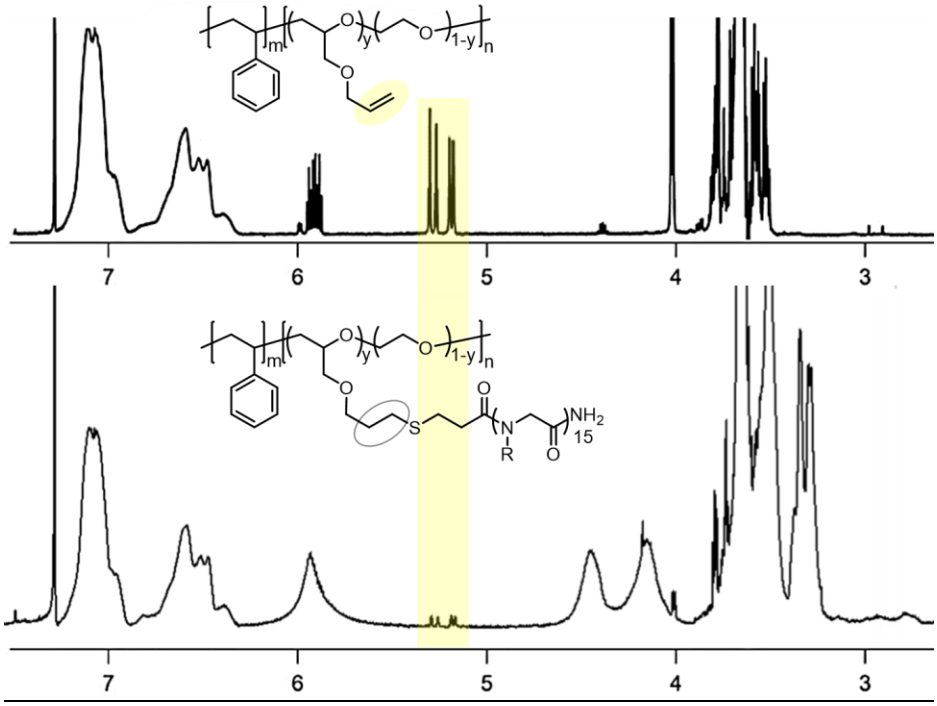

b) PEO-peptoid click attachment

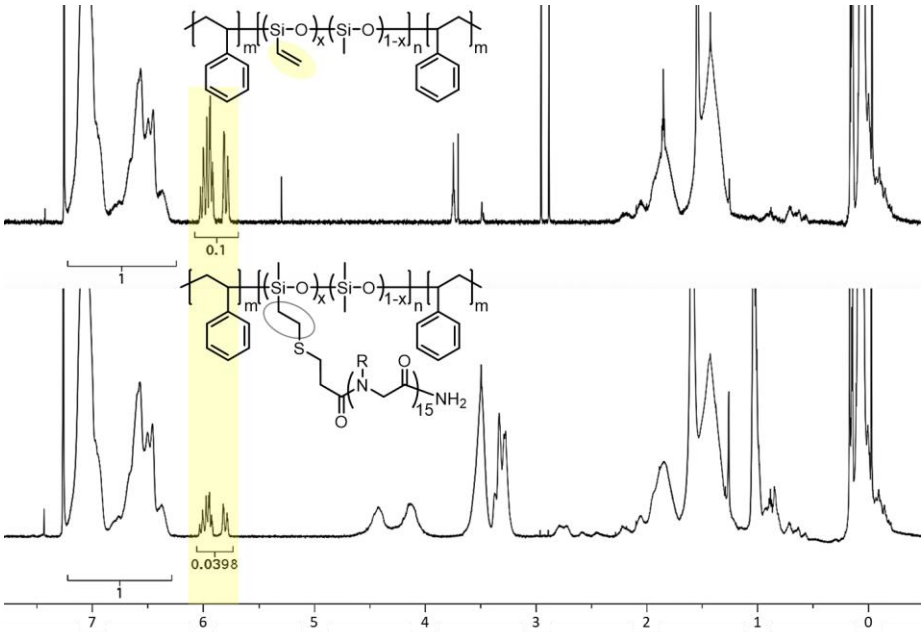

Figure B5. Reduction in allyl and vinyl components were indicative of polypeptoid attachment during thiol-ene click reaction. Due to steric hindrance resulting from the trivinyl siloxane comonomer, the PDMS-peptoid copolymer reached approximately 60% completion. This represents attachment at approximately two of the three vinyl groups per comonomer.

3.7 References

(1) Callow, J. A.; Callow, M. E. Trends in the Development of Environmentally Friendly Fouling-Resistant Marine Coatings. *Nat. Commun.* **2011**, *2* (1), 244. https://doi.org/10.1038/ncomms1251.

(2) Leonardi, A. K.; Ober, C. K. Polymer-Based Marine Antifouling and Fouling Release Surfaces: Strategies for Synthesis and Modification. *Annu. Rev. Chem. Biomol. Eng.* **2019**, *10* (1), 241–264. https://doi.org/10.1146/annurev-chembioeng-060718-030401.

(3) Gu, Y.; Yu, L.; Mou, J.; Wu, D.; Xu, M.; Zhou, P.; Ren, Y. Research Strategies to Develop Environmentally Friendly Marine Antifouling Coatings. *Mar. Drugs* **2020**, *18* (7), 371. https://doi.org/10.3390/md18070371.

(4) Hellio, C.; Yebra, D. M. 1 - Introduction. In *Advances in Marine Antifouling Coatings and Technologies*; Hellio, C., Yebra, D., Eds.; Woodhead Publishing Series in Metals and Surface Engineering; Woodhead Publishing, 2009; pp 1–15. https://doi.org/10.1533/9781845696313.1.

(5) Lim, J. Y.; Tay, T. S.; Lim, C. S.; Lee, S. S. C.; Teo, S. L.-M.; Tan, K. S. Mytella Strigata (Bivalvia: Mytilidae): An Alien Mussel Recently Introduced to Singapore and Spreading Rapidly. *Molluscan Res.* **2018**, *38* (3), 170–186. https://doi.org/10.1080/13235818.2018.1423858.

(6) Sanpanich, K.; Wells, F. Mytella Strigata (Hanley, 1843) Emerging as an Invasive Marine Threat in Southeast Asia. *BioInvasions Rec.* **2019**, *8*. https://doi.org/10.3391/bir.2019.8.2.16.

(7) Krishnan, S.; J. Weinman, C.; K. Ober, C. Advances in Polymers for Anti-Biofouling Surfaces. *J. Mater. Chem.* **2008**, *18* (29), 3405–3413. https://doi.org/10.1039/B801491D.

(8) Yang, W. J.; Neoh, K.-G.; Kang, E.-T.; Teo, S. L.-M.; Rittschof, D. Polymer Brush Coatings for Combating Marine Biofouling. *Prog. Polym. Sci.* **2014**, *39* (5), 1017–1042. https://doi.org/10.1016/j.progpolymsci.2014.02.002.

(9) He, M.; Gao, K.; Zhou, L.; Jiao, Z.; Wu, M.; Cao, J.; You, X.; Cai, Z.; Su, Y.; Jiang, Z. Zwitterionic Materials for Antifouling Membrane Surface Construction. *Acta Biomater.* **2016**, *40*, 142–152. https://doi.org/10.1016/j.actbio.2016.03.038.

(10) Murosaki, T.; Ahmed, N.; Gong, J. P. Antifouling Properties of Hydrogels. *Sci. Technol. Adv. Mater.* **2011**, *12* (6), 064706. https://doi.org/10.1088/1468-6996/12/6/064706.

(11) Lejars, M.; Margaillan, A.; Bressy, C. Fouling Release Coatings: A Nontoxic Alternative to Biocidal Antifouling Coatings. *Chem. Rev.* **2012**, *112* (8), 4347–4390. https://doi.org/10.1021/cr200350v.

(12) Magin, C. M.; Cooper, S. P.; Brennan, A. B. Non-Toxic Antifouling Strategies. *Mater. Today* **2010**, *13* (4), 36–44. https://doi.org/10.1016/S1369-7021(10)70058-4.

(13) Leng, C.; Buss, H. G.; Segalman, R. A.; Chen, Z. Surface Structure and Hydration of Sequence-Specific Amphiphilic Polypeptoids for Antifouling/Fouling Release Applications. *Langmuir* **2015**, *31* (34), 9306–9311. https://doi.org/10.1021/acs.langmuir.5b01440.

(14) Rufin, M. A.; Gruetzner, J. A.; Hurley, M. J.; Hawkins, M. L.; Raymond, E. S.; Raymond, J. E.; Grunlan, M. A. Enhancing the Protein Resistance of Silicone via Surface-Restructuring PEO–Silane Amphiphiles with Variable PEO Length. *J. Mater. Chem. B* **2015**, *3* (14), 2816–2825. https://doi.org/10.1039/C4TB02042A.

(15) Ge, A.; Qiao, L.; Seo, J.-H.; Yui, N.; Ye, S. Surface-Restructuring Differences between Polyrotaxanes and Random Copolymers in Aqueous Environment. *Langmuir* **2018**, *34* (41), 12463–12470. https://doi.org/10.1021/acs.langmuir.8b02676.

(16) Dimitriou, M. D.; Zhou, Z.; Yoo, H.-S.; Killops, K. L.; Finlay, J. A.; Cone, G.; Sundaram, H. S.; Lynd, N. A.; Barteau, K. P.; Campos, L. M.; Fischer, D. A.; Callow, M. E.; Callow, J. A.; Ober, C. K.; Hawker, C. J.; Kramer, E. J. A General Approach to Controlling the Surface Composition of Poly(Ethylene Oxide)-Based Block Copolymers for Antifouling Coatings. *Langmuir* **2011**, *27* (22), 13762–13772. https://doi.org/10.1021/la202509m.

(17) Wang, Y.; Betts, D. E.; Finlay, J. A.; Brewer, L.; Callow, M. E.; Callow, J. A.; Wendt, D. E.; DeSimone, J. M. Photocurable Amphiphilic Perfluoropolyether/Poly(Ethylene Glycol) Networks for Fouling-Release Coatings. *Macromolecules* **2011**, *44* (4), 878–885. https://doi.org/10.1021/ma102271t.

(18) van Zoelen, W.; Buss, H. G.; Ellebracht, N. C.; Lynd, N. A.; Fischer, D. A.; Finlay, J.; Hill, S.; Callow, M. E.; Callow, J. A.; Kramer, E. J.; Zuckermann, R. N.; Segalman, R. A. Sequence of Hydrophobic and Hydrophilic Residues in Amphiphilic Polymer Coatings Affects Surface Structure and Marine

Antifouling/Fouling Release Properties. *ACS Macro Lett.* **2014**, *3* (4), 364–368. https://doi.org/10.1021/mz500090n.

(19) Martinelli, E.; Suffredini, M.; Galli, G.; Glisenti, A.; Pettitt, M. E.; Callow, M. E.; Callow, J. A.; Williams, D.; Lyall, G. Amphiphilic Block Copolymer/Poly(Dimethylsiloxane) (PDMS) Blends and Nanocomposites for Improved Fouling-Release. *Biofouling* **2011**, *27* (5), 529–541. https://doi.org/10.1080/08927014.2011.584972.

(20) Martinelli, E.; Sarvothaman, M. K.; Galli, G.; Pettitt, M. E.; Callow, M. E.; Callow, J. A.; Conlan, S. L.; Clare, A. S.; Sugiharto, A. B.; Davies, C.; Williams, D. Poly(Dimethyl Siloxane) (PDMS) Network Blends of Amphiphilic Acrylic Copolymers with Poly(Ethylene Glycol)-Fluoroalkyl Side Chains for Fouling-Release Coatings. II. Laboratory Assays and Field Immersion Trials. *Biofouling* **2012**, *28* (6), 571–582. https://doi.org/10.1080/08927014.2012.697897.

(21) Faÿ, F.; Hawkins, M. L.; Réhel, K.; Grunlan, M. A.; Linossier, I. Non-Toxic, Anti-Fouling Silicones with Variable PEO–Silane Amphiphile Content. *Green Mater.* **2016**, *4* (2), 53–62. https://doi.org/10.1680/jgrma.16.00003.

(22) Galhenage, T. P.; Webster, D. C.; Moreira, A. M. S.; Burgett, R. J.; Stafslien, S. J.; Vanderwal, L.; Finlay, J. A.; Franco, S. C.; Clare, A. S. Poly(Ethylene) Glycol-Modified, Amphiphilic, Siloxane–Polyurethane Coatings and Their Performance as Fouling-Release Surfaces. *J. Coat. Technol. Res.* **2017**, *14* (2), 307–322. https://doi.org/10.1007/s11998-016-9862-9.

(23) Zouaghi, S.; Barry, M. E.; Bellayer, S.; Lyskawa, J.; André, C.; Delaplace, G.; Grunlan, M. A.; Jimenez, M. Antifouling Amphiphilic Silicone Coatings for Dairy Fouling Mitigation on Stainless Steel. *Biofouling* **2018**, *34* (7), 769–783. https://doi.org/10.1080/08927014.2018.1502275.

(24) Sundaram, H. S.; Cho, Y.; Dimitriou, M. D.; Weinman, C. J.; Finlay, J. A.; Cone, G.; Callow, M. E.; Callow, J. A.; Kramer, E. J.; Ober, C. K. Fluorine-Free Mixed Amphiphilic Polymers Based on PDMS and PEG Side Chains for Fouling Release Applications. *Biofouling* **2011**, *27* (6), 589–602. https://doi.org/10.1080/08927014.2011.587662.

(25) Ma, W.; Rajabzadeh, S.; Shaikh, A. R.; Kakihana, Y.; Sun, Y.; Matsuyama, H. Effect of Type of Poly(Ethylene Glycol) (PEG) Based Amphiphilic Copolymer on Antifouling Properties of Copolymer/Poly(Vinylidene Fluoride) (PVDF) Blend Membranes. *J. Membr. Sci.* **2016**, *514*, 429–439. https://doi.org/10.1016/j.memsci.2016.05.021.

(26) Quiñones-Pérez, M.; Cieza, R. J.; Ngo, B. K. D.; Grunlan, M. A.; Domenech, M. Amphiphilic Silicones to Reduce the Absorption of Small Hydrophobic Molecules. *Acta Biomater.* **2021**, *121*, 339–348. https://doi.org/10.1016/j.actbio.2020.11.041.

(27) Guo, H.; Chen, P.; Tian, S.; Ma, Y.; Li, Q.; Wen, C.; Yang, J.; Zhang, L. Amphiphilic Marine Antifouling Coatings Based on a Hydrophilic Polyvinylpyrrolidone and Hydrophobic Fluorine–Silicon-Containing Block Copolymer. *Langmuir* **2020**, *36* (48), 14573–14581. https://doi.org/10.1021/acs.langmuir.0c02329.

(28) Rahimi, A.; Stafslien, S. J.; Vanderwal, L.; Finlay, J. A.; Clare, A. S.; Webster, D. C. Amphiphilic Zwitterionic-PDMS-Based Surface-Modifying Additives to Tune Fouling-Release of Siloxane-Polyurethane Marine Coatings. *Prog. Org. Coat.* **2020**, *149*, 105931. https://doi.org/10.1016/j.porgcoat.2020.105931.

(29) Wang, J.; Zhang, S.; Wu, P.; Shi, W.; Wang, Z.; Hu, Y. In Situ Surface Modification of Thin-Film Composite Polyamide Membrane with Zwitterions for Enhanced Chlorine Resistance and Transport Properties. *ACS Appl. Mater. Interfaces* **2019**, *11* (12), 12043–12052. https://doi.org/10.1021/acsami.8b21572.

(30) Zuckermann, R. N.; Kerr, J. M.; Kent, S. B. H.; Moos, W. H. Efficient Method for the Preparation of Peptoids [Oligo(N-Substituted Glycines)] by Submonomer Solid-Phase Synthesis. *J. Am. Chem. Soc.* **1992**, *114* (26), 10646–10647. https://doi.org/10.1021/ja00052a076.

(31) Zuckermann, R. N. Peptoid Origins. *Pept. Sci.* **2011**, *96* (5), 545–555. https://doi.org/10.1002/bip.21573.

(32) Lau, K. H. A.; Sileika, T. S.; Park, S. H.; Sousa, A. M. L.; Burch, P.; Szleifer, I.; Messersmith, P. B. Molecular Design of Antifouling Polymer Brushes Using Sequence-Specific Peptoids. *Adv. Mater. Interfaces* **2015**, *2* (1), 1400225. https://doi.org/10.1002/admi.201400225.

(33) Ganesh, S. D.; Saha, N.; Zandraa, O.; Zuckermann, R. N.; Sáha, P. Peptoids and Polypeptoids: Biomimetic and Bioinspired Materials for Biomedical Applications. *Polym. Bull.* **2017**, *74* (8), 3455–3466. https://doi.org/10.1007/s00289-016-1902-1.

(34) Patterson, A. L.; Wenning, B.; Rizis, G.; Calabrese, D. R.; Finlay, J. A.; Franco, S. C.; Zuckermann, R. N.; Clare, A. S.; Kramer, E. J.; Ober, C. K.; Segalman, R. A. Role of Backbone Chemistry and Monomer Sequence in Amphiphilic Oligopeptide- and Oligopeptoid-Functionalized PDMS- and PEO-Based Block Copolymers for

Marine Antifouling and Fouling Release Coatings. *Macromolecules* **2017**, *50* (7), 2656–2667. https://doi.org/10.1021/acs.macromol.6b02505.

(35) Barry, M. E.; Davidson, E. C.; Zhang, C.; Patterson, A. L.; Yu, B.; Leonardi, A. K.; Duzen, N.; Malaviya, K.; Clarke, J. L.; Finlay, J. A.; Clare, A. S.; Chen, Z.; Ober, C. K.; Segalman, R. A. The Role of Hydrogen Bonding in Peptoid-Based Marine Antifouling Coatings. *Macromolecules* **2019**, *52* (3), 1287–1295. https://doi.org/10.1021/acs.macromol.8b02390.

(36) Chen, Z. Investigating Buried Polymer Interfaces Using Sum Frequency Generation Vibrational Spectroscopy. *Prog. Polym. Sci.* **2010**, *35* (11), 1376–1402. https://doi.org/10.1016/j.progpolymsci.2010.07.003.

(37) Monroe, J.; Barry, M.; DeStefano, A.; Gokturk, P. A.; Jiao, S.; Robinson-Brown, D.; Webber, T.; Crumlin, E. J.; Han, S.; Shell, M. S. Water Structure and Properties at Hydrophilic and Hydrophobic Surfaces. *Annu. Rev. Chem. Biomol. Eng.* **2020**, *11* (1), null. https://doi.org/10.1146/annurev-chembioeng-120919-114657.

(38) Cheng, J.-X.; Pautot, S.; Weitz, D. A.; Xie, X. S. Ordering of Water Molecules between Phospholipid Bilayers Visualized by Coherent Anti-Stokes Raman Scattering Microscopy. *Proc. Natl. Acad. Sci.* **2003**, *100* (17), 9826–9830. https://doi.org/10.1073/pnas.1732202100.

(39) Czanderna, A. W. Introduction. In *Methods of Surface Analysis*; Czanderna, A. W., Ed.; Elsevier, 1975; pp 1–4. https://doi.org/10.1016/C2009-0-07448-0.

(40) Shavorskiy, A.; Karslioglu, O.; Zegkinoglou, I.; Bluhm, H. Synchrotron-Based Ambient Pressure X-Ray Photoelectron Spectroscopy. *Synchrotron Radiat. News* **2014**, *27* (2), 14–23. https://doi.org/10.1080/08940886.2014.889547.

(41) Yamamoto, S.; Bluhm, H.; Andersson, K.; Ketteler, G.; Ogasawara, H.; Salmeron, M.; Nilsson, A. In Situx-Ray Photoelectron Spectroscopy Studies of Water on Metals and Oxides at Ambient Conditions. *J. Phys. Condens. Matter* **2008**, *20* (18), 184025. https://doi.org/10.1088/0953-8984/20/18/184025.

(42) Ketteler, G.; Yamamoto, S.; Bluhm, H.; Andersson, K.; Starr, D. E.; Ogletree, D. F.; Ogasawara, H.; Nilsson, A.; Salmeron, M. The Nature of Water Nucleation Sites on TiO2(110) Surfaces Revealed by Ambient Pressure X-Ray Photoelectron Spectroscopy. *J. Phys. Chem. C* **2007**, *111* (23), 8278–8282. https://doi.org/10.1021/jp068606i.

(43) Gokturk, P. A.; Barry, M.; Segalman, R.; Crumlin, E. J. Directly Probing Polymer Thin Film Chemistry and Counterion Influence on Water Sorption. *ACS Appl. Polym. Mater.* **2020**, *2* (11), 4752–4761. https://doi.org/10.1021/acsapm.0c00756.

(44) Axnanda, S.; Crumlin, E. J.; Mao, B.; Rani, S.; Chang, R.; Karlsson, P. G.; Edwards, M. O. M.; Lundqvist, M.; Moberg, R.; Ross, P.; Hussain, Z.; Liu, Z. Using "Tender" X-Ray Ambient Pressure X-Ray Photoelectron Spectroscopy as A Direct Probe of Solid-Liquid Interface. *Sci. Rep.* **2015**, *5* (1), 9788. https://doi.org/10.1038/srep09788.

(45) Salmeron, M.; Schlögl, R. Ambient Pressure Photoelectron Spectroscopy: A New Tool for Surface Science and Nanotechnology. *Surf. Sci. Rep.* **2008**, *63* (4), 169–199. https://doi.org/10.1016/j.surfrep.2008.01.001.

(46) Schnadt, J.; Knudsen, J.; Johansson, N. Present and New Frontiers in Materials Research by Ambient Pressure X-Ray Photoelectron Spectroscopy. *J. Phys. Condens. Matter* **2020**, *32* (41), 413003. https://doi.org/10.1088/1361-648X/ab9565.

(47) Han, Y.; Zhang, H.; Yu, Y.; Liu, Z. In Situ Characterization of Catalysis and Electrocatalysis Using APXPS. *ACS Catal.* **2021**, *11* (3), 1464–1484. https://doi.org/10.1021/acscatal.0c04251.

(48) Favaro, M.; Jeong, B.; Ross, P. N.; Yano, J.; Hussain, Z.; Liu, Z.; Crumlin, E. J. Unravelling the Electrochemical Double Layer by Direct Probing of the Solid/Liquid Interface. *Nat. Commun.* **2016**, *7* (1), 12695. https://doi.org/10.1038/ncomms12695.

(49) Favaro, M.; Yang, J.; Nappini, S.; Magnano, E.; Toma, F. M.; Crumlin, E. J.; Yano, J.; Sharp, I. D. Understanding the Oxygen Evolution Reaction Mechanism on CoOx Using Operando Ambient-Pressure X-Ray Photoelectron Spectroscopy. *J. Am. Chem. Soc.* **2017**, *139* (26), 8960–8970. https://doi.org/10.1021/jacs.7b03211.

(50) Křepelová, A.; Newberg, J.; Huthwelker, T.; Bluhm, H.; Ammann, M. The Nature of Nitrate at the Ice Surface Studied by XPS and NEXAFS. *Phys. Chem. Chem. Phys.* **2010**, *12* (31), 8870–8880. https://doi.org/10.1039/C0CP00359J.

(51) Bluhm, H. Photoelectron Spectroscopy of Surfaces under Humid Conditions. *Water Hydrog. Bonds* **2010**, *177* (2), 71–84. https://doi.org/10.1016/j.elspec.2009.08.006.

(52) Kong, X.; Castarède, D.; Boucly, A.; Artiglia, L.; Ammann, M.; Bartels-Rausch, T.; Thomson, E. S.; Pettersson, J. B. C. Reversibly Physisorbed and Chemisorbed Water on Carboxylic Salt Surfaces Under Atmospheric Conditions. *J. Phys. Chem. C* **2020**, *124* (9), 5263–5269. https://doi.org/10.1021/acs.jpcc.0c00319.

(53) Ketteler, G.; Ashby, P.; Mun, B. S.; Ratera, I.; Bluhm, H.; Kasemo, B.; Salmeron, M. In Situphotoelectron Spectroscopy Study of Water Adsorption on Model Biomaterial Surfaces. *J. Phys. Condens. Matter* **2008**, *20* (18), 184024. https://doi.org/10.1088/0953-8984/20/18/184024.

(54) Valero-Vidal, C.; Favaro, M.; Yu, Y.; Crumlin, E. J. Electrochemical Characterization of the Titanium/Pbs Interface By Ambient Pressure X-Ray Photoelectron Spectroscopy. *ECS Meet. Abstr.* **2016**, *MA2016-02* (10), 1203. https://doi.org/10.1149/MA2016-02/10/1203.

(55) Buechner, C.; Gericke, S. M.; Trotochaud, L.; Karslıoğlu, O.; Raso, J.; Bluhm, H. Quantitative Characterization of a Desalination Membrane Model System by X-Ray Photoelectron Spectroscopy. *Langmuir* **2019**, *35* (35), 11315–11321. https://doi.org/10.1021/acs.langmuir.9b01838.

(56) Gericke, S. M.; Mulhearn, W. D.; Goodacre, D. E.; Raso, J.; Miller, D. J.; Carver, L.; Nemšák, S.; Karslıoğlu, O.; Trotochaud, L.; Bluhm, H.; Stafford, C. M.; Buechner, C. Water-Polyamide Chemical Interplay in Desalination Membranes Explored by Ambient Pressure X-Ray Photoelectron Spectroscopy. *Phys. Chem. Chem. Phys.* **2020**, *22* (27), 15658–15663. https://doi.org/10.1039/D0CP01842B.

(57) Trotochaud, L.; Head, A. R.; Pletincx, S.; Karslıoğlu, O.; Yu, Y.; Waldner, A.; Kyhl, L.; Hauffman, T.; Terryn, H.; Eichhorn, B.; Bluhm, H. Water Adsorption and Dissociation on Polycrystalline Copper Oxides: Effects of Environmental Contamination and Experimental Protocol. *J. Phys. Chem. B* **2018**, *122* (2), 1000–1008. https://doi.org/10.1021/acs.jpcb.7b10732.

(58) Qian, J.; Ye, Y.; Yang, H.; Yano, J.; Crumlin, E. J.; Goddard, W. A. Initial Steps in Forming the Electrode–Electrolyte Interface: H2O Adsorption and Complex Formation on the Ag(111) Surface from Combining Quantum Mechanics Calculations and Ambient Pressure X-Ray Photoelectron Spectroscopy. *J. Am. Chem. Soc.* **2019**, *141* (17), 6946–6954. https://doi.org/10.1021/jacs.8b13672.

(59) Deng, X.; Herranz, T.; Weis, C.; Bluhm, H.; Salmeron, M. Adsorption of Water on Cu2O and Al2O3 Thin Films. *J. Phys. Chem. C* **2008**, *112* (26), 9668–9672. https://doi.org/10.1021/jp800944r.

(60) Newberg, J. T.; Starr, D. E.; Yamamoto, S.; Kaya, S.; Kendelewicz, T.; Mysak, E. R.; Porsgaard, S.; Salmeron, M. B.; Brown, G. E.; Nilsson, A.; Bluhm, H. Formation of Hydroxyl and Water Layers on MgO Films Studied with Ambient Pressure XPS. *Surf. Sci.* **2011**, *605* (1), 89–94. https://doi.org/10.1016/j.susc.2010.10.004.

(61) Gervais, M.; Douy, A.; Gallot, B.; Erre, R. Surface Analysis of Lipopeptides Using X-Ray Photoelectron Spectroscopy: I. Lipopeptides with Polysarcosine Peptidic Chains. *J. Colloid Interface Sci.* **1988**, *125* (1), 146–154. https://doi.org/10.1016/0021-9797(88)90063-X.

(62) G. Beamson; D. Briggs. *High Resolution XPS of Organic Polymers: The Scienta ESCA300 Database*; Wiley-VCH, 1992.

(63) Cumpson, P. J. Estimation of Inelastic Mean Free Paths for Polymers and Other Organic Materials: Use of Quantitative Structure–Property Relationships. *Surf. Interface Anal.* **2001**, *31* (1), 23–34. https://doi.org/10.1002/sia.948.

(64) Hofmann, S. Quantitative Analysis (Data Evaluation). In *Auger- and X-Ray Photoelectron Spectroscopy in Materials Science: A User-Oriented Guide*; Springer Science & Business Media, 2012; pp 77–201.

Chapter 4
Investigating solvent adsorption affinity for organic surfaces with ambient-pressure XPS

Adsorption-mediating interactions between the surface and small molecules crucially affect material functionality for many applications including pervaporation and water purification membranes, medical implants, and antifouling coatings. While recent research efforts have elucidated interactions between water molecules and the surface, understanding the affinity of organic species is also critical for materials design in circumstances where these species will interact with the surface either in vapor or solution phases. Hydrogen bonding interactions are known to significantly affect adsorption affinity, but the strength of interactions between polar solvents and the surface is variable dependent on chemistry, makes comparisons difficult. Self-assembled monolayers (SAMs) serve as an excellent model system for investigating such interactions, presenting a single functional group at a surface with sub-nanometer roughness. In this work, the adsorption affinities of acetic acid, 1-butanol, and water for methyl (CH_3), hydroxyl (OH), and carboxylic acid (COOH) SAMs were quantitatively probed using ambient pressure X-ray

photoelectron spectroscopy. Acetic acid displayed higher adsorption affinity for OH and COOH SAMs than butanol and water, but showed differences in electronic environment once adsorbed, deprotonating only on the COOH SAM surface. The effects of surface and solvent identity were not interchangeable: acetic acid adsorbed onto the OH SAM surface, but butanol failed to adsorb onto the carboxylic acid SAM. These findings suggest that the role of the surface in facilitating adsorption is distinct from that of the adsorbing species, possibly due to the spacing of functional groups, and that the surface chemistry can be tuned to induce particular interactions, such as deprotonation.

4.1 Introduction

Adsorption-mediating interactions at organic surfaces are significant for many fields, especially water/gas filtration membranes, biology, medicine, and marine antifouling coatings. For membrane applications, understanding of surface-mediated interactions between water, solutes, and the surface is especially critical for improving selectivity and overall yields. Recently, experimental and computational efforts have vastly improved current understanding of the way that water and surfaces interact.[1,2] While this is essential for water purification, most separations involve highly complex aqueous mixtures with other species that also interact with membrane surfaces. Small organic molecules are highly prevalent in waste streams,[3,4] and others have high economic potential in biofuel production. For instance, butanol is advantageous as a replacement for motor fuel, even more so than ethanol:[5–7] it contains close to the same energy density as gasoline (nearly 1.5 times that of ethanol), has a lower vapor pressure that allows it to be used in

existing gasoline supply channels, and is less to partition with water when present in gasoline mixtures.[8] However, its high toxicity to microorganisms means that separations must be able to remove it at very low concentrations in water.[9] Pervaporation is similarly dependent on solvent–surface interactions. Leveraging a thin membrane that separates liquid-phase and low vacuum environments, this process allows for the removal of organic solvents from aqueous mixtures and vice versa, or for separation of organic mixtures.[10,11] In order for separation to occur, the solvent must preferentially adsorb onto the membrane material and travel to the low-pressure side: acetic acid is a common byproduct in biofuel production pretreatment stages, but due to its toxicity must be removed in order to avoid interference with microorganism metabolism.[12] Removal of this acid via pervaporation is known to be challenging,[13] but is enhanced by the incorporation of Brønsted acidic sites,[14] which likely increase affinity.

For both aqueous and vapor phase separations of polar organic molecules, hydrogen bonding plays a key role in initiating surface interactions.[15] This has been particularly followed by the antifouling community, which uses either materials with a strong affinity for water (such as zwitterions, PEG, or polysaccharides)[16–19] or materials with low surface energy (including fluorinated functionalities and siloxanes)[16,17,20] to mitigate adsorption interactions. While hydrophilicity has often been used as a metric for preventing adsorption, it is apparent that hydrogen bonding can instigate water structuring and still also lead to stronger interactions with solutes or microorganisms.[21] Common design rules note that hydrophilicity without the use of hydrogen bond donors produces a superior antifouling surface than one where hydrogen bond donors are incorporated.[22–24]

However, the nuances and breadth of hydrogen bonding interactions is still under exploration, particularly by computational methods.[25] In addition to the molecular makeup of the hydrogen bond donor or acceptor itself, the electronegativity of adjacent functionalities can further strengthen or weaken hydrogen bonds as electron donators or acceptors.[26] The distance between hydrogen bonds as well as the number of participating groups can further increase strength: a single hydrogen bond donor or acceptor can interact with two acceptors or donors in a "bifurcated" hydrogen bonding system, while bidentate hydrogen bonds involve two adjacent hydrogen bond donor/acceptor pairs.[25,27] The effects of varying hydrogen bonding interaction strengths are widely apparent in nature, giving promise for better design of future materials. For instance, bidentate catechol functionalities provide mussels with the ability to adhere to many types of underwater surfaces (despite the presence of water that screens hydrogen bonding interactions)[28] and have become adopted in many bioinspired adhesives and self-healing materials.[29–31]

Despite the pressing need for widescale design rules to support or suppress adsorption, the chemical and structural complexity of most coatings and membranes make direct relations of chemistry to adsorption-mediating interactions difficult. Self-assembled monolayers (SAMs) are advantageous for investigating the roles of particular functional group chemistries without the effects of morphology or heterogeneity.[32] These consist of densely packed monomolecular layers made by the adsorption and spontaneous assembly of organic molecules, and contain a head group that presents at the outer surface, an oligomeric backbone chain, and a reactive linker for binding to the substrate. Ultimately, the surface consists of the singular head group chemistry with sub-nanometer roughness, enabling study of interactions between functional groups on a flat, homogeneous

surface.[33,34] While several distinctive classes of SAM molecular chemistries have been formed, the most prevalent consist of thiols linked to gold or other oxide-free metals, or silanes bound to hydroxylated surfaces such as silica.[35] The former are known to consistently form a well-packed single molecule layer and provide access to a wide range of surface chemistries such as methyl, alcohol, and carboxylic acid terminal functionalities.[32,36] Experimental adsorption affinity of solvents can thus be linked to common biological and polymeric functional groups.

Ambient pressure X-ray photoelectron spectroscopy (APXPS) has gained recognition for its ability to quantify surface-mediated processes such as adsorption and subsequent reactions.[37–40] This technique uses ejected photoelectrons to characterize the composition and electronic environment of the top few nanometers of the surface with fine control over the pressure and temperature within the analysis chamber.[41] In addition to exploring adsorption of water onto a variety of organic[36,42,43] and inorganic[44–47] surfaces, APXPS has been useful for probing the adsorption of organic solvents, such as isopropanol,[48] acetone,[49] and acetic acid,[50] onto the surface of ice. Notably, these three solvents were shown to follow a Langmuir adsorption isotherm, indicating primary interactions with the surface are necessary and limit coverage to a singular molecular layer.[51] As a result, APXPS is highly useful for understanding surface interactions as are relevant for membrane processes as well as other similar applications.

In this work, the affinity of model polar solvents (i.e., acetic acid, butanol, and water) for SAM surfaces containing methyl (CH_3), hydroxyl (OH), and carboxylic acid (COOH) head groups was probed using APXPS (**Figure 1**). The functional group chemistries of both the solvent and surface collaboratively determined surface affinity.

Only acetic acid was found to adsorb at the explored pressures, doing so on the hydrogen bonding OH- and COOH-terminated surfaces, with widespread deprotonation on the latter. Notably, the role of the surface and solvent species was not interchangeable: acetic acid easily adsorbed onto hydroxylated surfaces, but butanol was not found to adsorb onto carboxylic acid surfaces. These findings show that surfaces and adsorbing species play distinct roles in adsorption and desorption processes, possibly affected by the spacing of functional groups on the surface, and that surface chemistries can be tuned to promote desirable interactions, such as deprotonation.

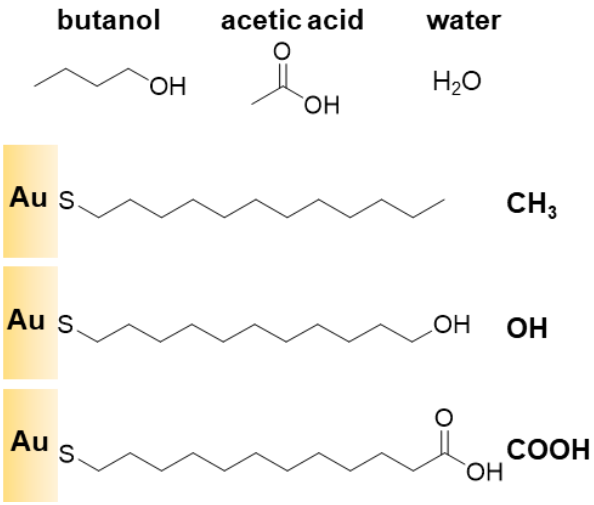

Figure 1. Top: Selected polar solvents included butanol, acetic acid, and water, which contain varying numbers of hydrogen bond acceptors and donors. Bottom: Thiol SAM chemistries displayed surfaces consisting of methyl, hydroxyl, or carboxylic acid head groups.

4.2 Experimental Methods

4.2.1 Materials

1-dodecanethiol, 11-mercaptoundecanol, and 12-mercaptododecanoic acid used in preparing self-assembled monolayers (SAMs) were purchased from Sigma Aldrich. Glacial acetic acid, 200 proof anhydrous ethanol, and anhydrous n-butanol were also obtained from Sigma Aldrich.

4.2.2 Template stripping of gold

Template-stripped gold as a substrate for self-assembled monolayers was leveraged due to its ability to provide a clean and ultrasmooth surface on demand.[52–54] Briefly, prime grade silicon wafers were cleaned with O_2 plasma for 5 minutes before vapor deposition of 250 nm Au. Small droplets of adhesive epoxy (EPO-TEK 377) were then placed onto the gold surface and covered with ~1 cm^2 silicon wafer pieces. After curing for 1 hour at 150 C, the wafer piece was attached to the 250 nm Au layer. Immediately before SAM preparation, the wafer and gold was stripped from the prime grade silicon substrate, revealing a clean and smooth gold surface underneath.

4.2.3 SAMs fabrication

Preparation of self-assembled monolayer (SAM) surfaces is well-established in literature.[32,55] Thiol SAMs were prepared by immersing freshly-exposed gold wafer pieces in 3 mM thiol solutions for 24 hours under inert atmosphere. 1-dodecanethiol and 11-mercaptoundecanol were dissolved in anhydrous ethanol while 12-mercaptododecanoic acid was dissolved in a low pH ethanol/water/acetic acid solution (85/10/5, v/v/v).[56] After 24 hours, CH_3, OH, and COOH SAMs were rinsed with ethanol to remove excess thiol. (OH and COOH SAMs were also sonicated for ~3 minutes to remove any residual hydrogen bound thiol.) The SAMs were then dried with nitrogen, placed into a nitrogen glove bag, and then loaded into the APXPS preparatory chamber within 30 minutes. Exposure to oxygen atmosphere was limited to under 5 minutes. XPS analysis confirms that oxidation was insignificant, as the sulfur-Au linkages were bound to gold with no free thiol (**Figure C3**).

4.2.4 APXPS measurements

All XPS measurements were conducted at the Advanced Light Source (ALS) of the Lawrence Berkeley National Laboratory with 100 eV pass energy at Beamline 9.3.2.[57] X-ray photon energy ranged from 325-690 eV. Due to the minimal thickness of the SAMs on gold, surface charging was insignificant. However, the SAMs exhibited beam-induced damage within a few minutes, so rastering methods were used during data acquisition to minimize damage.[42] Spectra were collected in 1-2 minutes in a single position before movement, and were found to be consistent from position to position (**Figure C2**). Summation of these spectra was done to improve the signal-to-noise ratio, particularly for the S 2p and O 1s core levels. The gold substrate's Au 4f core level was used for calibration of all peak intensities. No contributions were detected from the cured EPO-TEK 377 epoxy used to adhere the gold to the wafer piece due to the thickness of the 250 nm gold underlayer.

For *in situ* measurements, anhydrous butanol, glacial acetic acid, and Milli-Q water were each added to a glass bulb and degassed by three freeze−pump−thaw cycles before introduction into the analysis chambers. Using a precision leak valve, pressures of 250 mTorr for butanol and acetic acid vapor and 750 mTorr for water vapor were added to the analysis chamber at Beamline 9.3.2. These are for each solvent 5.5%, 2.1%, and 4.3% of the maximum vapor pressure at room temperature, respectively. After introduction of solvent to the chamber, samples were equilibrated for at least 15 minutes before data collection. No changes were seen thereafter over several hours, indicating equilibrium was established. All fitting procedures were performed on Casa XPS software with Shirley

background subtraction and 50/50 symmetrical Gaussian/Lorentzian product function line shapes for surface components.

4.2.5 AFM measurements

Tapping-mode AFM measurements were made using a Veeco MultiMode Scanning Probe Microscope. Images were collected using Nanosensors long cantilevers at 1.00 Hz.

4.3 Results and Discussion

4.3.1 Chemistry of SAMs and solvents

The ways that organic surfaces interact with solvents in the vapor phase for applications such as pervaporation are determined in large part by the chemistry of both the solvent and surface. Three relevant solvents for industry include water, butanol, and acetic acid. All three have similar vapor pressures, reducing the likelihood of differences in coverage being ascribed to differences in partial pressure in the Langmuir adsorption model.[51] All are also capable of participating in hydrogen bonding interactions: butanol and water have one and two hydrogen bond donors, respectively, while acetic acid has both a hydrogen bond donor and acceptor. Furthermore, each has a potentially labile proton, with acetic acid predictably being the strongest Brønsted acid, followed by water and finally butanol (**Table C1**). Use of SAMs terminated with methyl, alcohol, and carboxylic acid functionalities enables similar comparisons among the chemistries, while still being relevant as groups commonly present in biological and polymeric systems. From these properties, it is most likely that acetic is best at adsorbing onto surfaces, containing both a hydrogen bond donor and acceptor. The relatively higher vapor pressure of water would be expected to limit adsorption at 250 mTorr, so measurements were also taken at 750 mTorr water vapor pressure (4.3% RH) to be similar to butanol (5.5% P_0) and acetic acid (2.1% P_0) at 250 mTorr.

To isolate the effects of functional group chemistry on adsorption interactions, self-assembled monolayers (SAMs) were fabricated on gold. An ultrasmooth surface was created by template stripping of the gold from silicon (RMS roughness <0.2 nm; **Figure C1**), and the chemical purity of the produced SAM surfaces was investigated using XPS.

The monolayer samples were confirmed to be attached during measurement by their negligible thiol content and the S-Au 3/2 peak at 162.1 eV (**Figure C3**).

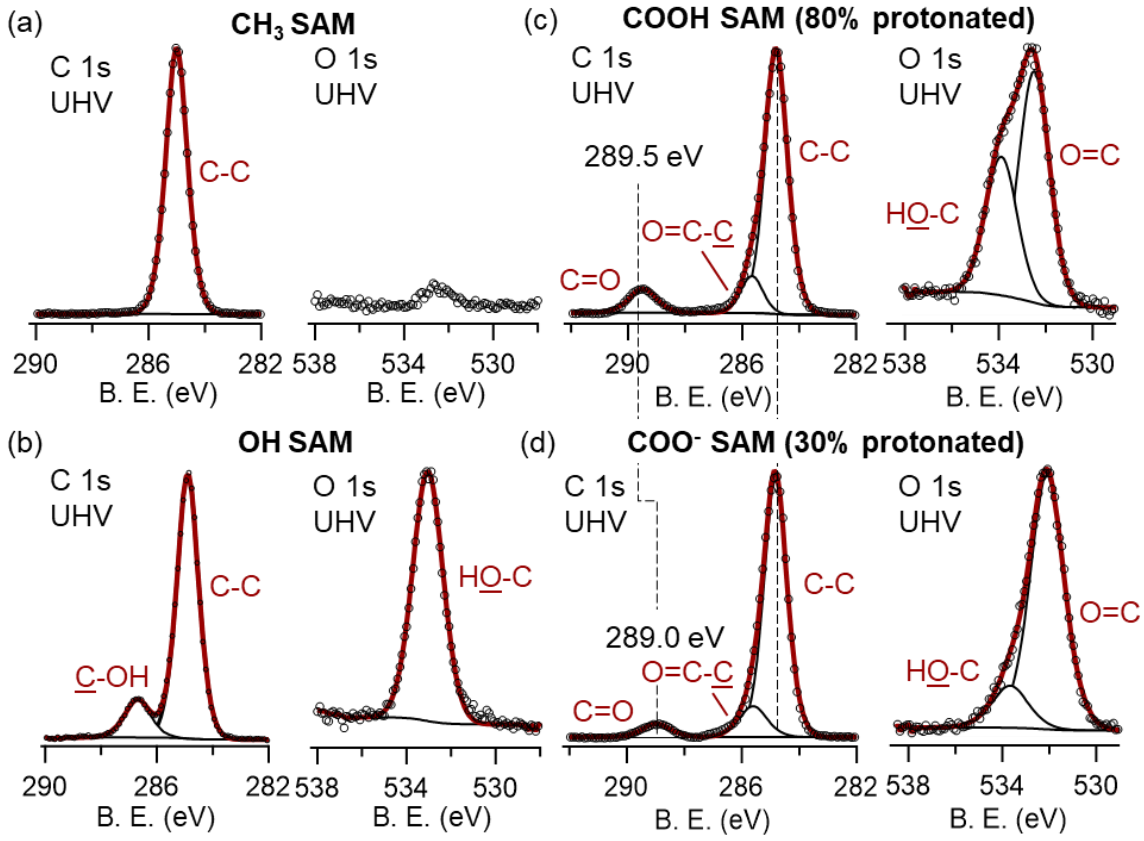

Figure 4-2. C 1s (445 eV) and O 1s (690 eV) spectra of (a) CH3, (b) OH, (c) majority protonated and (d) majority deprotonated COOH self-assembled monolayer surfaces under ultrahigh vacuum conditions. Minor amounts of oxygen impurity were detected in methyl SAM surfaces, while the degree of protonation for COOH SAM surfaces affected COOH position in the C 1s and C-OH magnitude.

CH_3, OH, and COOH SAMs all share a large C 1s 284.9 eV peak indicative of the SAM alkyl chain plus the sulfur-linked hydrocarbon (**Figure 4-2**). The terminal hydroxyl carbon is found at 286.7, while the primary and secondary carboxylic acid carbons (C=O and O=C-C, respectively) are present at 289.5 eV and 285.7 eV. Oxygen components probed to the same depth (**Figure 4-2**) are unique to each SAM chemistry. Small amounts of an impurity can be detected in the CH_3 SAM O 1s spectra, while the OH SAM's alcohol

component can be found at 533.8 eV. The acidic (HO-C) and carbonyl oxygens in the COOH SAM at 533.9 eV and 532.5 eV were found in different ratios depending on the method of preparation: low pH solutions yielded SAMs that were ~80% protonated as shown in **Figure 4-2c**, which is consistent with previous efforts in literature.[36] Deprotonated carboxyl groups (**Figure 4-2d**) have both reduced acidic oxygen intensity and lower electron binding energy to the primary carboxylic acid carbon (C=O). The asymmetry of the acid carbon peaks above are likely due to the presence of minority deprotonated and protonated groups in **Figures 4-2c** and **4-2d**, respectively.

4.3.2. Adsorption by solvent vapor

To investigate the affinity of relevant solvents in industry, the samples were exposed to 1-butanol, acetic acid, and water. All three solvents can participate in hydrogen bonding, and have a lower vapor pressure that makes adsorption more conducive during APXPS measurements. The SAM surfaces were found to display chemistry-dependent responses to vapor exposure (**Figure 4-3**).

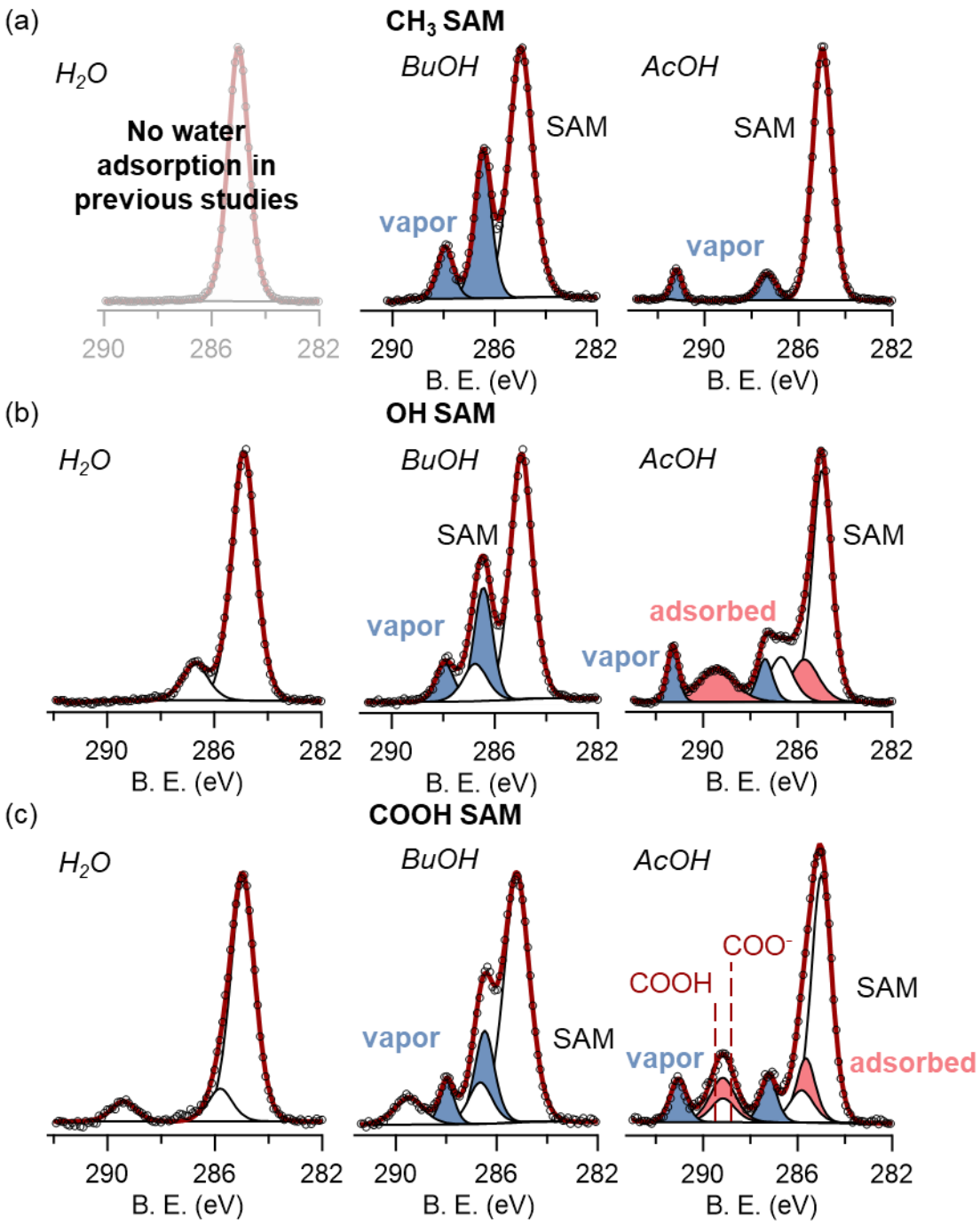

Figure 4-3. C 1s (445 eV) spectra of (a) CH3, (b) OH, and (c) COOH SAMs exposed to 750 mTorr water (left), 250 mTorr butanol (center) and 250 mTorr acetic acid (right) vapors. Methyl-terminated SAMs have previously been shown to not participate in water adsorption[36] and here show no interaction with any organic vapor species. OH and COOH SAMs both show acetic acid adsorption, but not butanol adsorption. As expected, addition of water has minimal effect on C 1s composition.

The methyl-terminated SAM never showed adsorption to butanol or acetic acid, and has been previously shown to not interact with water at low pressures.[36] Exposure to water, as expected, did not affect the C 1s composition of either the OH or COOH SAM surfaces. At 250 mTorr, butanol was not found to adsorb onto either COOH or OH SAM surfaces. Because the OH SAM and butanol consist of the same alcoholic carbon and oxygen chemical environments, quantitative core level comparisons were made according to a layered model to definitively confirm a lack of adsorption. Further details can be found in Appendix C.

However, acetic acid was found to adsorb onto both the OH- and COOH-terminated self-assembled monolayer upon exposure to 250 mTorr acid vapor, the same pressure at which butanol failed to adsorb. Molecular adsorption in the C 1s spectrum can be identified with the appearance of broad (salmon-colored) primary and secondary carboxylic acid peaks. For the OH SAM, the primary acid carbon is centered at 289.4 eV, indicating the acid is predominantly protonated, and is much broader than other components with a FWHM at 1.7 eV. It is possible that this wide breadth could be due to variability in hydrogen bonding interactions with the surface, such as bidentate or bifurcated H-bonds, though simulations would be necessary to confirm. The COOH SAM gains additional primary and secondary acid carbons from adsorption that are visible by the increased peak intensity near 289 eV and more significant shoulder at 285.7 eV. Unlike the OH SAM, the COOH SAM's combined acid peak is positioned in between the binding energies of protonated and deprotonated acidic carbons. Consequently, the adsorbed and SAM acid carbons are likely split into COOH and COO^- subcomponents. Because the components

overlap, it is difficult to ascertain whether the SAM surface or adsorbed acid participate equally in deprotonation or if one largely dominates.

O 1s spectra of surfaces in contact with water, butanol, and acetic acid vapor confirm that adsorption is limited to acetic acid. Water adsorption measurements were collected up to 750 mTorr water vapor pressure, but no increases in oxygen content or changes in trace shape were seen for either the OH or COOH SAM component (**Figures 4-4a** and **4-4e**, respectively). No adsorbed butanol was detected either (**Figures 4-4b and 4-4f**), corroborating observations of the C 1s spectra for the OH and COOH SAM.

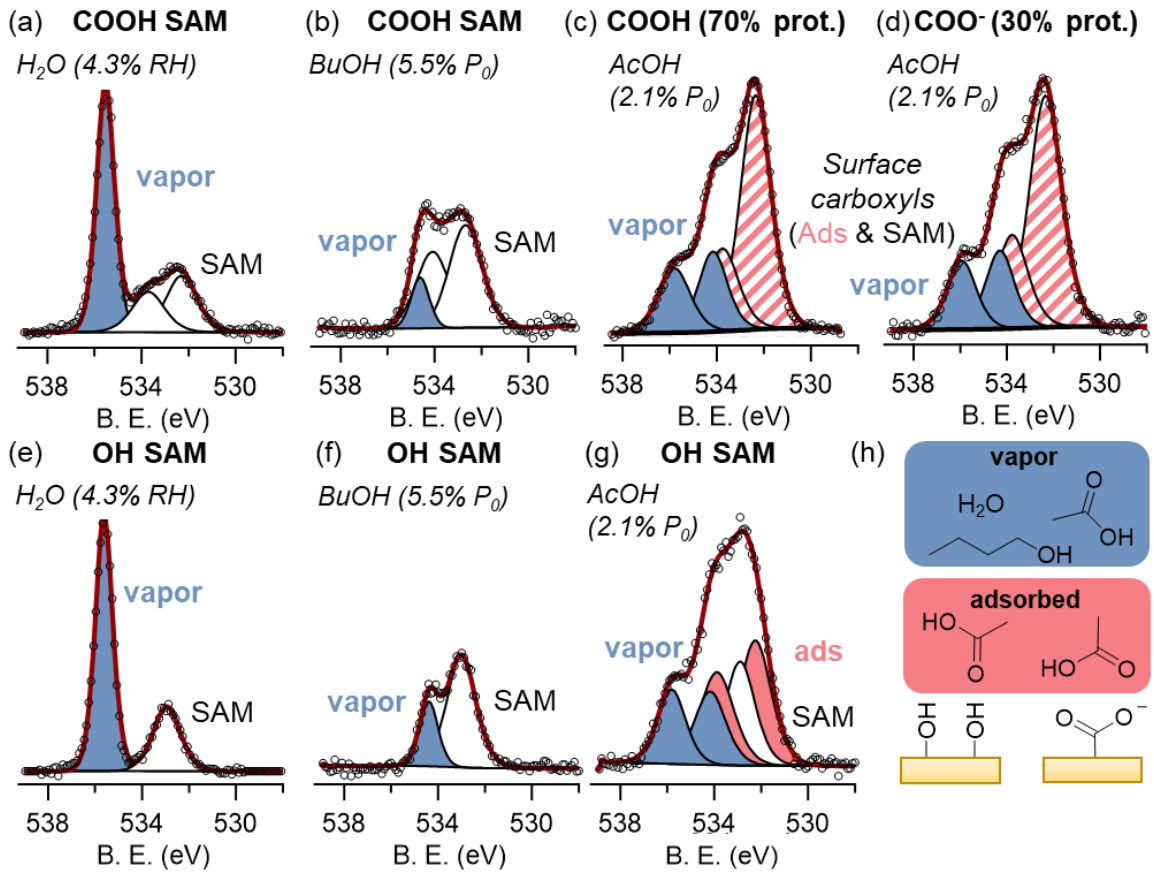

Figure 4-4. O 1s spectra of COOH (top; a-d) and OH (bottom; e-g) SAM surfaces at equivalent depths with C 1s. Measurements were taken of (a,e) 750 mTorr water, (b,f) 250 mTorr butanol, and (c,d,g) acetic acid vapors, which are 4.3%, 5.5%, and 2.1% of the room temperature vapor pressure. (h) Schematic showing all adsorbed and vapor species for the

OH and COOH SAMs; acetic acid has a higher affinity than water or butanol. CH_3 SAM O 1s spectra can be found in Appendix C.

Further information on acid deprotonation can be ascertained from the O 1s spectrum, where the ratios of the carboxyl oxygen components are indicative of the degree of protonation. When a carboxylic acid deprotonates, the extra electron is shared equally amongst the two oxygens with an O 1s binding energy matching that of the O=C component.[36] This causes even slight deprotonation to be visible as increases in carbonyl-character oxygen are 1:1 with decreases in hydroxyl-character oxygen. For the COOH SAM surface, introduction of acetic acid reduced the protonation of carboxylic acid groups by nearly 30% (**Figure 4-4c**). Interestingly, the initial degree of protonation had little effect on the final equilibrium content: COOH and COO^- surfaces that initially were 80% and 30% protonated, respectively, both reached 55% protonation under exposure to 250 mTorr acetic acid vapor (**Figure 4-4d**). This contrasts strongly with the OH SAM, where the C 1s core level suggests that deprotonation is not occurring, and the position of O 1s carbonyl and acidic oxygen components are within ~10% of full protonation depending on the fit (**Figure 4-4g**).

Acetic acid is well-known to dissociate in aqueous solutions and has been observed to deprotonate when it adsorbs onto ice surfaces.[50] While the COOH SAM did not change protonation upon exposure to water vapor, the COOH SAM surface seemed to interact with acetic acid in a way that was comparable to the ice surface. Acid dissociation was apparent, with nearly one COOH deprotonated per hydrogen bonding pair. Regardless of whether the unbound proton remains nearby or is replaced by another counterion, the surface likely dynamically undergoes protonation and deprotonation as the adsorbed layer exchanges

with the gas phase. However, the gas phase is predominantly protonated (**Figure C4**), indicating this is a surface-induced phenomenon that affects a negligible fraction of all acetic acid molecules, despite its strong effects on the observed SAM and adsorbed phases. The absence of this process on the OH SAM suggests the two surfaces interact with individual acetic acid molecules with different extents of hydrogen bonding or for different durations.

While acetic acid was seen to interact differently with OH and COOH SAM surfaces, deprotonating the latter, both displayed overall similar affinity in terms of adsorption. The thickness of the acetic acid layer (d_{aa}) can be quantitatively determined from the attenuation of peak intensity that occurs as electrons escape through the adsorbed acid. Acetic acid C=O integrated intensity (I_{aa}) through a finite layer can be quantified as according to equations previously defined in literature:

$$I_{\mathrm{aa}} \approx N_{\mathrm{aa}}\sigma_{\mathrm{aa}} \int_0^{d_{\mathrm{aa}}} \exp\left(-\frac{z}{l_{\mathrm{aa}}}\right) dz = N_{\mathrm{aa}}\sigma_{\mathrm{aa}} l_{\mathrm{aa}} \left[1 - \exp\left(-\frac{d_{\mathrm{aa}}}{l_{\mathrm{aa}}}\right)\right] \quad \text{(Eqn. 4.1)}$$

where N is the atomic density, σ represents the X-ray photoionization cross section, and l indicates the electron mean free path.[58] Values for each of these parameters in the acetic acid/SAM system can be found in **Table 4-1.** Photoelectrons traveling from the SAM through an adsorbed layer carry an additional decay prefactor due to attenuation through the entire thickness of the adsorbed acid layer:

$$I_{\mathrm{SAM}} \approx N_{\mathrm{SAM}}\sigma_{\mathrm{SAM}} \exp\left(-\frac{d_{aa}}{l_{aa}}\right) \int_0^{d_{\mathrm{SAM}}} \exp\left(-\frac{z'}{l_{\mathrm{SAM}}}\right) dz' \quad \text{(Eqn. 4.2)}$$

Integrating and solving for the unknown thickness of the acid layer (d_{aa}), the relationship between the component intensities becomes:

$$d_{aa} = l_{aa} \ln\left(\left[\frac{I_{aa}N_{SAM}\sigma_{SAM}l_{SAM}}{I_{SAM}N_{aa}\sigma_{aa}l_{aa}}\right]\left[1 - \exp\left(-\frac{d_{SAM}}{l_{SAM}}\right)\right]\right) \quad \text{(Eqn. 4.3)}$$

Table 4-1. Parameters for calculation of acetic acid layer thickness.*

	Acetic acid C=O	**SAM C-C**
N [cm^{-3}]	4.51×10^{22}	4.51×10^{22}
σ [Mb]	0.360	0.360
l [Å]	9.59	9.55
d [Å]		10.4

* N, σ, *l*, and d represent the carbon atomic density, photoionization cross section,[59] TPP-2M calculated electron inelastic mean free path at 160 eV,[60] and layer thickness, respectively. The atomic density and layer thickness of the self-assembled monolayer were calculated using the contour length of a SAM chain at 30° from the surface normal.[55] Further details are in Appendix C.

The calculated thickness of an acetic acid layer is 1.4-1.5 Å for the OH and COOH SAM surfaces, leveraging the parameter values indicated in **Table 4-1**. Given that a layer of acetic acid is ~3.5 Å with the carboxyl group facing the surface, the surfaces of both SAMs are at a coverage of approximately 0.4-0.5 (equivalent) monolayers. This coverage is actually denser than acetic acid within its bulk liquid state, due to the high density of SAM headgroups (21.4 $Å^2$/chain)[55] that serve as available adsorption sites. It is likely that both maintain similar orientations with the carboxyl group facing toward the surface, where it can participate in hydrogen bonding interactions with the polar headgroups (**Figure 4-5**). While the OH SAM contains only a single proton donor, it is possible that acetic acid could interact with multiple headgroups in a bifurcated hydrogen bond (in addition to singular H-bonding).[25] Uncharged carboxylic acid functional groups are capable of forming two H-bonds from the donator acidic oxygen and the acceptor carbonyl oxygen. As such, the

COOH SAM surface likely forms bidentate bonds with adsorbed acetic acid. Charged acetate groups contain two donor oxygens due to the resonance structure that distributes the extra electron, and can interact with either one donator acidic oxygen or two, if bifurcated. Because APXPS cannot provide such structural information, further experiments on ambient pressure NEXAFS or development of computational models would be ideal for investigating the organization of the adsorbed layer.

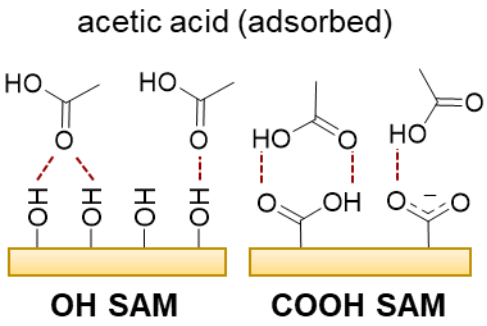

Figure 4-5. Possible hydrogen bonding interactions that take place at the acetic acid–SAM surface. It is possible that single and bifurcated hydrogen bonds take place on OH SAMs, while the COOH SAM can also participate in bidentate hydrogen bonding of uncharged acids.

4.3.3 Solvent adsorption and kinetics

The extent of adsorption can be further related to the equilibrium favorability of adsorption and desorption processes. The Langmuir adsorption model is applicable for ideal, flat surfaces that host up to one full monolayer that adsorb from the gas or vapor phase. Adsorption of organic solvents including alcohols and acetic acid onto ice surfaces have been shown to follow such a model,[48,50] and should interact similarly with SAM surfaces. The coverage θ_A of a single species on these system as a function of pressure can be approximated as

$$\theta_A = \frac{K_{eq}^A P_A}{1 + K_{eq}^A P_A} \qquad K_{eq}^A = \frac{\mathrm{k_{ad}}}{k_d} \qquad \text{(Eqn. 4.4)}$$

where K_{eq}^{A} represents the equilibrium adsorption constant relating the adsorption (k_{ad}) and desorption (k_d) rate constants, and P_A is the partial pressure (P_0).[51] Because the coverage is has been previously shown to be significantly affected by solvent saturation pressure,[48] solvents with similar and low vapor pressures were selected to emphasize differences in adsorption and desorption kinetics. At room temperature, the partial pressures of butanol (250 mTorr), water (750 mTorr), and acetic acid (250 mTorr) are 5.5%, 4.3%, and 2.1% relative to P_0, respectively. Among these three solvents, only acetic acid was observed to adsorb onto the self-assembled monolayer surface. Differences in its coverage can be attributed to differences primarily in desorption rate constants, increasing K_{eq}^{acid}. For the ~45% coverage seen, K_{eq}^{acid} could be estimated to be approximately 3.3 $Torr^{-1}$. However, a full adsorption isotherm would be beneficial for confirming the Langmuir adsorption model and for extracting a more accurate equilibrium constant.

In general, adsorption was seen to depend on the identity of the solvent and surface, but the roles are not interchangeable. In this work, butanol was not found on the COOH SAM surface while acetic acid adsorbed in substantial quantities on the OH SAM. While there are subtle differences from the slight degree of deprotonation seen on the COOH SAM that may have greater scale impacts, these findings suggests that the role of the surface in facilitating adsorption may be distinct from that of the adsorbing species that initiates adsorption events. These are bolstered by additional past research: organic acids and alcohols are known to adsorb onto ice at low pressures (reaching ~1 ML by a partial pressure of 0.9% P_0),[48,50,61] but water shows much lower adsorption affinity for acetic acid[62] and other organic surfaces under similar conditions.[63] Minimally quantifiable (ad)sorption onto charged and hydrophilic polymers has been observed at 0.5% relative humidity (RH),

increasing sluggishly until reaching 100% RH.[42] Compared with oxides such as MgO, ZnO, VO_2, and Fe_3O_4 that exhibit water dissociation at ~0.01% RH[45,64,65] and molecular adsorption at ~0.1% RH[66] even these hydrophilic organic surfaces are comparatively hydrophobic. Possible explanations for the disparity in adsorption affinity of water for organic surfaces (versus the adsorption of organic surfaces onto ice) include differences in surface energy between the species and effects from functional group density at the surface. Future simulations would be particularly advantageous for investigating these possibilities.

4.4 Conclusions

Controlling adsorption-mediating interactions between organic surfaces and solvents is critical for effective materials function in applications ranging from membrane processes, such as pervaporation, to antifouling coatings. Self-assembled monolayers (SAMs) are a useful model system for investigating the effects of organic molecule surface chemistry on the surface affinity of organic solvents and water. In this work, we demonstrated that acetic acid displays higher adsorption affinities for hydrophilic OH- and COOH-terminated SAMs than 1-butanol and water, and it adsorbed similar quantities onto both surfaces at 0.4-0.5 equivalent monolayers. However, the surface chemistry was seen to direct distinctive acetic acid interactions at the surface: adsorbed acid and the COOH SAM headgroup were found to participate in deprotonation, which also occurs on the surface of ice and other metals, while the OH SAM facilitated molecular acetic acid adsorption. These findings suggest that even materials with similar affinities towards a

solvent species may be further capable of eliciting distinct interactions, giving widespread implications for material design and tunability.

Furthermore, distinct roles between the surface and solute were observed for interactions between alcohol and carboxylic acid functionalities. Butanol was not found to adsorb onto the surface of the hydroxylated SAM, but acetic acid adsorbed in large quantities. Previous experiments have suggested organic alcohols and acids easily adsorb to water at very low pressures (0.9% P_0), but our results indicate that water resists adsorption even at 5 times that pressure (4.3% RH). This suggests that the role of the surface in adsorption and desorption is distinct from that of the adsorbing species, and raises additional questions on whether the spacing of functional groups on a surface influences adsorption. Future simulations investigating the ability of a single acetic acid molecule to participate in multiple hydrogen bonding interactions with hydroxylated surfaces may be of use in explaining our experimentally-observed differences.

4.5 Acknowledgements

This work was supported as part of the Center for Materials for Water and Energy Systems (M-WET), an Energy Frontier Research Center funded by the U.S. Department of Energy (DOE), Office of Science, Basic Energy Sciences (BES) under Award #DE-SC0019272. E.J.C. was partially supported by an Early Career Award in the Condensed Phase and Interfacial Molecular Science Program, in the Chemical Sciences Geosciences and Biosciences Division of the Office of Basic Energy Sciences of the DOE under contract DE-AC02-05CH11231. M.E.B. gratefully acknowledges the National Science Foundation

for a graduate fellowship under Award #DGE 1650114 and the Office of Naval Research (ONR) from Awards N00014-17-1-2047. This research used resources of the Advanced Light Source and the Molecular Foundry, which are DOE Office of Science User Facilities supported by the Office of Science, Office of Basic Energy Sciences, of the U.S. Department of Energy, under Contract DE-AC02-05CH11231.

4.6 Appendix C

4.6.1 AFM images

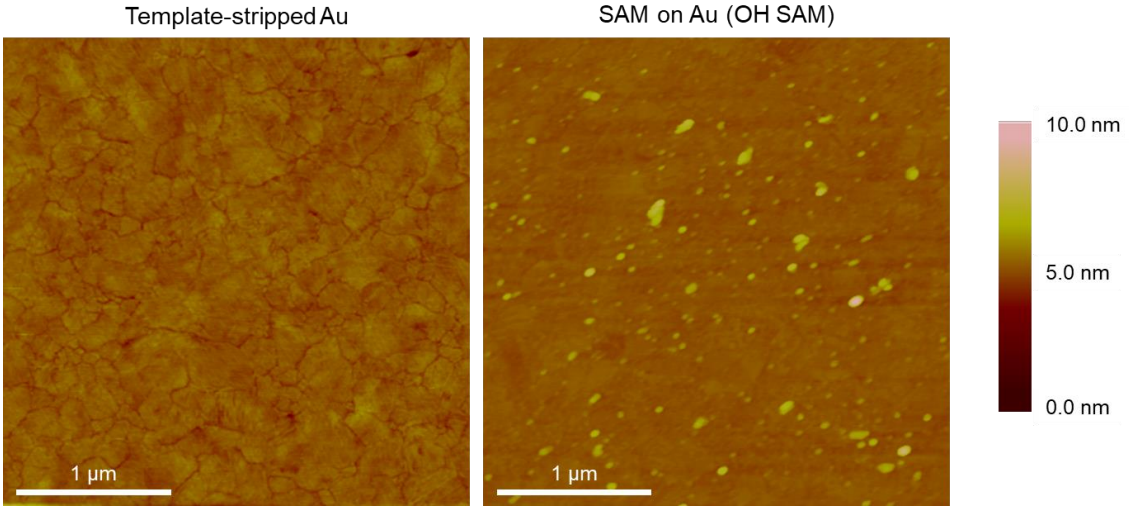

Figure C1. AFM image showing morphology of (left) fresh template-stripped gold surface and (right) representative OH SAM after fabrication. The RMS surface roughness is <0.2 nm for both surfaces.

Table C1. Solvent and surface properties

	H-bond donors	**H-bond acceptors**	**Vapor pressure (20 °C)**	**pKa**
1-butanol	1	0	4.5 Torr[67]	16[68]
Acetic acid	1	1	11.9 Torr[69]	4.5[70]
Water	2	0	17.5 Torr[71]	14[72]
COOH SAM	1	1	–	~4.5
OH SAM	1	0	–	~16
CH_3 SAM	0	0	–	~50[73]

4.6.2 Beam stability

Beam stability testing and development of rastering protocols was conducted as previously described.[42] Degradation studies were first performed to identify spectral changes as a function of time and the timing of their onset. For instance, the C-OH of the OH SAM was found to degrade beginning at around 3-4 minutes of measurement (**Figure C2**, left). Rastering protocols that involved moving the sample every 1.5 minutes prevented this damage (**Figure C2**, right), while summation could be performed as necessary for core levels with lower signal-to-noise.

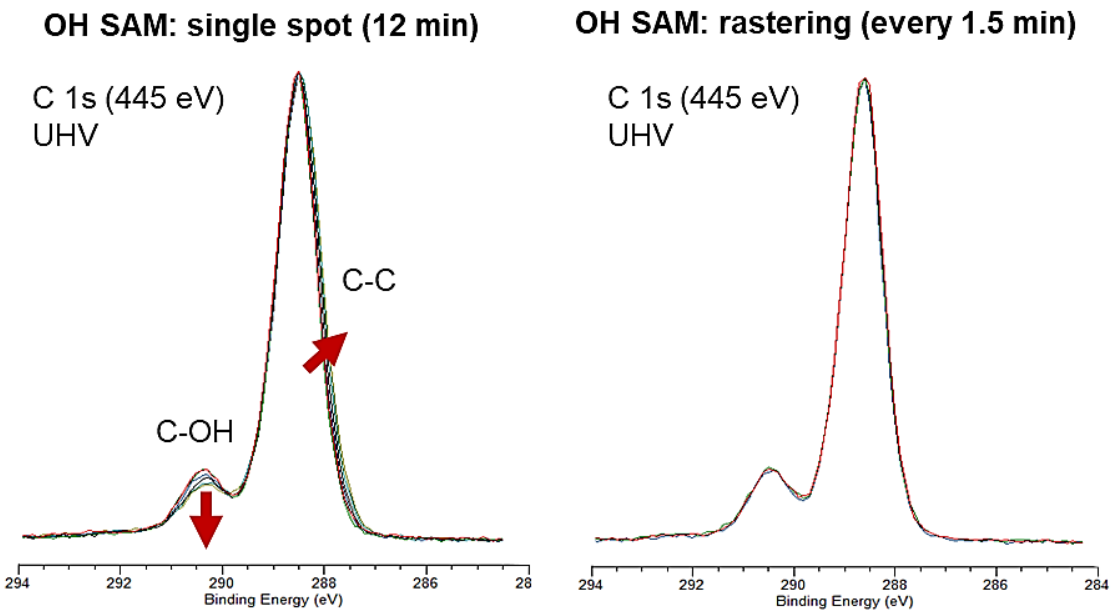

Figure C2. The location and timing of X-ray damage due to beam exposure were identified for each sample, and then minimized using a rastering method. For the OH SAM C 1s, rastering every 1.5 minutes was sufficient to prevent beam damage artefacts from affecting spectra.

SAM purity: S 2p core levels

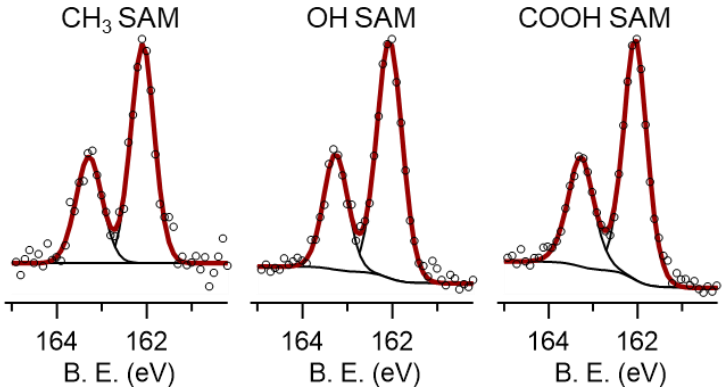

Figure C3. S 2p spectra of CH_3, OH, and COOH SAMs. The ratio of S 2p 3/2 and 1/2 doublets are 2:1 as expected for the case where the bound S-Au is the sole sulfur species.

CH_3 SAM spectra

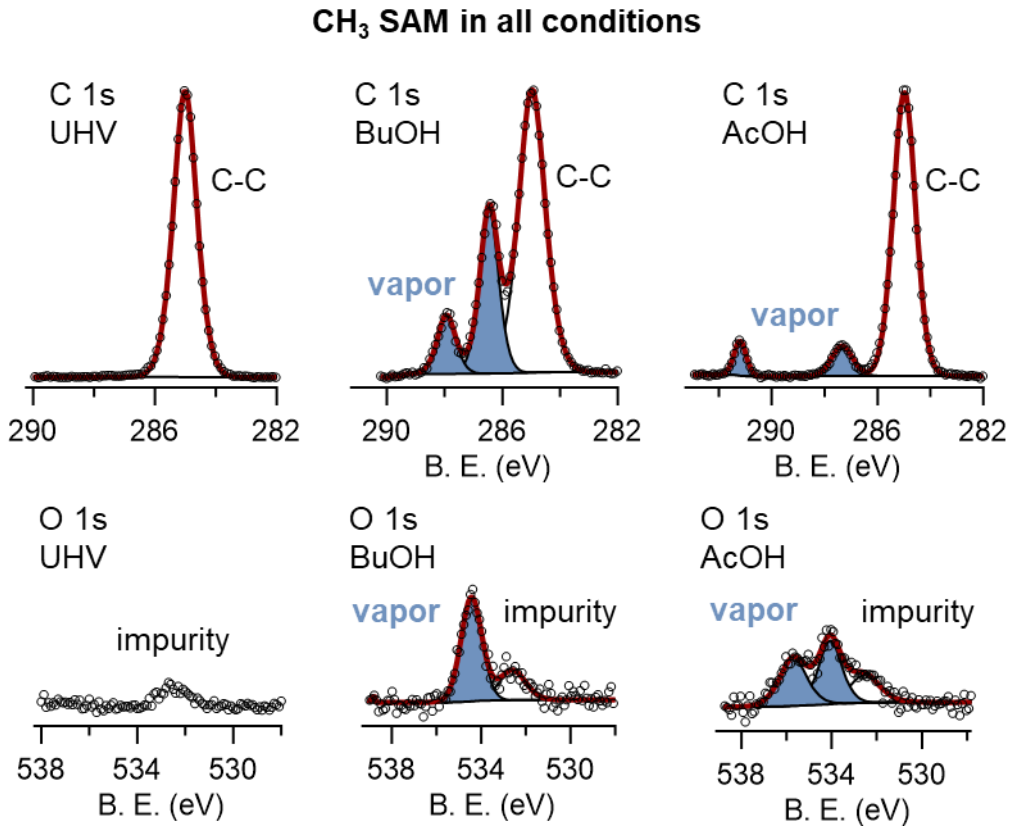

Figure C4. C 1s and O 1s spectra showing SAM composition under UHV, butanol, and acetic acid vapors. No adsorption was observed. From reference

4.6.3 Vapor phase spectra

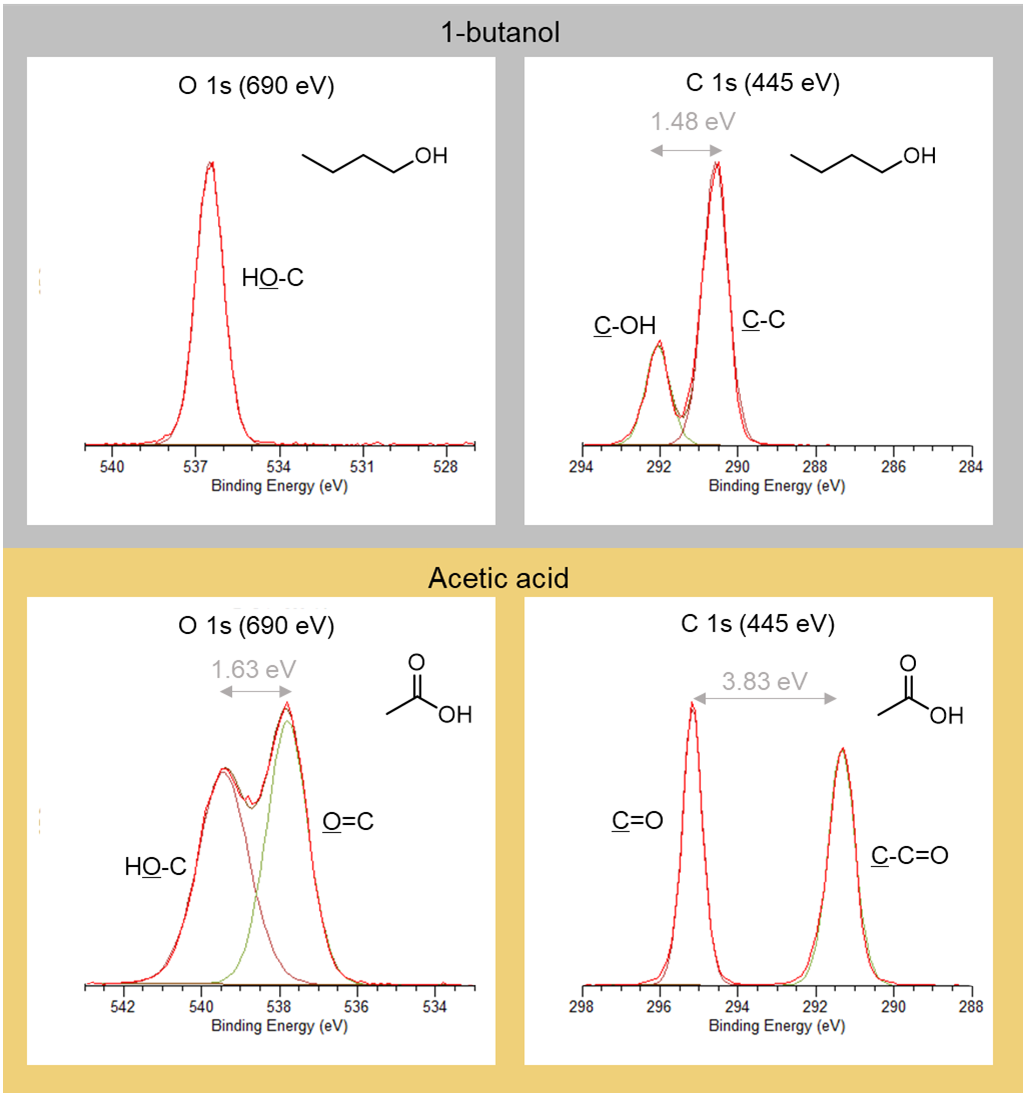

Figure C5. Vapor phase O 1s and C 1s spectra for 1-butanol and acetic acid. Ratios and gap widths were used to constrain the vapor phase in all surface fits.

4.6.4 General fitting methods

For spectra that contained large numbers of overlapping peaks (i.e., SAM, adsorbed, and/or vapor), certain key constraints were initially used. The SAM chemistry was initialized with the relative component ratios and position as found under vacuum conditions. Adsorbed and/or vapor species were initialized with set gap widths and ratios based on vapor phase spectra. Several cycles of fitting with varying tightness of constraints were then conducted before concluding whether adsorption was occurring. For one particular spectrum, the OH SAM C 1s with 250 mTorr butanol, additional quantification was necessary due to the ambiguity of the spectra as explained later.

4.6.5 Calculations of atomic density

Atomic density for the SAM and solvent layer were determined based on published densities for alkyl self-assembled monolayer chains. Each chain is reported in literature to occupy an area of 21.4 Å at an angle averaging 30 degrees relative to the surface normal.[74] A contour length of 12.0 Å (from the C-C bond lengths for the 10 alkyl carbon atoms) therefore indicates a vertical height of 10.4 Å for the alkyl portion of the chain. Combined, this suggests a volumetric density of 4.51×10^{21} chains/cm^3. Since there are 10 (alkyl) carbon atoms per chain, the C-C atomic density is 4.51×10^{22} atoms/cm^{-3}.

For Langmuir adsorption, the density of adsorbed vapor is presumed to be based on the number of available adsorption sites. Consequently, the density of adsorbed acetic acid would be 4.51×10^{22} atoms/cm^{-3} as well up to a one monolayer maximum.

4.6.6 Determination of OH SAM and butanol C 1s spectrum

The OH SAM C 1s spectrum in the presence of butanol could involve either 4 or 6 overlapping components depending on whether adsorption is or is not occurring. Because of the degree of overlap, two fits with and without adsorption both were feasible matches to the raw spectrum (**Figure C4**).

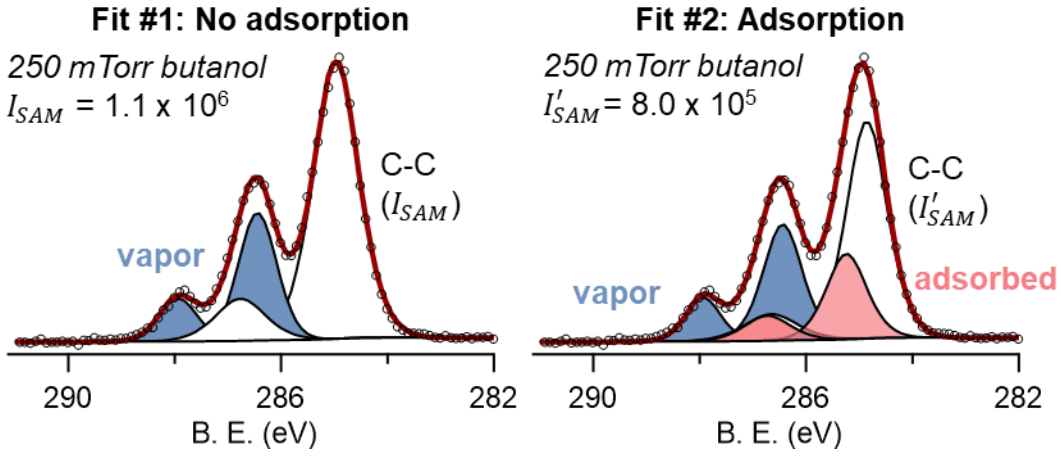

Figure C6. Two different fits for the same C 1s spectrum of the OH SAM under 250 mTorr butanol vapor. They differ primarily by the intensity of the C-C SAM backbone component (I_{SAM}), which is ~40% smaller when adsorption is presumed to be occurring versus not occurring.

However, the overall intensity of the C-C components differs significantly enough between the two fits to leverage quantitative analysis based on signal attenuation. Specifically, the intensity of the Au 4f spectrum and C 1s spectrum are quantitatively related and can be predicted according to a layered model with adsorbed solvent on top of the SAM, and finally gold at the bottom.

The SAM intensity, measured as the area of the C-C component in the C 1s spectrum, can be quantitatively described using equations from literature:[58]

$$I_{\mathrm{SAM}} \approx N_{\mathrm{SAM}}\sigma_{\mathrm{SAM}}l_{\mathrm{SAM}}\exp\left(-\frac{d_{butanol}}{l_{butanol}}\right)\int_0^{d_{\mathrm{SAM}}}\exp\left(-\frac{z}{l_{\mathrm{aa}}}\right)dz$$
$$= N_{\mathrm{SAM}}\sigma_{\mathrm{SAM}}l_{\mathrm{SAM}}\exp\left(-\frac{d_{butanol}}{l_{butanol}}\right)\left[1-\exp\left(-\frac{d_{SAM}}{l_{SAM}}\right)\right] \qquad \text{(Eqn. C1)}$$

Here, *N* represents the atomic density, σ represents the X-ray photoionization cross section, *l* indicates the electron mean free path, and *d* is the thickness of the layer as before. Electron attenuation through a butanol layer is included as an exponential decay term. The intensity of the gold substrate is similar to that of the SAM C-C, but accounts for electron attenuation due to traveling through the SAM layer. Note that the gold has effectively infinite depth.

$$I_{\mathrm{Au}} \approx N_{\mathrm{Au}}\sigma_{\mathrm{Au}}l_{\mathrm{Au}}\exp\left(-\frac{d_{butanol}}{l_{butanol}}\right)\exp\left(-\frac{d_{\mathrm{SAM}}}{l_{SAM}}\right)\int_0^{d_{\mathrm{Au}}}\exp\left(-\frac{z}{l_{\mathrm{Au}}}\right)dz$$
$$= N_{\mathrm{Au}}\sigma_{\mathrm{Au}}l_{\mathrm{Au}}\exp\left(-\frac{d_{butanol}}{l_{butanol}}\right)\exp\left(-\frac{d_{\mathrm{SAM}}}{l_{SAM}}\right) \qquad \text{(Eqn. C2)}$$

The ratio between the intensities can be approximated as

$$\frac{I_{\mathrm{SAM}}}{I_{Au}} = \frac{N_{\mathrm{SAM}}\sigma_{\mathrm{SAM}}l_{\mathrm{SAM}}}{N_{\mathrm{Au}}\sigma_{\mathrm{Au}}l_{\mathrm{Au}}}\left[\exp\left(+\frac{d_{SAM}}{l_{SAM}}\right)-1\right] \qquad \text{(Eqn. C3)}$$

Electrons from the SAM and Au layers experience equal attenuation from all layers above them (such as the vapor, adsorbed solvent, and even the SAM headgroup), and the decay terms are correspondingly canceled out in this equation. The remaining parameters can be calculated and are shown below for X-rays with 445 eV photon energy:

Table C2: Parameters factoring into calculation of predicted component intensities

	Au 4f	**SAM C-C**
n [cm^{-3}]	5.90 x 10^{22}	4.51 × 10^{22}
σ [Mb]	4.24	0.360
l [Å]	6.83	9.55
d [Å]	(inf)	10.4

In addition to predicting SAM content at 250 mTorr butanol, the model was tested at lower butanol pressures, under UHV conditions, and with 250 mTorr acetic acid, as shown in **Table C2**. In general, the model shows a ~10% difference from the expected fit, making it a suitable estimate. For the 250 mTorr butanol case, the prediction overestimated the C-C content by ~20% making the non-adsorption case (Fit #1) much closer than the alternative. Therefore, the attenuation quantification results indicate it is more likely that butanol is not adsorbing onto the surface at 250 mTorr and 78 mTorr.

Table C3: Predicted and fitted intensities for different environmental conditions

	250 mTorr butanol	78 mTorr butanol	UHV	250 mTorr acetic acid
I_{Au}	8.00×10^6	20.1×10^6	18.5×10^6	5.97×10^6
$I_{C\text{-}C}$ (predicted)	1.4×10^6	3.6×10^6	3.3×10^6	1.1×10^6
$I_{C\text{-}C}$ (Fit #1; no adsorption)	1.1×10^6	3.3×10^6	3.4×10^6	--
$I_{C\text{-}C}$ (Fit #2; adsorption)	0.8×10^6	3.0×10^6	--	1.0×10^6
Percent difference	21%	8%	3%	8%

Table C4: Summary of adsorption results

SAM	Butanol (250 mTorr / 5.5% P_0)	Acetic acid (250 mTorr / 2.1% P_0)	Water (750 mTorr / 4.2% RH)
CH_3	N	N	N[36]
OH	N	Y (0.4-0.5 ML)	N
COOH	N	Y (0.4-0.5 ML)	N

4.7 References

(1) Monroe, J.; Barry, M.; DeStefano, A.; Gokturk, P. A.; Jiao, S.; Robinson-Brown, D.; Webber, T.; Crumlin, E. J.; Han, S.; Shell, M. S. Water Structure and Properties at Hydrophilic and Hydrophobic Surfaces. *Annu. Rev. Chem. Biomol. Eng.* **2020**, *11* (1), null. https://doi.org/10.1146/annurev-chembioeng-120919-114657.

(2) Henderson, M. A. The Interaction of Water with Solid Surfaces: Fundamental Aspects Revisited. *Surf. Sci. Rep.* **2002**, *46* (1), 1–308. https://doi.org/10.1016/S0167-5729(01)00020-6.

(3) Landsman, M. R.; Sujanani, R.; Brodfuehrer, S. H.; Cooper, C. M.; Darr, A. G.; Justin Davis, R.; Kim, K.; Kum, S.; Nalley, L. K.; Nomaan, S. M.; Oden, C. P.; Paspureddi, A.; Reimund, K. K.; Rowles, L. S.; Yeo, S.; Lawler, D. F.; Freeman, B. D.; Katz, L. E. Water Treatment: Are Membranes the Panacea? *Annu. Rev. Chem. Biomol. Eng.* **2020**, *11* (1), null. https://doi.org/10.1146/annurev-chembioeng-111919-091940.

(4) Bolong, N.; Ismail, A. F.; Salim, M. R.; Matsuura, T. A Review of the Effects of Emerging Contaminants in Wastewater and Options for Their Removal. *Desalination* **2009**, *239* (1), 229–246. https://doi.org/10.1016/j.desal.2008.03.020.

(5) Qureshi, N.; Ezeji, T. C. Butanol, 'a Superior Biofuel' Production from Agricultural Residues (Renewable Biomass): Recent Progress in Technology. *Biofuels Bioprod. Biorefining* **2008**, *2* (4), 319–330. https://doi.org/10.1002/bbb.85.

(6) Lee, S. Y.; Park, J. H.; Jang, S. H.; Nielsen, L. K.; Kim, J.; Jung, K. S. Fermentative Butanol Production by Clostridia. *Biotechnol. Bioeng.* **2008**, *101* (2), 209–228. https://doi.org/10.1002/bit.22003.

(7) Ezeji, T. C.; Qureshi, N.; Blaschek, H. P. Bioproduction of Butanol from Biomass: From Genes to Bioreactors. *Curr. Opin. Biotechnol.* **2007**, *18* (3), 220–227. https://doi.org/10.1016/j.copbio.2007.04.002.

(8) Ranjan, A.; Moholkar, V. S. Biobutanol: Science, Engineering, and Economics. *Int. J. Energy Res.* **2012**, *36* (3), 277–323. https://doi.org/10.1002/er.1948.

(9) Abdehagh, N.; Tezel, F. H.; Thibault, J. Separation Techniques in Butanol Production: Challenges and Developments. *Biomass Bioenergy* **2014**, *60*, 222–246. https://doi.org/10.1016/j.biombioe.2013.10.003.

(10) Azimi, H.; Thibault, J.; Tezel, F. H. Separation of Butanol Using Pervaporation: A Review of Mass Transfer Models. *J. Fluid Flow Heat Mass Transf. JFFHMT* **2019**, *5* (4), 53–82.

(11) Hrubesh, L. W.; Coronado, P. R.; Satcher, J. H. Solvent Removal from Water with Hydrophobic Aerogels. *J. Non-Cryst. Solids* **2001**, *285* (1), 328–332. https://doi.org/10.1016/S0022-3093(01)00475-6.

(12) Grzenia, D. L.; Schell, D. J.; Wickramasinghe, S. R. Membrane Extraction for Removal of Acetic Acid from Biomass Hydrolysates. *J. Membr. Sci.* **2008**, *322* (1), 189–195. https://doi.org/10.1016/j.memsci.2008.05.030.

(13) Yeom, C.-K.; Lee, K.-H. Pervaporation Separation of Water-Acetic Acid Mixtures through Poly(Vinyl Alcohol) Membranes Crosslinked with Glutaraldehyde. *J. Membr. Sci.* **1996**, *109* (2), 257–265. https://doi.org/10.1016/0376-7388(95)00196-4.

(14) Sano, T.; Ejiri, S.; Yamada, K.; Kawakami, Y.; Yanagishita, H. Separation of Acetic Acid-Water Mixtures by Pervaporation through Silicalite Membrane. *J. Membr. Sci.* **1997**, *123* (2), 225–233. https://doi.org/10.1016/S0376-7388(96)00224-4.

(15) Parthasarathi, R.; Subramanian, V. Characterization of Hydrogen Bonding: From van Der Waals Interactions to Covalency. In *Hydrogen Bonding—New Insights*; Grabowski, S. J., Ed.; Springer Netherlands: Dordrecht, 2006; pp 1–50. https://doi.org/10.1007/978-1-4020-4853-1_1.

(16) Leonardi, A. K.; Ober, C. K. Polymer-Based Marine Antifouling and Fouling Release Surfaces: Strategies for Synthesis and Modification. *Annu. Rev. Chem. Biomol. Eng.* **2019**, *10* (1), 241–264. https://doi.org/10.1146/annurev-chembioeng-060718-030401.

(17) Yang, W. J.; Neoh, K.-G.; Kang, E.-T.; Teo, S. L.-M.; Rittschof, D. Polymer Brush Coatings for Combating Marine Biofouling. *Prog. Polym. Sci.* **2014**, *39* (5), 1017–1042. https://doi.org/10.1016/j.progpolymsci.2014.02.002.

(18) He, M.; Gao, K.; Zhou, L.; Jiao, Z.; Wu, M.; Cao, J.; You, X.; Cai, Z.; Su, Y.; Jiang, Z. Zwitterionic Materials for Antifouling Membrane Surface Construction. *Acta Biomater.* **2016**, *40*, 142–152. https://doi.org/10.1016/j.actbio.2016.03.038.

(19) Murosaki, T.; Ahmed, N.; Gong, J. P. Antifouling Properties of Hydrogels. *Sci. Technol. Adv. Mater.* **2011**, *12* (6), 064706. https://doi.org/10.1088/1468-6996/12/6/064706.

(20) Lejars, M.; Margaillan, A.; Bressy, C. Fouling Release Coatings: A Nontoxic Alternative to Biocidal Antifouling Coatings. *Chem. Rev.* **2012**, *112* (8), 4347–4390. https://doi.org/10.1021/cr200350v.

(21) Barry, M. E.; Davidson, E. C.; Zhang, C.; Patterson, A. L.; Yu, B.; Leonardi, A. K.; Duzen, N.; Malaviya, K.; Clarke, J. L.; Finlay, J. A.; Clare, A. S.; Chen, Z.; Ober, C. K.; Segalman, R. A. The Role of Hydrogen Bonding in Peptoid-Based Marine Antifouling Coatings. *Macromolecules* **2019**, *52* (3), 1287–1295. https://doi.org/10.1021/acs.macromol.8b02390.

(22) Ostuni, E.; Chapman, R. G.; Holmlin, R. E.; Takayama, S.; Whitesides, G. M. A Survey of Structure−Property Relationships of Surfaces That Resist the Adsorption of Protein. *Langmuir* **2001**, *17* (18), 5605–5620. https://doi.org/10.1021/la010384m.

(23) Dalsin, J. L.; Messersmith, P. B. Bioinspired Antifouling Polymers. *Mater. Today* **2005**, *8* (9), 38–46. https://doi.org/10.1016/S1369-7021(05)71079-8.

(24) Merrill, E. W. Distinctions and Correspondences among Surfaces Contacting Blood. *Ann. N. Y. Acad. Sci.* **1987**, *516* (1), 196–203. https://doi.org/10.1111/j.1749-6632.1987.tb33041.x.

(25) Rozas, I. On the Nature of Hydrogen Bonds: An Overview on Computational Studies and a Word about Patterns. *Phys. Chem. Chem. Phys.* **2007**, *9* (22), 2782–2790. https://doi.org/10.1039/B618225A.

(26) Lee, H. M.; Singh, N. J.; Kim, K. S. Weak to Strong Hydrogen Bonds. In *Hydrogen Bonding—New Insights*; Grabowski, S. J., Ed.; Springer Netherlands: Dordrecht, 2006; pp 149–192. https://doi.org/10.1007/978-1-4020-4853-1_4.

(27) Shimoni, L.; Glusker, J. P. Hydrogen Bonding Motifs of Protein Side Chains: Descriptions of Binding of Arginine and Amide Groups. *Protein Sci.* **1995**, *4* (1), 65–74. https://doi.org/10.1002/pro.5560040109.

(28) Waite, J. H. Nature's Underwater Adhesive Specialist. *Int. J. Adhes. Adhes.* **1987**, *7* (1), 9–14. https://doi.org/10.1016/0143-7496(87)90048-0.

(29) Lee, B. P.; Messersmith, P. B.; Israelachvili, J. N.; Waite, J. H. Mussel-Inspired Adhesives and Coatings. *Annu. Rev. Mater. Res.* **2011**, *41* (1), 99–132. https://doi.org/10.1146/annurev-matsci-062910-100429.

(30) Forooshani, P. K.; Lee, B. P. Recent Approaches in Designing Bioadhesive Materials Inspired by Mussel Adhesive Protein. *J. Polym. Sci. Part Polym. Chem.* **2017**, *55* (1), 9–33. https://doi.org/10.1002/pola.28368.

(31) Ahn, B. K.; Lee, D. W.; Israelachvili, J. N.; Waite, J. H. Surface-Initiated Self-Healing of Polymers in Aqueous Media. *Nat. Mater.* **2014**, *13* (9), 867–872. https://doi.org/10.1038/nmat4037.

(32) Bain, C. D.; Whitesides, G. M. Molecular-Level Control over Surface Order in Self-Assembled Monolayer Films of Thiols on Gold. *Science* **1988**, *240* (4848), 62–63. https://doi.org/10.1126/science.240.4848.62.

(33) Vericat, C.; Vela, M. E.; Benitez, G.; Carro, P.; Salvarezza, R. C. Self-Assembled Monolayers of Thiols and Dithiols on Gold: New Challenges for a Well-Known System. *Chem. Soc. Rev.* **2010**, *39* (5), 1805–1834. https://doi.org/10.1039/B907301A.

(34) Gooding, J. J.; Mearns, F.; Yang, W.; Liu, J. Self-Assembled Monolayers into the 21st Century: Recent Advances and Applications. *Electroanalysis* **2003**, *15* (2), 81–96. https://doi.org/10.1002/elan.200390017.

(35) Mandler, D.; Kraus-Ophir, S. Self-Assembled Monolayers (SAMs) for Electrochemical Sensing. *J. Solid State Electrochem.* **2011**, *15* (7), 1535. https://doi.org/10.1007/s10008-011-1493-6.

(36) Ketteler, G.; Ashby, P.; Mun, B. S.; Ratera, I.; Bluhm, H.; Kasemo, B.; Salmeron, M. In Situphotoelectron Spectroscopy Study of Water Adsorption on Model Biomaterial Surfaces. *J. Phys. Condens. Matter* **2008**, *20* (18), 184024. https://doi.org/10.1088/0953-8984/20/18/184024.

(37) Salmeron, M.; Schlögl, R. Ambient Pressure Photoelectron Spectroscopy: A New Tool for Surface Science and Nanotechnology. *Surf. Sci. Rep.* **2008**, *63* (4), 169–199. https://doi.org/10.1016/j.surfrep.2008.01.001.

(38) Starr, D. E.; Liu, Z.; Hävecker, M.; Knop-Gericke, A.; Bluhm, H. Investigation of Solid/Vapor Interfaces Using Ambient Pressure X-Ray Photoelectron Spectroscopy. *Chem. Soc. Rev.* **2013**, *42* (13), 5833–5857. https://doi.org/10.1039/C3CS60057B.

(39) Zhong, L.; Chen, D.; Zafeiratos, S. A Mini Review of in Situ Near-Ambient Pressure XPS Studies on Non-Noble, Late Transition Metal Catalysts. *Catal. Sci. Technol.* **2019**, *9* (15), 3851–3867. https://doi.org/10.1039/C9CY00632J.

(40) Schnadt, J.; Knudsen, J.; Johansson, N. Present and New Frontiers in Materials Research by Ambient Pressure X-Ray Photoelectron Spectroscopy. *J. Phys. Condens. Matter* **2020**, *32* (41), 413003. https://doi.org/10.1088/1361-648X/ab9565.

(41) Karslıoğlu, O.; Bluhm, H. Ambient-Pressure X-Ray Photoelectron Spectroscopy (APXPS). In *Operando Research in Heterogeneous Catalysis*; Frenken, J., Groot, I., Eds.; Springer Series in Chemical Physics; Springer International Publishing: Cham, 2017; pp 31–57. https://doi.org/10.1007/978-3-319-44439-0_2.

(42) Gokturk, P. A.; Barry, M.; Segalman, R.; Crumlin, E. J. Directly Probing Polymer Thin Film Chemistry and Counterion Influence on Water Sorption. *ACS Appl. Polym. Mater.* **2020**, *2* (11), 4752–4761. https://doi.org/10.1021/acsapm.0c00756.

(43) Gericke, S. M.; Mulhearn, W. D.; Goodacre, D. E.; Raso, J.; Miller, D. J.; Carver, L.; Nemšák, S.; Karslıoğlu, O.; Trotochaud, L.; Bluhm, H.; Stafford, C. M.; Buechner, C. Water-Polyamide Chemical Interplay in Desalination Membranes Explored by Ambient Pressure X-Ray Photoelectron Spectroscopy. *Phys. Chem. Chem. Phys.* **2020**, *22* (27), 15658–15663. https://doi.org/10.1039/D0CP01842B.

(44) Deng, X.; Herranz, T.; Weis, C.; Bluhm, H.; Salmeron, M. Adsorption of Water on Cu2O and Al2O3 Thin Films. *J. Phys. Chem. C* **2008**, *112* (26), 9668–9672. https://doi.org/10.1021/jp800944r.

(45) Goodacre, D.; Blum, M.; Buechner, C.; Hoek, H.; Gericke, S. M.; Jovic, V.; Franklin, J. B.; Kittiwatanakul, S.; Söhnel, T.; Bluhm, H.; Smith, K. E. Water

Adsorption on Vanadium Oxide Thin Films in Ambient Relative Humidity. *J. Chem. Phys.* **2020**, *152* (4), 044715. https://doi.org/10.1063/1.5138959.

(46) Trotochaud, L.; Head, A. R.; Pletincx, S.; Karslıoğlu, O.; Yu, Y.; Waldner, A.; Kyhl, L.; Hauffman, T.; Terryn, H.; Eichhorn, B.; Bluhm, H. Water Adsorption and Dissociation on Polycrystalline Copper Oxides: Effects of Environmental Contamination and Experimental Protocol. *J. Phys. Chem. B* **2018**, *122* (2), 1000–1008. https://doi.org/10.1021/acs.jpcb.7b10732.

(47) Arima, K.; Jiang, P.; Deng, X.; Bluhm, H.; Salmeron, M. Water Adsorption, Solvation, and Deliquescence of Potassium Bromide Thin Films on SiO2 Studied by Ambient-Pressure X-Ray Photoelectron Spectroscopy. *J. Phys. Chem. C* **2010**, *114* (35), 14900–14906. https://doi.org/10.1021/jp101683z.

(48) T. Newberg, J.; Bluhm, H. Adsorption of 2-Propanol on Ice Probed by Ambient Pressure X-Ray Photoelectron Spectroscopy. *Phys. Chem. Chem. Phys.* **2015**, *17* (36), 23554–23558. https://doi.org/10.1039/C5CP03821A.

(49) Starr, D. E.; Pan, D.; Newberg, J. T.; Ammann, M.; Wang, G. E.; Michaelides, A.; Bluhm, H. Acetone Adsorption on Ice Investigated by X-Ray Spectroscopy and Density Functional Theory. *Phys. Chem. Chem. Phys.* **2011**, *13* (44), 19988–19996. https://doi.org/10.1039/C1CP21493D.

(50) Křepelová, A.; Bartels-Rausch, T.; Brown, M. A.; Bluhm, H.; Ammann, M. Adsorption of Acetic Acid on Ice Studied by Ambient-Pressure XPS and Partial-Electron-Yield NEXAFS Spectroscopy at 230–240 K. *J. Phys. Chem. A* **2013**, *117* (2), 401–409. https://doi.org/10.1021/jp3102332.

(51) Masel, R. I. 4.3 Langmuir Adsorption Model. In *Principles of Adsorption and Reaction on Solid Surfaces*; John Wiley & Sons, 1996; p 240.

(52) Vogel, N.; Zieleniecki, J.; Köper, I. As Flat as It Gets: Ultrasmooth Surfaces from Template-Stripping Procedures. *Nanoscale* **2012**, *4* (13), 3820–3832. https://doi.org/10.1039/C2NR30434A.

(53) Weiss, E. A.; Kaufman, G. K.; Kriebel, J. K.; Li, Z.; Schalek, R.; Whitesides, G. M. Si/SiO2-Templated Formation of Ultraflat Metal Surfaces on Glass, Polymer, and Solder Supports: Their Use as Substrates for Self-Assembled Monolayers. *Langmuir* **2007**, *23* (19), 9686–9694. https://doi.org/10.1021/la701919r.

(54) Naumann, R.; Schiller, S. M.; Giess, F.; Grohe, B.; Hartman, K. B.; Kärcher, I.; Köper, I.; Lübben, J.; Vasilev, K.; Knoll, W. Tethered Lipid Bilayers on Ultraflat

Gold Surfaces. *Langmuir* **2003**, *19* (13), 5435–5443. https://doi.org/10.1021/la0342060.

(55) Strong, L.; Whitesides, G. M. Structures of Self-Assembled Monolayer Films of Organosulfur Compounds Adsorbed on Gold Single Crystals: Electron Diffraction Studies. *Langmuir* **1988**, *4* (3), 546–558. https://doi.org/10.1021/la00081a009.

(56) Chapman, R. G.; Ostuni, E.; Yan, L.; Whitesides, G. M. Preparation of Mixed Self-Assembled Monolayers (SAMs) That Resist Adsorption of Proteins Using the Reaction of Amines with a SAM That Presents Interchain Carboxylic Anhydride Groups. *Langmuir* **2000**, *16* (17), 6927–6936. https://doi.org/10.1021/la991579l.

(57) Grass, M. E.; Karlsson, P. G.; Aksoy, F.; Lundqvist, M.; Wannberg, B.; Mun, B. S.; Hussain, Z.; Liu, Z. New Ambient Pressure Photoemission Endstation at Advanced Light Source Beamline 9.3.2. *Rev. Sci. Instrum.* **2010**, *81* (5), 053106. https://doi.org/10.1063/1.3427218.

(58) Hofmann, S. Quantitative Analysis (Data Evaluation). In *Auger- and X-Ray Photoelectron Spectroscopy in Materials Science: A User-Oriented Guide*; Springer Science & Business Media, 2012; pp 77–201.

(59) Yeh, J. J.; Lindau, I. Atomic Subshell Photoionization Cross Sections and Asymmetry Parameters: $1 \leqslant Z \leqslant 103$. *At. Data Nucl. Data Tables* **1985**, *32* (1), 1–155. https://doi.org/10.1016/0092-640X(85)90016-6.

(60) Powell, C. J.; Jablonski, A. *NIST Electron Inelastic-Mean-Free-Path Database*, Version 1.2.; SRD 71, National Institute of Standards and Technology, Gaithersburg, MD, 2010.

(61) Sokolov, O.; Abbatt, J. P. D. Adsorption to Ice of N-Alcohols (Ethanol to 1-Hexanol), Acetic Acid, and Hexanal. *J. Phys. Chem. A* **2002**, *106* (5), 775–782. https://doi.org/10.1021/jp013291m.

(62) Papagiannakopoulos, P.; Kong, X.; Thomson, E. S.; Pettersson, J. B. C. Water Interactions with Acetic Acid Layers on Ice and Graphite. *J. Phys. Chem. B* **2014**, *118* (47), 13333–13340. https://doi.org/10.1021/jp503552w.

(63) Tu, A.; Kwag, H. R.; Barnette, A. L.; Kim, S. H. Water Adsorption Isotherms on CH3-, OH-, and COOH-Terminated Organic Surfaces at Ambient Conditions Measured with PM-RAIRS. *Langmuir* **2012**, *28* (43), 15263–15269. https://doi.org/10.1021/la302848k.

(64) Newberg, J. T.; Goodwin, C.; Arble, C.; Khalifa, Y.; Boscoboinik, J. A.; Rani, S. ZnO(10$\bar{1}$0) Surface Hydroxylation under Ambient Water Vapor. *J. Phys. Chem. B* **2018**, *122* (2), 472–478. https://doi.org/10.1021/acs.jpcb.7b03335.

(65) Kendelewicz, T.; Kaya, S.; Newberg, J. T.; Bluhm, H.; Mulakaluri, N.; Moritz, W.; Scheffler, M.; Nilsson, A.; Pentcheva, R.; Brown, G. E. X-Ray Photoemission and Density Functional Theory Study of the Interaction of Water Vapor with the Fe3O4(001) Surface at Near-Ambient Conditions. *J. Phys. Chem. C* **2013**, *117* (6), 2719–2733. https://doi.org/10.1021/jp3078024.

(66) Newberg, J. T.; Starr, D. E.; Yamamoto, S.; Kaya, S.; Kendelewicz, T.; Mysak, E. R.; Porsgaard, S.; Salmeron, M. B.; Brown, G. E.; Nilsson, A.; Bluhm, H. Formation of Hydroxyl and Water Layers on MgO Films Studied with Ambient Pressure XPS. *Surf. Sci.* **2011**, *605* (1), 89–94. https://doi.org/10.1016/j.susc.2010.10.004.

(67) Kemme, H. R.; Kreps, S. I. Vapor Pressure of Primary N-Alkyl Chlorides and Alcohols. *J. Chem. Eng. Data* **1969**, *14* (1), 98–102. https://doi.org/10.1021/je60040a011.

(68) International Union of Pure and Applied Chemistry; Commission on Equilibrium Data; Serjeant, E. P.; Dempsey, B.; International Union of Pure and Applied Chemistry; Commission on Electrochemical Data. *Ionisation Constants of Organic Acids in Aqueous Solution*; Pergamon Press: Oxford; New York, 1979.

(69) McDonald, R. A.; Shrader, S. A.; Stull, D. R. Vapor Pressures and Freezing Points of Thirty Pure Organic Compounds. *J. Chem. Eng. Data* **1959**, *4* (4), 311–313. https://doi.org/10.1021/je60004a009.

(70) Sun, N.; Avdeef, A. Biorelevant PKa (37°C) Predicted from the 2D Structure of the Molecule and Its PKa at 25°C. *J. Pharm. Biomed. Anal.* **2011**, *56* (2), 173–182. https://doi.org/10.1016/j.jpba.2011.05.007.

(71) Bridgeman, O. C.; Aldrich, E. W. Vapor Pressure Tables for Water. *J. Heat Transf.* **1964**, *86* (2), 279–286. https://doi.org/10.1115/1.3687121.

(72) Silverstein, T. P.; Heller, S. T. PKa Values in the Undergraduate Curriculum: What Is the Real PKa of Water? *J. Chem. Educ.* **2017**, *94* (6), 690–695. https://doi.org/10.1021/acs.jchemed.6b00623.

(73) Alkorta, I.; Elguero, J. Carbon Acidity and Ring Strain: A Hybrid HF-DFT Approach (Becke3LYP/6–311++G∗∗). *Tetrahedron* **1997**, *53* (28), 9741–9748. https://doi.org/10.1016/S0040-4020(97)00597-8.

(74) Strong, L.; Whitesides, G. M. Structures of Self-Assembled Monolayer Films of Organosulfur Compounds Adsorbed on Gold Single Crystals: Electron Diffraction Studies. 13.

Chapter 5

Conclusions and Outlook

In summary, this dissertation investigates the complex relationship between surface chemistry and interfacial interactions for polymers in aqueous conditions, and how each both influence and are influenced by the other. This codependence has significant implications for applications ranging from marine antifouling coatings to water purification membranes, and exploration of both was made possible by forming highly-controlled polymer and organic surfaces that could be studied with recently developed surface characterization techniques.

Chapters 2 and 4 emphasized the effect of hydrogen bonding interactions on fouling and adsorption processes, respectively. In Chapter 2, the use of peptoids as side chains in PDMS-based fouling release copolymers enabled minor modifications of side chain chemistry to determine the ways that hydrogen bonding influences marine antifouling coating suitability. The two analogous hydrogen-bonding and non-hydrogen-bonding

peptoid surfaces (with peptoids that contained or lacked a single amide bond in the hydrophilic pendant group) showed vastly different responses to *Ulva linza* algae, despite presenting similar hydrophilicity in contact angle goniometry. The non-hydrogen-bonding surface showed higher initial settlement, but drastically improved fouling release of algae left the surface far cleaner than other samples. Sum frequency generation spectroscopy showed that these two materials interacted differently with water, with the hydrogen-bonding surface instigating a structured water layer that likely reduced initial settlement. However, these hydrogen bonds also strengthened interactions with algae and inhibited removal when compared with the non-hydrogen-bonding material.

Chapter 4 demonstrates that hydrogen bonding interactions similarly govern adsorption from vapor phase conditions. In this study, self-assembled monolayers (SAMs) provided ultrasmooth surfaces consisting of either COOH, OH, or CH_3 head groups to determine the effects of surface chemistry on adsorption of water, 1-butanol, and acetic acid. Hydrogen bonds were essential for adsorption, but key differences were observed between the surface and solvent pairs. Acetic acid that adsorbed onto COOH-terminated SAMs was found to trigger widespread acid deprotonation: approximately 45% of the total acetic acid components were deprotonated based on O 1s spectra. This was paired with a change in the C 1s carboxyl carbon binding energy to an intermediate value between COOH and COO^- positions. Conversely, butanol did not show signs of deprotonation in either O 1s or C 1s spectra. From this, it is clear that solvent surface affinity can differ beyond adsorption to include different electronic environments.

In addition, Chapters 2 and 3 depicted the changes in surface chemistry that can result from exposure to water vapor or immersion underwater. Chapter 3 focused

predominantly on the effects of polypeptoids on polymer surface chemistry in vacuum and hydrated conditions up to 100% relative humidity (RH). When amphiphilic polypeptoids were incorporated into PEO-based block copolymer systems as side chains, fluorinated monomers were able to drive surface segregation as had been previously seen by the group. The addition of water did not induce restructuring of the polypeptoid components away from the surface, likely as a result of the hydrophilic polypeptoid backbone and ether monomers. However, restructuring of the PDMS-polypeptoid system was apparent when water was added to the system. There, increases in polypeptoid content were directly correlated with increases in water affinity. This correlates well with sum frequency generational spectroscopy of the antifouling PDMS-based system with shorter peptoid side chains from Chapter 2. Side chain surface restructuring was apparent between ambient air and underwater conditions by the appearance of the peptoid amide bend for the latter.

While this work represents significant progress in understanding interactions that take place between the surface and water or organic adsorbates, much must be done in order to understand the surface and interactions present in complex aqueous systems. A key next step in this process is investigating the effects that water has on surface adsorption. To this point, hydrogen bonding has been seen to instigate adsorption of polar solvents to the surface (Chapter 4), but also instigate formation of structured water layers in aqueous conditions (Chapter 2). These two effects are in opposition, and observing competition between water and solvents for adsorption sites will be particularly useful in understanding the ways that hydrogen bonding affects adsorption and fouling.

Another area for growth lies in the materials studied. Self-assembled monolayers were particularly convenient for characterizing surface adsorption onto particular

functional groups, but differ rather significantly from polymer coatings or membranes which can also sorb water. Future experiments should begin to bridge the gap between idealized assembled monolayers and realistic polymers that participate in both adsorption and absorption. In particular, development of a surface with flexible brushes that can interact with water and solutes all along the chain, rather than solely the end, may be a suitable intermediate. Leveraging polypeptoids for this work could be advantageous, as they can be studied as surface brushes and as side chains in block copolymers.

The final, and perhaps most significant, challenge lies with characterization of these surfaces. This dissertation focused on development of ambient pressure XPS (APXPS) for characterization of polymeric surfaces in underwater conditions. While we have successfully studied polymer materials in hydrated conditions without inducing beam degradation or excessive charging, major improvements can still be made. Reaching both nanometer-level surface sensitivity and underwater conditions is challenging for any spectroscopy that relies on signal from electrons; lower energy electrons (from lower energy photons) will more purely come from the surface, but cannot travel far through an aqueous layer or even through vapor phases. We have gotten around this problem by extrapolating data from the top 2-5 nm in moderate pressures (below ~1 Torr) to data collected at full saturation (~20 Torr) with surface sensitivity on the order of 20-30 nm. Future efforts must continue until collecting all of this information at a single time is possible to answer the key question of functional group surface density at the top surface in fully hydrated conditions.

Improving polymer compatibility for underwater applications will remain a significant focus for research and industry for decades to come. This work lays down

methodologies for creating and characterizing tunable polymer surfaces in such conditions. As generations of such works develop over time, understanding of and control over underwater surfaces will improve, yielding increasingly rapid innovations for underwater applications ranging from membranes to antifouling coatings.